Development and Characterization of Optimum Process Parameters for Metallic Composites made by Ultrasonic Consolidation

THESIS

Presented in Partial Fulfillment of the Requirements for the Degree Master of Science in the Graduate School of The Ohio State University

By

Christopher D. Hopkins, B.S.

Graduate Program in Mechanical Engineering

The Ohio State University

2010

Thesis Committee:

Dr. Marcelo J. Dapino, Advisor

Dr. Sudarsanam Suresh Babu

ABSTRACT

Ultrasonic consolidation (UC), also referred to as ultrasonic additive manufacturing (UAM), is a recent solid-state, low temperature fabrication process that can be used for layered creation of solid metal structures. The process uses ultrasonic energy to induce plastic deformation and nascent surface formation at the interface between layers of metal foil causing bonding between the surfaces. UAM is an inherently stochastic process with a number of unknown facets that can affect the bond quality between layers. In order to take advantage of the unique benefits of UAM, it is necessary to understand the relationship between manufacturing parameters (machine settings) and bond quality by quantifying the mechanical strength of UAM builds. The goal of this thesis is to identify the optimum combination of processing parameters for manufacture of metallic composites.

The research presented consists of three parts; the first part deals with characterizing the mechanical strength of titanium-aluminum builds by statistically analyzing the effects of four main process parameters on the USS and UTTS of the builds. A multi-factorial experiment was designed to study the effects of the manufacturing parameters normal force, oscillation amplitude, weld speed, and number of bilayers on the outcome measures Ultimate Shear Strength (USS) and Ultimate Transverse Tensile Strength (UTTS). For a given factor, the operating levels were selected to

cover the full range of machine capabilities. A generalized linear model was formulated to study the statistical significance of each factor. Transverse shear and transverse tensile experiments were conducted to evaluate the bond strength of the builds. Optimum levels of each parameter were established based upon the statistical contrast trend analyses. The results from trend analyses indicate that high mechanical strength can be achieved with a process window bounded by a 1500 N normal force, 30 μm oscillation amplitude, about 42 mm/s weld speed, and two bilayers. The effects of each process parameter on bond strength are discussed and explained. Microstructural analysis was performed on samples in order to evaluate interfacial bonding and indicated that the composites strength were mainly due to mechanical interlocking between the soft aluminum and hard titanium layers.

The second part investigates the effect of the process parameters tack force, weld force, oscillation amplitude, and weld rate on the USS and UTTS of 3003-H18 aluminum UAM built samples. A multi-factorial experiment was designed and an analysis of variance was performed. Additional statistical tools were employed in order to develop a complete understanding of the effects and interactions of the process parameters. The results of the statistical analyses indicate that a relatively high mechanical strength can be achieved with a process window bounded by a 350 N tack force, 1000 N weld force, 26 μm oscillation amplitude, and about 42 mm/s weld rate. The effects of each process parameter on bond strength are discussed and explained. A correlation and proposed hypothesis between the process parameters, the mechanical strength of the specimens, and their resulting microstructure was developed based upon analyses using optical microscopy. Bond characterization analyses indicate that there all the specimens had close to the same amount of percent bonded area and

that a high linear weld density (LWD) did not directly correlate to a high mechanical strength. The final part of this thesis explores the fatigue life of 3003 aluminum UAM built specimens loaded axially using fully reversible bending.

ACKNOWLEDGMENTS

I would like to begin by acknowledging all of those who have contributed to the success of this research. First, I would like to thank my adviser, Dr. Marcelo Dapino, for providing the opportunity to work in the Smart Materials and Structures Laboratory on this project. His continuous support and dedication were invaluable during my M.S. program. I would also like to thank Professor Suresh Babu for serving on my exam committee and for all of his metallurgical insights.

I am grateful to Dr. Karl Graff, Matt Short, and Gary Thompson at Edison Welding Institute for their exceptional support and assistance without which this research would not be possible. Thanks to John Sheridan and Chris Fitzgerald at Solidica, Inc., and the Smart Vehicle Concepts Center for making close collaboration with these companies possible.

I am thankful to Professor Angela Dean from the OSU Department of Statistics and Soledad Fernandez from the Center for Biostatistics for their help and technical guidance with all of my statistical work. I would also like to thank David Schick and Sriraman Ramanujam, from the OSU Welding Engineering Department for their guidance and assistance with all things metallurgical.

I thank all of my colleagues at the Smart Materials and Structures Lab, especially Shravan Bharadwaj, Suryarghya Chakrabarti, Daniel Foster, Ryan Hahnlen, John Larson, and Arjun Mahadevan for all of their help, advice, support, and friendship. I

thank Neil Gardner of the Student Machine shop who willingly volunteered his time and know-how to help me with all of my machining tasks.

I would like to express my sincerest gratitude towards my parents for their continued love, support and advice throughout my college career. Thank you Mom, Dad, and Aunt Dee for everything you've done for me. Your constant encouragement and reassurance have motivated me to accomplish my dreams and goals. Finally, I am truly indebted to Colleen for her unwavering support and faith in me. She has been key in keeping me calm, focused and grounded during my graduate studies. I could not have done it without her.

VITA

August 22, 1985	Born - Ewing, New Jersey
June 2004	Honors Diploma, West Windsor-Plainsboro High School North
May 2008	B.S. Mechanical Engineering Magna Cum Laude, Miami University
2008	Graduate Teaching Assistant, The Ohio State University
2009 - Present	Graduate Research Associate, The Ohio State University

FIELDS OF STUDY

Major Field: Mechanical Engineering

Studies in Smart Materials and Structures: Dr. Marcelo Dapino

Major Field: Mechanical Engineering

TABLE OF CONTENTS

Page

LIST OF TABLES

LIST OF FIGURES

CHAPTER 1

INTRODUCTION

1.1 Ultrasonic Additive Manufacturing (UAM)

Ultrasonic additive manufacturing (UAM) or ultrasonic consolidation (UC) is a state-of-the-art manufacturing process that combines principles from ultrasonic welding, layered manufacturing techniques, and subtractive processes to create metal parts with arbitrary shapes and features [6]. UAM is a solid-state welding process that allows joining of metallic materials far below their respective melting temperatures. The locally generated heat due to ultrasonic vibration during the UAM process ranges between 30-50% of the melting temperature of the base metal [20]. Being a relatively low-temperature process, UAM offers unprecedented opportunities to create parts with embedded smart materials or electronic components [18, 29]. Further, the subtractive stage integrated within the UAM system allows for the simultaneous incorporation of arbitrarily shaped internal features such as cooling channels or designed anisotropies. Finally, UAM has been utilized to embed and join both difficult and dissimilar metals and materials such as Ti, Al, Cu, Mg, and stainless steel alloys (a few representative builds are shown in Figure 1.1).

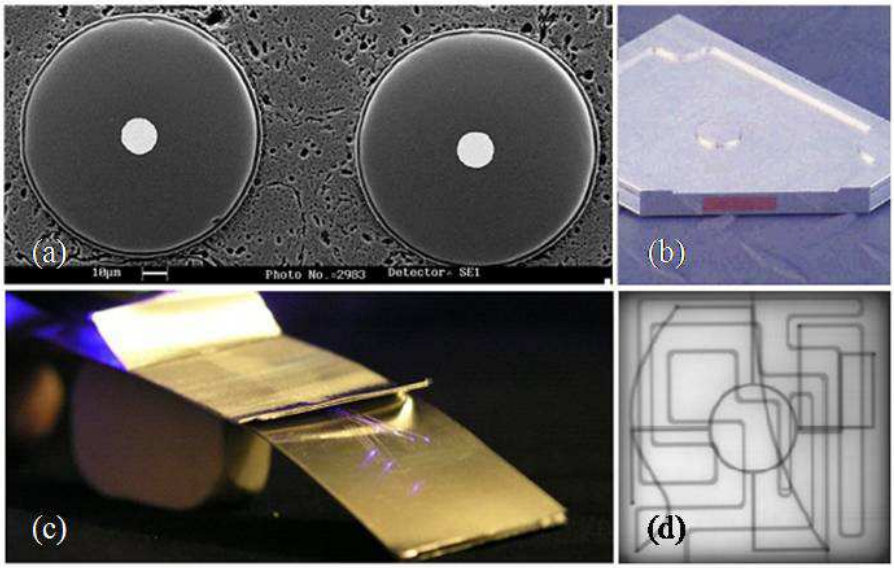

Figure 1.1: (a) Micrograph of 102 μm (0.004") diameter sigma fibers embedded in aluminum [18]. (b) Aluminum UAM build with embedded copper block. (c) Fiber optics embedded between aluminum tapes. (d) X-ray image of a UAM build with arbitrary multi-level internal channels made using subtractive processes. (Photographs (b) and (c) courtesy of Solidica, Inc., Image (d) courtesy of EWI)

In UAM, (like in UMW) a sonotrode or horn is used to apply a normal force at the interface between two metal work pieces. Piezoelectric ultrasonic transducers drive the transversely vibrating sonotrode which imparts a motion to the top work piece and creates a relative, friction-like action at the interface of the two work pieces. This scrubbing motion causes shear deformations of contacting surface asperities resulting in dispersion of interface oxides and contaminants [25]. The combination of imparted static normal force and transverse motion leads to increasing areas of clean metal-to-metal contact and ultimately brings about solid-state bonding and adhesion between the faying surfaces [30]. A diagram of the UAM process is seen in Figure 1.2.

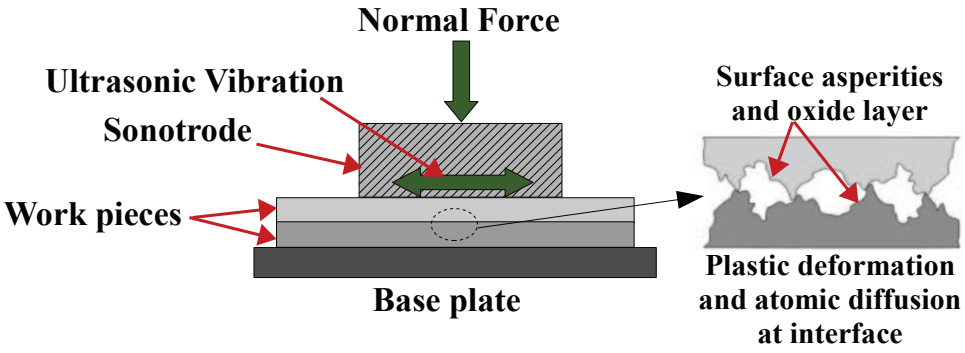

Figure 1.2: Schematic representation of ultrasonic additive manufacturing at the interface between two metal surfaces.

On a metallurgical scale, in UMW processes, the weld zone shows local plastic deformation within a small thickness (less than 100 μm). This layer has a very fine grain structure resulting from heavy plastic deformation and recrystallization [6]. The grain structure just outside the weld zone is generally undisturbed, while the weld zone consists of an irregular pattern of fine grains or amorphous structures. This pattern has some undulation which at times seems to transfer to near-turbulent patterns of mixing in some regions [6]. It is still unclear how parts made by UAM relate metallurgically to parts made by UMW, but the basic phenomena outlined here are analogous to those found to exist thus far in specimens built by UAM.

The UAM system is distinct from conventional UMW systems; it consists of a rotating transducer, booster, and horn arrangement. As shown in Figure 1.3, instead of a spot contact, vibrations generated by a piezoelectric ultrasonic transducer are transmitted into the parts through a rolling sonotrode. The speed at which the

sonotrode travels across the build is referred to as the weld speed and is an operator-defined process parameter. The vibrations propagate longitudinally at a frequency of 20 kHz from the transducer to the sonotrode through tuned waveguides. The amplitude of these vibrations is considered a process parameter that can be adjusted. Normal force can be adjusted and is applied to the vibrating sonotrode as it rolls along the work piece and the vibrations transmitted to the weld interface cause a solid-state bond between the parts.

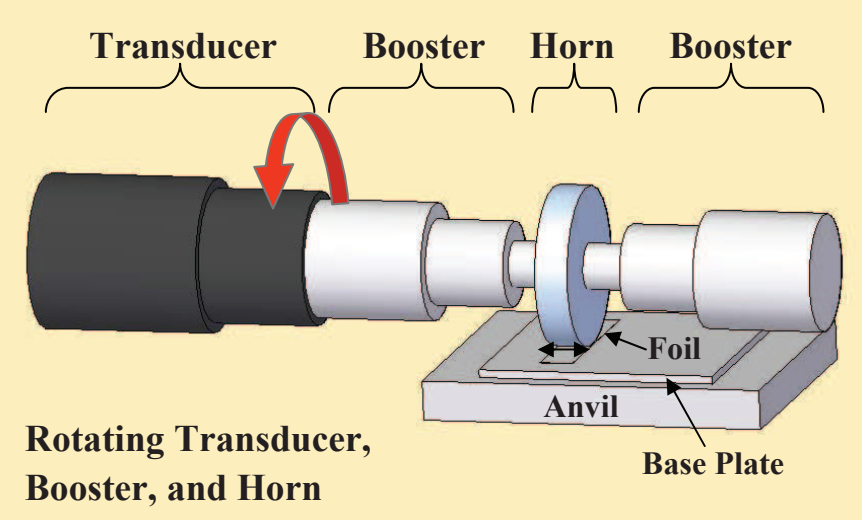

Figure 1.3: Diagram of UAM system where successive layers of metal tape are bonded together for creating bulk metallic parts.

Current UAM systems achieve the most effective bonding on thin metal layers of approximately 152 μm (0.006") thickness. The most sophisticated UAM system therefore employs an automated feed mechanism for allowing successive layers of metal tapes, drawn from a continuous spool, or thin sheets to be bonded together

for creating larger bulk builds. A subtractive CNC machining stage is also fully automatic and integrated within the UAM system [30]. Figure 1.4 is a photograph of the outside of Solidica, Inc.'s Formation machine, while Figure 1.5 shows the internal layout. Presently, Edison Welding Institute (EWI) has a UAM test bed, referred to as the VHP-UAM machine, which can supply up to 10 kW of ultrasonic power during a weld cycle as opposed to the 2 kW maximum that the current Formation system can supply.

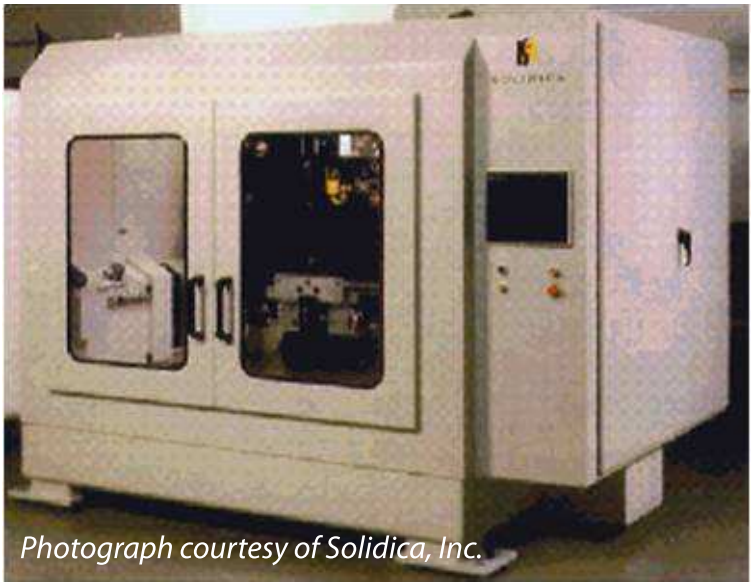

Figure 1.4: Photograph of Solidica, Inc.'s UAM Formation machine.

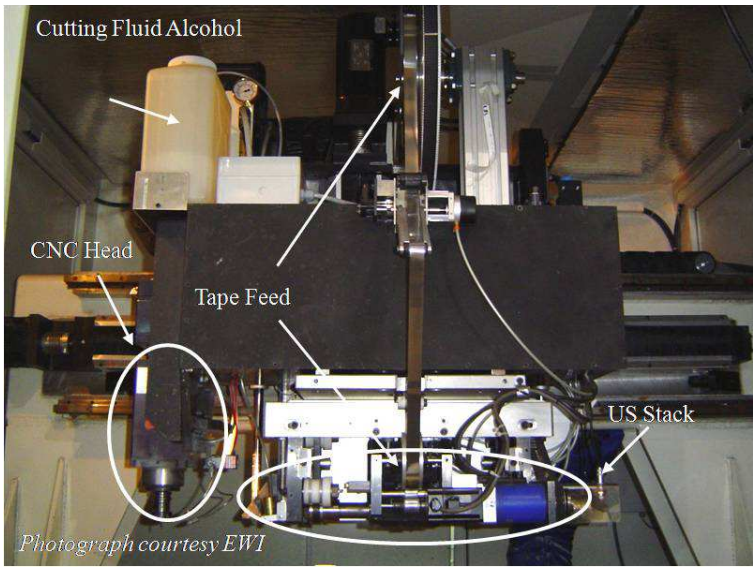

Figure 1.5: Photograph of ultrasonic transducer, booster and horn system, tape feed mechanism and integrated CNC mill.

1.2 Design of Experiments (DOE)

1.2.1 Overview and the Taguchi Method

Design of Experiments (DOE) is a structured, organized approach to determining the relationship between different factors affecting a process and the output of that process. Typically, several factors are examined at once because it is more efficient to examine all possible causes of variation simultaneously rather than one at a time. Fewer observations are needed and more information can be gained about the system being studied. There are several steps that are involved in the design and analysis of an experiment which are key to collecting data correctly and efficiently to allow a good analysis with the required precision. The steps are [4]:

(a) Define the objectives of the experiment.

(b) Identify all sources of variation.

(c) Choose a rule for assigning the experimental units to the treatments (experimental design).

(d) Specify the measurements to be made, the experimental procedure, and the anticipated difficulties.

(e) Specify the model.

(f) Outline the analysis.

(g) Review the above decisions. Revise, if necessary.

Steps (a), (b), and (d) require an understanding of the process, its parameters, and the precise questions that are to be addressed by the experiment. Step (c) is the point at which an experimental design is chosen for assigning which experimental units are to be observed under which treatments [4].

There are many different types of experimental designs including completely randomized, block, nested, full-factorial, and fractional factorial designs. The research presented within this document focuses on a specific type of fractional factorial experiment that uses orthogonal arrays to select the treatment combinations. A treatment combination is any combination of levels of the factors that are of interest to the experimenter (treatment factors). Orthogonal arrays consist of a number of predetermined treatment combinations depending upon the number of treatment factors and the number of levels at which each factor will be used. Orthogonal arrays are advantageous because of their reduced number of observations, which has the advantage of saving both time and money in running the experiment, without confounding

main-effects and interactions. The term "confounded" refers to the indistinguishability of a treatment contrast and a block contrast, which should be avoided when selecting the factorial scheme [4].

One proponent of orthogonal arrays as an experimental design was Dr. Genechi Taguchi [23]. He devised several orthogonal arrays based upon ordinary fractional factorial designs, called Taguchi orthogonal arrays, in which the difference between treatment and noise factors is ignored at the design stage. His designs are commonly used for quality improvement in many industries. An example of a Taguchi L9 orthogonal array is displayed in Table 1.1 whose column elements (L, M, H) signify the low, medium and high levels (also represented by 1, 2, 3) of the column parameters (treatment factors) [23]. Each row represents a specific set of factor levels (treatment combination), sometimes referred to as the run number or experiment number. In practice, these treatment combinations would be then randomized and the response variable would be measured following the randomized order to avoid any biases due to manufacturing or measurement order.

While his experimental designs are based upon proven methods, Dr. Taguchi's data analysis methods, mainly signal-to-noise ratios, are not widely accepted by statisticians [23]. Therefore, the data analysis techniques that he promotes are not employed for the statistical analyses used in this research. Furthermore, there are several statistical tools that he does not mention that can be extremely useful for gleaning more information from the data.

Table 1.1: Example of a coded Taguchi L9 orthogonal array.

Treatment Combination	**Factor A**	**Factor B**	**Factor C**	**Factor D**
1	L	L	L	L
2	L	M	M	M
3	L	H	H	H
4	M	L	M	H
5	M	M	H	L
6	M	H	L	M
7	H	L	H	M
8	H	M	L	H
9	H	H	M	L

1.2.2 Analysis of Variance (ANOVA)

The most common and accepted way of statistically determining whether or not the treatments differ in terms of their effects on the response variables is by writing and testing a null hypothesis against an alternative hypothesis. The null hypothesis is of the general form,

H_0:{all levels of parameter A have an equal effect on the response variable}

and the alternative hypothesis is such that,

H_A:{at least two levels of parameter A differ in their effect on the response variable}.

A model equation is written and shows the dependence of the response variable upon the levels of the treatment factors [4]. The models that are used in this research are linear, meaning that the response variable is written as a linear function of the parameters. An example of a simple model with only one treatment factor, τ, at level i and mean μ is given by the following:

$$Y_{it} = \mu + \tau_i + \epsilon_{it}, \tag{1.1}$$

with $t = 1, ..., r_i$, $i = 1, ..., v$, and the assumptions that ϵ_{it} is of a normal distribution about zero with each replicate of ϵ_{it} being mutually independent.

In equation (1.1), Y_{it} is the response at level i, replicate t and is equal to the overall mean plus the effect of the treatment factor at level i and the error variable, ϵ_{it}. This model compares measures of variation and is the standard analysis of variance model. This serves as the foundation of all statistical analyses performed in this research.

The null hypothesis is tested by calculating several statistics including the sum of squares, the mean square, an F-ratio (from an F-distribution) and a p-value for the overall model, error, treatment factors, and any included interactions. These values are usually summarized in an analysis of variance table. Table 1.2 shows the results of an ANOVA performed on simulated data as an example of an ANOVA table.

Table 1.2: Example results of ANOVA produced by the statistical software SAS [9].

Source of Variation	**Degrees of freedom**	**Type III Sum of Squares**	**Mean Square**	**F-Ratio**	**p-value**
Parameter A	3	24248.538	6062.135	151.43	0.0001
Parameter B	3	502.956	167.652	4.16	0.0189
Parameter C	3	278.613	92.871	2.32	0.2701
Parameter D	3	9773.168	3257.723	81.38	0.0034
Error	51	2041.581	40.031		
Total	63	36844.856			

From the information presented in Table 1.2, the generalized null hypothesis can be tested. If the F-ratio for a given parameter is greater than the corresponding critical F-value (referenced from an F distribution table) then it can be concluded that there is sufficient evidence to reject the null hypothesis (no difference in effects)

in favor of the alternative hypothesis (there is a difference in effects). A simpler way of reaching this conclusion is by comparing the p-value for each parameter against a pre-selected Type I error probability or significance level, α. A Type I error probability is the probability of rejecting H_0 when in fact it is true [4]. Typically, α is chosen to be between 0.01 and 0.10 depending upon how important it is to not incur in a Type I error. Therefore, if the p-value for a given parameter is less than the chosen α level the null hypothesis can be rejected for the parameter and it can be reasoned that the parameter has a significant effect on the response variable.

In the example illustrated by Table 1.2, it can be concluded that different levels of Parameters A and D have an effect on the response variable at a significance level of 0.01 because the p-values for these parameters are less than 0.01. It can also be conjectured that because the p-value for Parameter A is much less than the p-value for Parameter D, Parameter A has a more significant effect on the response variable than Parameter D. There is not sufficient evidence at the 0.01 level to reject the null hypotheses for Parameters B and C, therefore it cannot be concluded that they have an effect on the response variable.

1.2.3 Interactions

In statistics, an interaction between treatment factors means that the simultaneous influence of two factors on a response variable is not additive [4]. When two factors interact, the relationship between each of the interacting factors and the response variable depends on the value of the other interacting variable. An example of an ANOVA model that includes an interaction between its two factors is

$$Y_{ijt} = \mu + \alpha_i + \beta_j + (\alpha\beta)_{ij} + \epsilon_{ijt}, \tag{1.2}$$

with $t = 1, ..., r_{ij}$, $i = 1, ..., a$, $j = 1, ..., b$, and the assumptions that ϵ_{ijt} is of a normal distribution about with each replicate of ϵ_{ijt} being mutually independent.

The interaction term $(\alpha\beta)_{ij}$ is added to the ANOVA table to be tested. If it is found to be a significant interaction (based on p-value comparison) then it may not be sensible to consider the factors involved in the interaction separately anymore [4]. Further, the interaction should be checked graphically because occasionally a perceived interaction from the statistical analysis may be negligible on the plot and vice versa. Example interaction plots are shown in Figures 1.6 and 1.7.

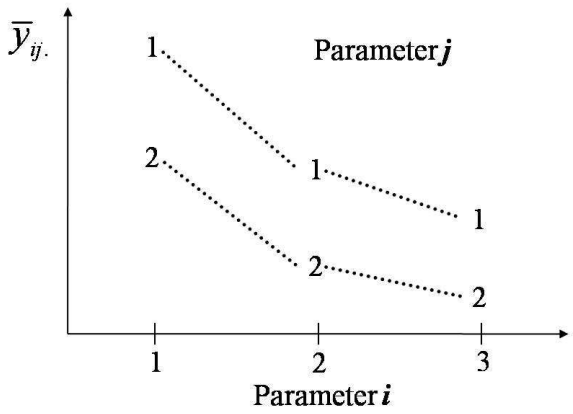

Figure 1.6: Example interaction plot showing no interaction between levels of Parameter i and Parameter j [4].

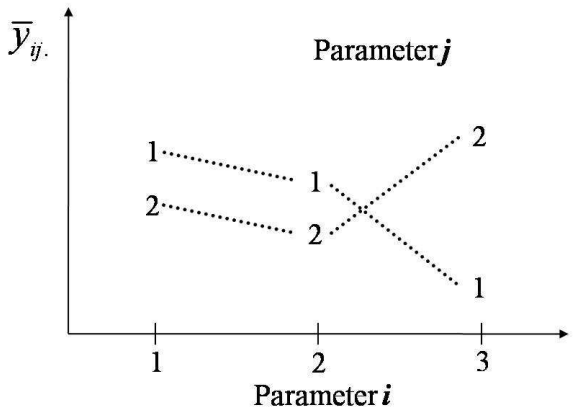

Figure 1.7: Example interaction plot showing an interaction with Parameter j at level 3 of Parameter i [4].

The example interaction plot given by Figure 1.6 indicates that all three levels of Parameter i obtain a higher response at level 1 of Parameter j. Also, level 1 of Parameter i has a higher response than the other two levels of Parameter i. Finally, it is concluded from this plot that no interaction exists between the given levels of Parameter i and Parameter j. Figure 1.7 shows that for levels 1 and 2 of Parameter i the response variable is higher when combined with level 1 of Parameter j, but at level 3 of Parameter i, level 2 of Parameter j produces a higher response. This effect is known as an interaction between Parameter i and Parameter j.

1.2.4 Confidence Intervals and Trend Contrasts

For the purposes of this research a contrast is defined as a linear combination of the parameters that can be used to compare the effects of the treatments. For example, a single contrast consists of the difference between the effects of two treatments, u and s. If that difference is equal to zero, then it can be said that treatments u and s

affect the response in the same way, thus the treatments do not differ. Otherwise, the treatments do have differing effects on the response variable. This difference can be determined by using contrasts to create confidence intervals. For a single confidence interval, the confidence level is based on the probability that the given interval will contain the true value of the contrast [4]. In this research, simultaneous confidence intervals were used because they provide intervals where the probability is based upon all of the intervals being simultaneously correct. This often produces wide intervals compared to single confidence intervals for a given confidence level, but they are necessary when multiple levels and parameters are used.

There are several accepted methods for calculating simultaneous confidence intervals, and the one used in this research is Tukey's method for all pairwise comparisons. This method was utilized because it can be unplanned and produces the smallest intervals when only pairwise difference contrasts are required. The general formula for calculating the confidence interval with an overall confidence level of at least 100(1-α)% is given by

$$\tau_i - \tau_s \in \left((\bar{y}_i - \bar{y}_s) \pm w_T \sqrt{msE \left(\frac{1}{r_i} + \frac{1}{r_s} \right)} \right), \tag{1.3}$$

where the critical coefficient, $w_T = q_{v,n-v,\alpha}/\sqrt{2}$, $\tau_i - \tau_s$ is the pairwise comparison, the $\bar{y}$'s are the averages for the levels examined, r is the number of replications at each level, and $q_{v,n-v,\alpha}$ is a tabulated critical value from a Studentized range distribution [4]. The confidence intervals that are created using this formulation are interpreted to determine if the levels of a given parameter affect the response variable and, if so, by what degree. For example, let Parameter A have levels 1 and 2, and, using Tukey's method, the resulting confidence limits are -3.104 and 3.091 at a 95% confidence level. Therefore, the results can be understood to say that because the

interval contains zero, and about half of the interval is negative and half is positive there is no difference in effect on the response variable between the two levels of this parameter. Suppose the confidence limits were instead -9.012 and -8.463, this would indicate that level 2 of Parameter A consistently results in a greater response than level 1 and that there is a 95% probability that the next contrast would be within this range as well. Alternatively, if the limits were 8.463 and 9.012, then level 1 of Parameter A would consistently result in a greater response than level 2.

Confidence intervals are used as a supporting tool to determine the individual effects of the levels of a given parameter on the response variable. Also, they can assist in interpreting unclear results from an ANOVA table because a confidence interval can help to determine the degree to which a parameter affects the response variable.

Trend contrasts are based on regression theory and are used to establish and/or verify any trends observed from a scatterplot of the response variable versus the levels of a given treatment factor. Linear, quadratic, cubic and higher order trends can be detected provided there are enough statistical degrees of freedom. The contrasts are based upon hypothesis testing and are a quantitative way of finding out whether an observed trend in the data is truly present or not. For example, suppose there are three levels of Parameter B and it is desired to know whether the value of the response variable increases or decreases as the level increases, and, if so, whether the rate of change remains constant [4]. These questions can be answered by estimating linear and quadratic trends in the response. A table similar to that of an overall ANOVA table can be produced with the contrast trends as the parameters being tested. A Type I error probability, α, is pre-selected and is used as a benchmark for comparing

the p-values that are produced for each trend being tested. If a p-value for a trend is less than α it can be concluded that that data trend is present in the data.

1.3 Problem Definition

In UAM, the normal force, oscillation amplitude, and weld speed can be adjusted over a broad range of values, but it is unclear how these parameters and combinations of them affect the process and resulting build's strength. There are several other parameters that can be adjusted, including the roughness of the sonotrode, the pattern of the texture on the sonotrode, and the substrate temperature or baseplate pre-heat temperature. These were not investigated here because their effect on the mechanical strength of a build is thought to be minimal. They could be included in future DOEs in order to evaluate their effective significance on a UAM build's mechanical strength.

Several studies have related bond quality to manufacturing parameters (machine settings), mainly normal force, oscillation amplitude, and weld speed. Most of these studies focused on 3003-H18 aluminum as the matrix material and assessed the bond quality by reporting either peel strength data or linear weld density (LWD) [14, 19, 20, 21]. In UAM studies, linear weld density is defined as the ratio of microscopically observable "bonded" regions to "unbonded" regions at the interface between layers and is reported as an averaged percent. Peel tests are only useful for comparison between parameter sets and other UAM samples, and are primarily used for measuring adhesive strength of tape, glue or other bonded surfaces [28]. Peel tests do not provide strength values useful for the design of bulk UAM parts and for direct comparison to typical bulk mechanical strength values such as ultimate shear and tensile strength. LWD is not a good indicator of bond strength because currently it is not known how

LWD relates to the mechanical strength of a build and, if there is a relationship, what value would result in a maximum (or minimum) mechanical strength of the build.

Studies focused on titanium-aluminum (Ti/Al) UAM composites have not been reported until now. Finally, fatigue test data of UAM built specimens where fully reversible axial loading is applied in the transverse direction is currently unreported.

1.4 Objectives

The chief objective of this research is to characterize the dependence of mechanical properties on process parameters for UAM composites comprising Ti/Al bilayers as well as 3003 aluminum. Statistical studies were conducted in order to account for the stochastic nature of the UAM process. Trends in the response variable data were detected and statistically verified. Titanium−aluminum builds were chosen to be investigated because of their relevance in high-strength composite applications. Builds consisting of layers of 3003 aluminum were also studied because it is currently the most commonly used material in the UAM community and a comprehensive DOE study of 3003 aluminum was needed to serve as a baseline for other materials and higher powered UAM machines. Finally, mechanical testing procedures were developed for this research which may be applicable to future UAM mechanical strength investigations.

Both studies use a design of experiment approach in order to fully explore the effects of normal force, oscillation amplitude, and weld speed (or weld rate) on the ultimate shear strength (USS) and ultimate transverse tensile strength (UTTS) of the builds. The DOE focusing on Ti/Al composites also included a parameter specific to multi-material builds called number of bilayers. A bilayer consists of one titanium

layer on top of one aluminum layer without any welding in between as shown in Figure 1.8. The parts are built by successively welding one bilayer onto another. The 3003 aluminum DOE did not include number of bilayers because that parameter is not necessary for single-material builds, but did include tack force as a fourth parameter. In the Beta machine, two passes are run across each layer with the first pass being called the tack pass, and the second being the weld pass. Generally, the tack pass has parameters that are lower than the weld pass; the tack pass is needed to hold the tape down in order to prevent it from slipping out from under the horn when higher parameter levels are used. Therefore, the tack force refers to the normal force that is applied during the tack pass. It is desired to determine whether varying the tack force significantly affects the overall build's strength.

Finally, fatigue specimens comprising 3003 aluminum were created under two combinations of process parameters and were tested until failure at varying stress levels in order to produce S-N plots that have yet to be reported.

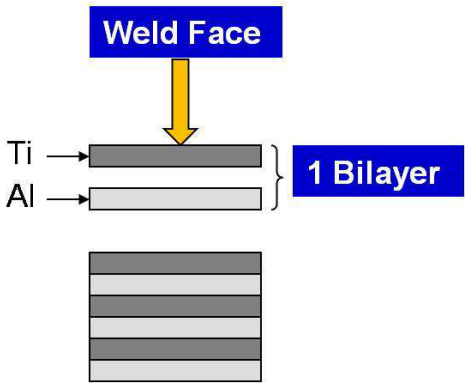

Figure 1.8: Schematic representation of Ti/Al bilayers.

CHAPTER 2

TITANIUM – ALUMINUM DOE

2.1 Experimental Methods

2.1.1 Sample Fabrication and Statistical Procedures

The materials used in this research were 0.005" (127 μm) thick sheets of commercially pure, annealed, grade 1 titanium and 1100-O aluminum. All samples were built by Solidica, Inc., Ann Arbor, MI and were 0.75" in height by 2.50" wide and 11.50" long (19 mm by 63.5 mm by 292 mm). The samples were all built at a baseplate preheat temperature of 150°C and were subjected to a post-process heat treatment of four hours at 480°C followed by furnace cooling. The samples were then machined to the geometries needed for testing.

A Taguchi L16 orthogonal array was employed for the experimental design. The Taguchi array is a statistically robust design that reduces the number of treatment combinations from 256 to 16 for a design consisting of four parameters at four levels each [23]. The process parameters and their corresponding levels are shown in Table 2.1. The levels for each of the manufacturing parameters were selected because they represent an even distribution across the range of machine operation limits for each setting.

Table 2.1: Process parameters and levels used for Ti/Al DOE.

Parameter	**Level 1**	**Level 2**	**Level 3**	**Level 4**
Normal Force (N)	500	1000	1500	2000
Oscillation Amplitude (μm)	15	20	25	30
Weld Speed[a] (in/min)	50	100	150	200
	(21 mm/sec)	(42 mm/sec)	(64 mm/sec)	(85 mm/sec)
Number of Bilayers[b]	2	4	6	8

[a]The default machine input unit is in/min. Reported values in mm/sec are rounded off to nearest integer.

[b]One bilayer consists of a layer of titanium on top of a layer of aluminum without any welding in between.

Table 2.2 shows the Taguchi orthogonal array with the coded parameter levels. The original statistical model used for this DOE was a generalized linear model (GLM) with four main effects, and the standard analysis of the data using this model, a four-way analysis of variance (ANOVA), was implemented. The linear model equation is

$$Y_{ijklt} = \mu + \alpha_i + \beta_j + \gamma_k + \delta_l + \epsilon_{ijklt}, \tag{2.1}$$

where it is assumed that ϵ_{ijklt} is of a normal distribution about zero, and all ϵ_{ijklt} are mutually independent with $i = j = k = l = t = 1, 2, 3, 4$.

The model equation summarizes the dependence of the response variable (USS or UTTS), Y_{ijklt}, upon the levels of the treatment factors [4]. In equation (2.1), μ denotes the overall mean of the response variable. The effects of each of the process parameters on the mean response are represented by α_i, β_j, γ_k, and δ_l, where α_i is the effect of normal force at the ith level on the response while the other three factors are fixed. Similarly, β_j, γ_k, and δ_l represent the effects of amplitude, weld speed,

and number of bilayers at the jth, kth, and lth levels, respectively, while the other factors are fixed. The error variable, ϵ_{ijklt} is a random variable with zero mean which denotes any nuisance variation in the response. In this model it is assumed that the error variables are independent and that they have a normal distribution with zero mean and constant variance. This is the most appropriate model to be used initially because there are no known interactions between the process parameters and it was not known if there would be enough statistical degrees of freedom to add more terms to the model. After sample production and testing the model needed to be reduced in order to determine the significance of the parameters. Four separate generalized linear models were used with two main-effect factors per model. This was found to produce useful information about the process parameters and their effects on the response variables.

Four shear and four transverse tensile samples were created and tested per experimental run. All mechanical tests were run on a 20 kip (89 kN) Interlaken load frame fitted with a $\pm$ 5000 lb (22.2 kN) load cell in series with the load train. The load frame was connected to an MTS 458.20 Micro Console controller that was coupled to a data acquisition system comprising a Data Physics Mobilyzer and PC. All tests were run under displacement control with a ramp (average rate of 0.01 in/sec) and hold input program. During testing, displacement was measured using the linear variable differential transformer (LVDT) integrated into the load frame. Because the LVDT measures the load frame's hydraulic ram displacement, all displacement data includes displacement generated with the load train as well as the specimen. Due to this, the shape of the force-displacement plots can only be used to determine if a given sample failed in brittle or ductile mode through qualitative analysis [28]. Further, this

data cannot be used to calculate specimen strain or related properties such as elastic modulus. Finally, the statistical analyses were performed using SAS 9.1 statistical software.

Table 2.2: Coded Taguchi L16 orthogonal array.

Treatment Combination	**Normal Force**	**Amplitude**	**Weld Speed**	**Number of Bilayers**
1	1	1	1	1
2	1	2	2	2
3	1	3	3	3
4	1	4	4	4
5	2	1	2	3
6	2	2	1	4
7	2	3	4	1
8	2	4	3	2
9	3	1	3	4
10	3	2	4	3
11	3	3	1	2
12	3	4	2	1
13	4	1	4	2
14	4	2	3	1
15	4	3	2	4
16	4	4	1	3

2.1.2 Transverse Shear Testing

UAM shear specimens were built based upon ASTM Standard Test Method for Lap Shear Strength of Sealants [10]. The specimens were designed such that a tape layer was along the shear plane as shown by Figure 2.1. The samples were received as 2.500" by 0.675" by 0.750" (63.50 mm by 17.15 mm by 19.05 mm) rectangular prisms then were machined down to nominal dimensions (Figure 2.1). Final design

dimensions can be seen in Appendix A. The samples were tested by placing them in a shear jig where one leg is supported and the other leg is loaded from the top (Figure 2.2). Figure 2.3 shows a sample in the shear jig just prior to being tested in the load frame. Loading was applied until sample failure while measuring force and hydraulic ram displacement.

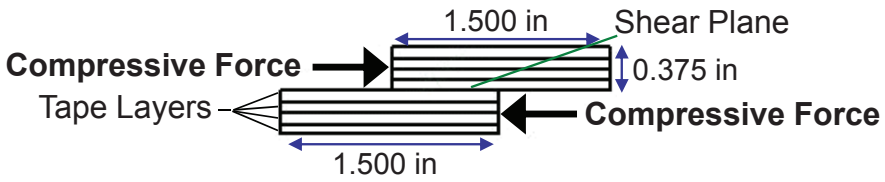

Figure 2.1: Loading scheme and tape diagram of shear specimens (not to scale).

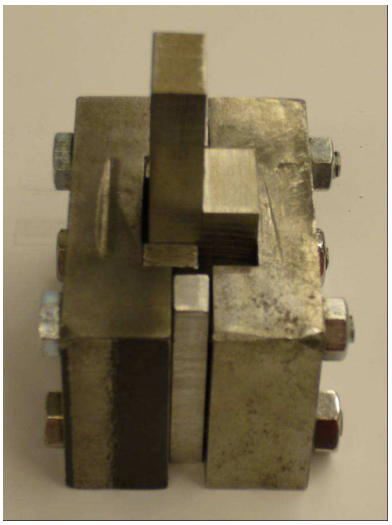

Figure 2.2: UAM shear specimen loaded in test jig.

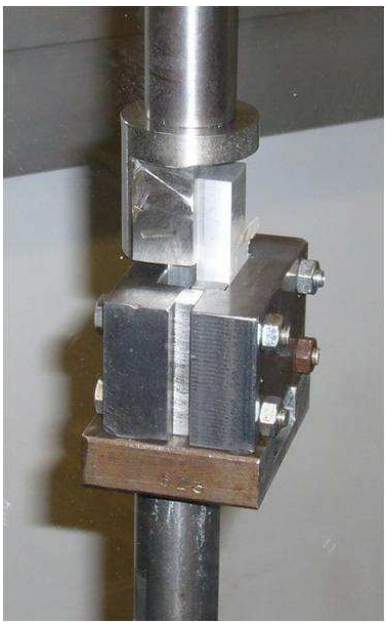

Figure 2.3: UAM shear specimen strength testing set-up.

2.1.3 Transverse Tensile Testing

UAM transverse tensile specimens were built such that the tape layers were perpendicular to the applied axial loading (Figure 2.4). The samples were received as 0.375" by 0.375" by 0.750" (9.53 mm by 9.53 mm by 19.05 mm) rectangular prisms then were then machined down to the nominal dimensions. The final design dimensions and geometry were selected because they allowed for a minimum number of layers to be used to create the transverse tensile samples and can be seen in Appendix A. Since this geometry and test method were not based upon any known standard configuration, control tests were run with a solid wrought piece of 3003 aluminum. Table 2.3 summarizes the results from these control tests. The ultimate tensile strength of solid 3003 aluminum is known to be about 152 MPa. Therefore,

it is found that the test does not bias the ultimate tensile strength and is repeatable. In turn, the geometry shown was used for the transverse tensile testing of the Ti/Al samples in this research. Tensile strength of the bonding between the layers was tested by placing the samples into specially designed grips. Figure 2.5 shows the configuration of the grips and the samples. The samples were placed under a tensile stress by being axially loaded until failure while the force and hydraulic ram displacement were measured.

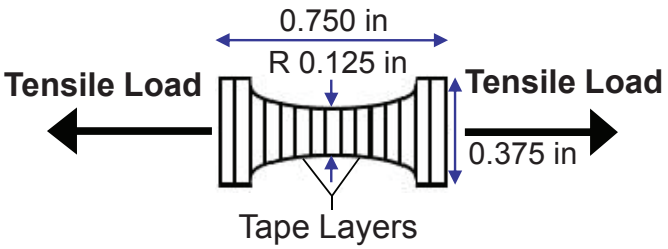

Figure 2.4: Loading scheme and tape diagram of transverse tensile specimens (not to scale).

Table 2.3: Transverse tensile mechanical testing results for control samples of solid 3003 aluminum.

Sample	**Breaking Force** (N)	**Gauge Area** (10^{-5} m^2)	**UTTS** (MPa)
Control 1	3.167	4857	153.0
Control 2	3.117	4787	153.6
Control 3	3.167	4865	153.6
		Average =	153.4
		Stand. Dev. =	0.3

Figure 2.5: (Left to Right) Transverse tensile sample grips, grips installed in jaws, sample in grips prior to testing.

2.1.4 Longitudinal Tensile Testing

Outside of the statistical DOE, the longitudinal tensile strength was examined for UAM built commercially pure, annealed, grade 1 titanium and 1100-O aluminum composites. The purpose of these tests was to investigate whether there was increased tensile strength due to grain refinement as previously found in UAM built 3003 aluminum samples [7], and to observe the consistency of the tensile strength between samples. Also, half of the samples were made with an aluminum base plate and the other half were made without it. This was done in order to study the effect of the aluminum base plate and determine if there is any significant difference in longitudinal tensile strength between samples made with the base plate and samples made without it.

All of the samples were created using the following process parameters: 1500 N normal force, 30 μm oscillation amplitude, 100 in/min (42 mm/sec) weld speed, and two bilayers. These values were chosen because they were found to be the approximate

optimal levels for Ti/Al composites based upon results of the Ti/Al DOE. UAM longitudinal tensile samples were adapted from ASTM Standard Test Method for Tension Testing of Metallic Materials [12] such that the tape interfaces were parallel to the applied axial force as shown by Figure 2.6. Nominal dimensions can be seen in Figure 2.7 and Table 2.4. Final design dimensions can be seen in Appendix A.

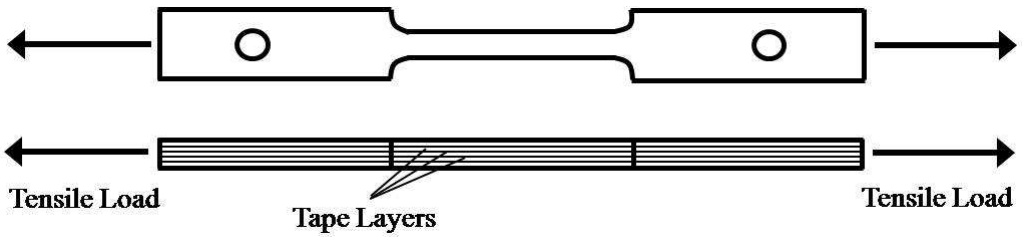

Figure 2.6: Loading scheme and tape diagram of longitudinal tensile specimens (not to scale).

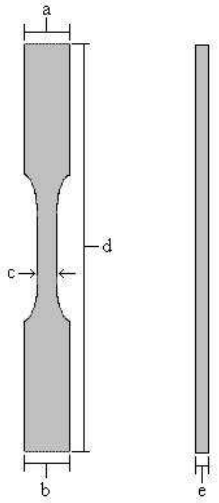

Figure 2.7: Longitudinal tensile sample dimensions.

Table 2.4: Nominal dimensions of UAM longitudinal tensile samples.

	a	**b**	**c**	**d**	**e**
Dimension (in)	0.375	0.375	0.150	3.870	0.125

These dimensions had been proven to work in the past with the load frame, pins, and grips that were available in the laboratory [7]. Longitudinal tensile specimens were carefully placed and aligned in the grips as shown by Figure 2.8.

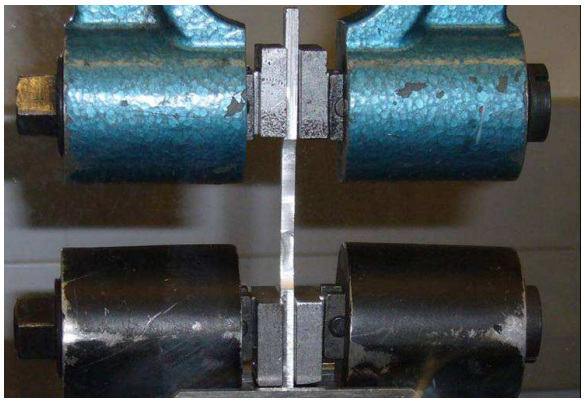

Figure 2.8: UAM longitudinal tensile specimen pinned in test jaws.

The specimens were axially loaded in tension until failure while measuring force and displacement. The maximum breaking force was noted and divided by the measured cross sectional area in the gauge region of the specimen in order to calculate the ultimate longitudinal tensile strength (ULTS) of the sample. For some of the tests, an extensometer was used to measure strain in order to obtain an estimate of

the elastic modulus of the samples. This was not done for all samples due to set-up issues with the extensometer.

2.1.5 Micrograph Preparation

After mechanical testing, certain samples were selected in order to examine the bond interface at a microscopic level and to determine if there is a correlation between macroscopic mechanical strength and micro-structure. Samples were cross-sectioned (perpendicular to weld direction) and hot mounted in a clear polymer matrix. Samples were polished using 120C, 400C, 600C, 800C and 3 μm grit paper, successively, followed by 30 minutes of vibratory polishing. Observations were conducted on as-polished samples using an inverted (metallurgical) optical microscope under various magnifications.

2.2 Mechanical Test Results

2.2.1 Transverse Shear Tests

Several samples could not be built due to delamination during manufacture or machining. The breaking force varied considerably between samples within individual experiments and between experiments. A typical force versus displacement plot for UAM Ti/Al composites tested in shear can be seen by Figure 2.9. All shear test results are tabulated and displayed in Appendix B. Figure 2.10 shows the USS averages over the sample replicates and the standard error. The standard error is defined as the standard deviation over the square root of the total number of samples studied. The recorded breaking force was the point at which the specimen underwent complete failure such that the force dropped off significantly. There are only 8 of 16 experimental runs that could be tested for shear.

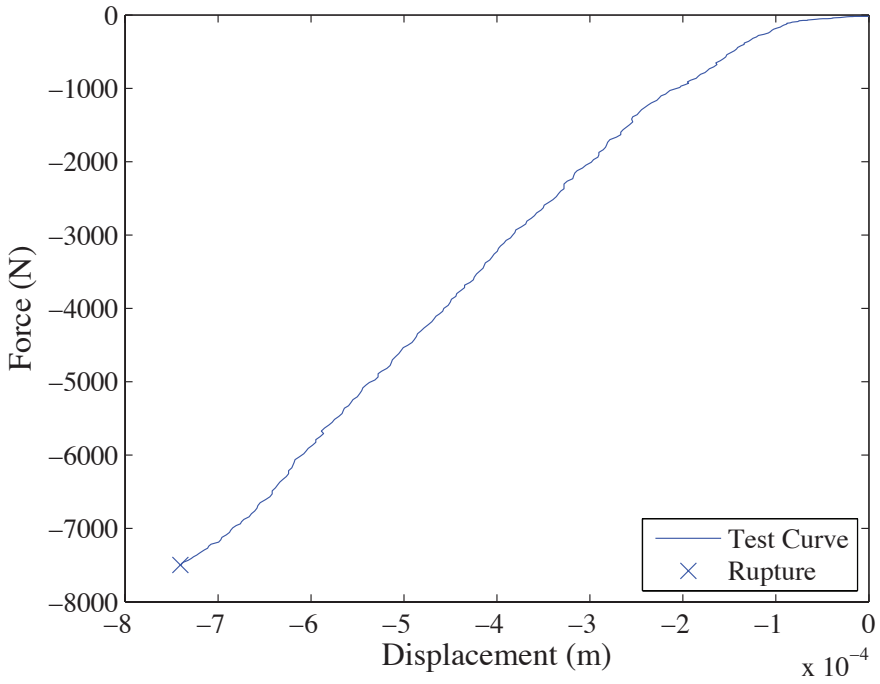

Figure 2.9: Force versus displacement plot from shear test for Expt. #11, Sample 4.

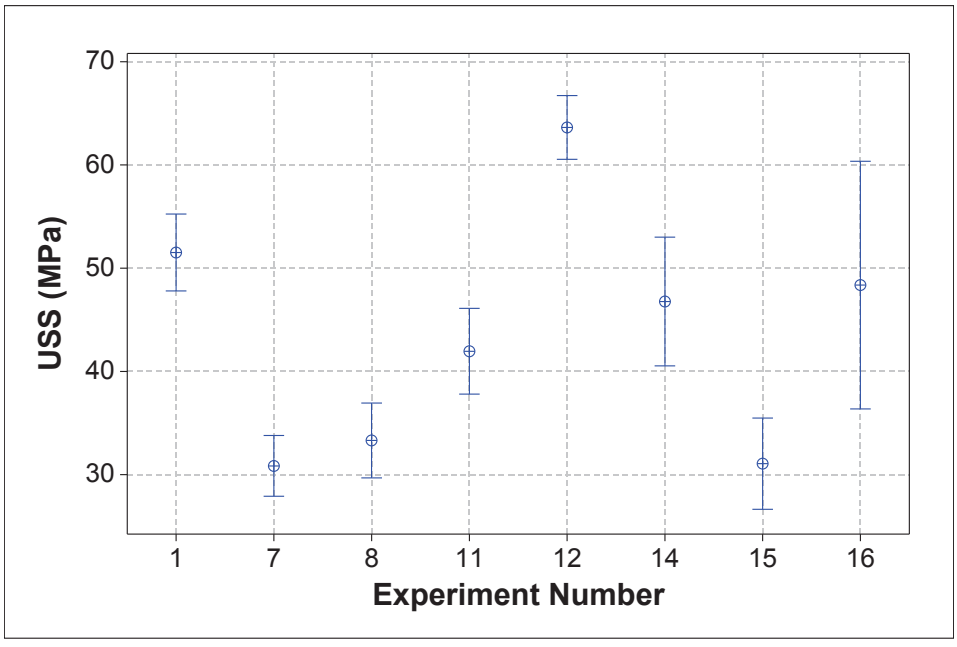

Figure 2.10: Interval plot showing ultimate shear strength (USS) for shear experiments–bars are one standard error from mean (crosshair).

Surface plots of the response variables for Ti/Al composites are shown in Figure 2.11. These indicate that attainment of the highest USS requires a combined selection of 1500 N normal force, 30 μm or more amplitude, 42 mm/s to 64 mm/s weld speed, and only two bilayers. Moreover, they indicate that there is most likely no interaction between the parameters at these levels because the levels that produce the highest response are the same between plots of varying combinations of parameters.

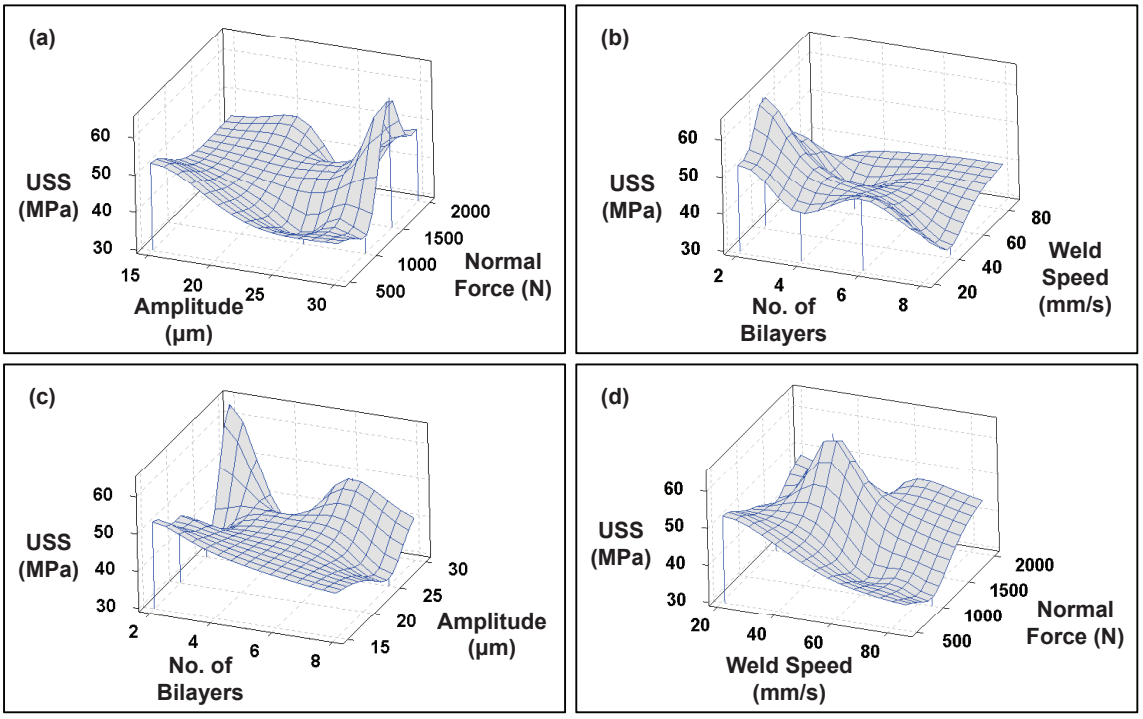

Figure 2.11: Surface plots of USS as as a function of (a) normal force and amplitude, (b) weld speed and no. of bilayers, (c) amplitude and no. of bilayers, and (d) normal force and weld speed.

2.2.2 Transverse Tensile Tests

Several samples could not be built due to delamination during manufacture or machining. The breaking force varied considerably between samples within individual experiments and between experiments. A typical force versus displacement plot for UAM Ti/Al composites tested in transverse tension can be seen by Figure 2.12. All transverse tensile test results (including fracture location) are tabulated and displayed in Appendix B. Figure 2.13 shows UTTS averages over the sample replicates and the standard error. The standard error is defined the same as in section 2.2.1. The recorded breaking force was the point at which the specimen underwent complete failure such that the force dropped off significantly. There are only 6 of 16 experimental runs that could tested for transverse tension.

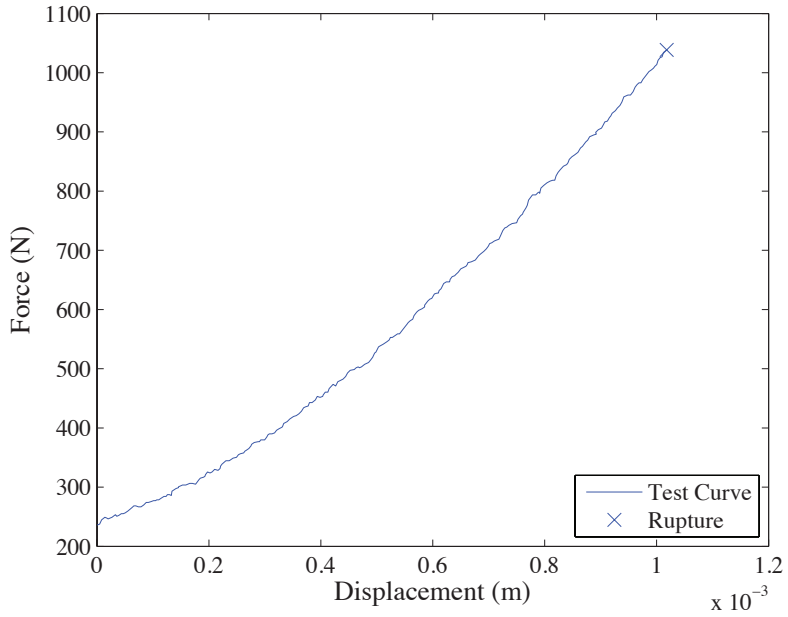

Figure 2.12: Force versus displacement plot from transverse tensile test for Expt. #12, Sample 1.

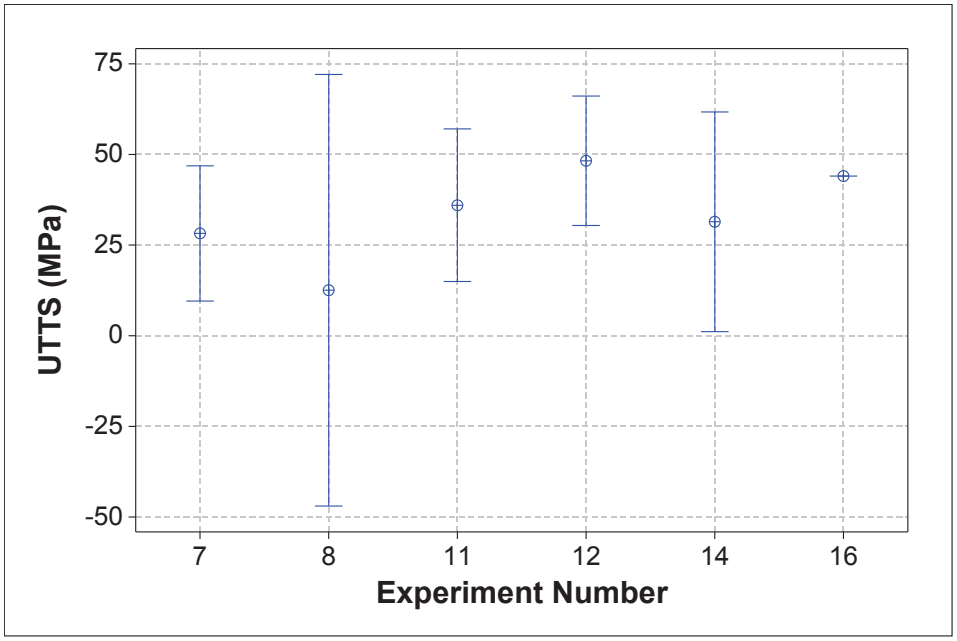

Figure 2.13: Interval plot showing ultimate transverse tensile strength (UTTS) for transverse tensile experiments–bars are one standard error from mean (crosshair).

Surface plots of the response variables for Ti/Al composites are shown in Figure 2.14. These indicate that attainment of the highest UTTS requires a combined selection of 1500 N normal force, 30 μm or more amplitude, 42 mm/s to 64 mm/s weld speed, and only two bilayers (same as shear tests). Moreover, they indicate that there is most likely no interaction between the parameters at these levels because the levels that produce the highest response are the same between plots of varying combinations of parameters.

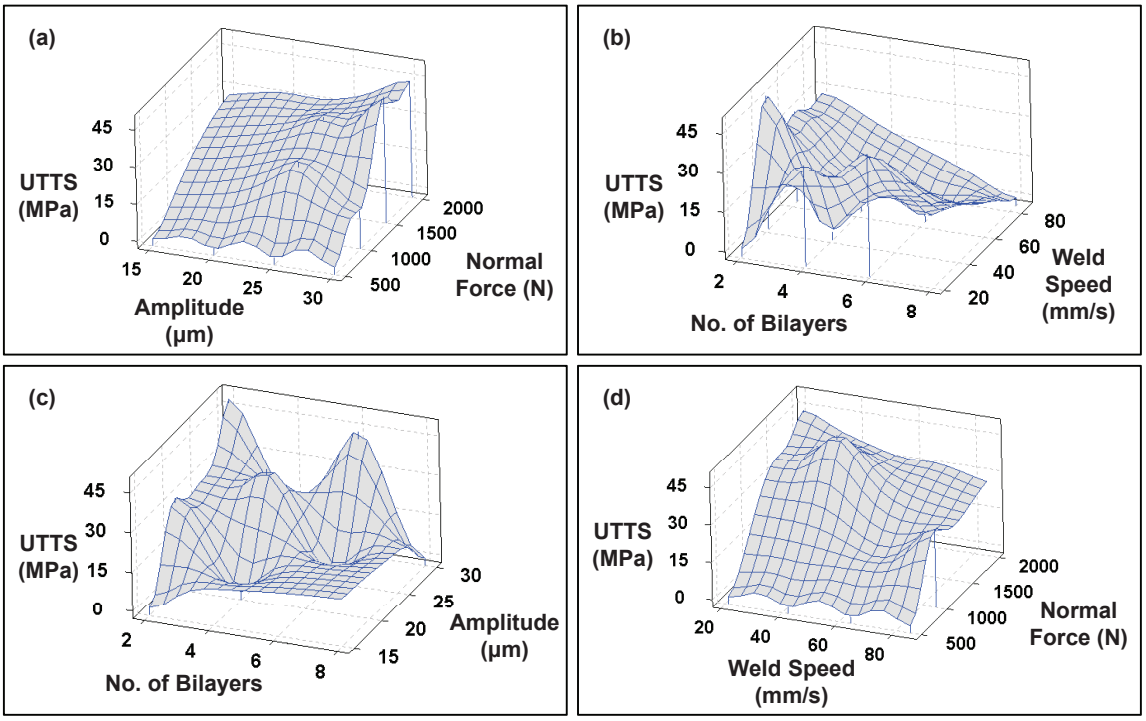

Figure 2.14: Surface plot illustrating UTTS as influenced by (a) normal force and amplitude, (b) weld speed and no. of bilayers, (c) amplitude and no. of bilayers, and (d) normal force and weld speed.

2.2.3 Longitudinal Tensile Tests

Figure 2.15 is a typical force versus displacement plot (extensometer data unavailable for these tests) for samples made with the base plate. Figure 2.16 is a typical force versus displacement plot and Figure 2.17 is a typical stress versus strain plot (extensometer data available for these tests) for samples made without the base plate. Figure 2.18 shows ULTS averages over the sample replicates and the standard error. The standard error is defined the same as in section 2.2.1. All longitudinal tensile test results, including estimated modulus of elasticity and percent elongation at failure, are tabulated and displayed in Appendix B.

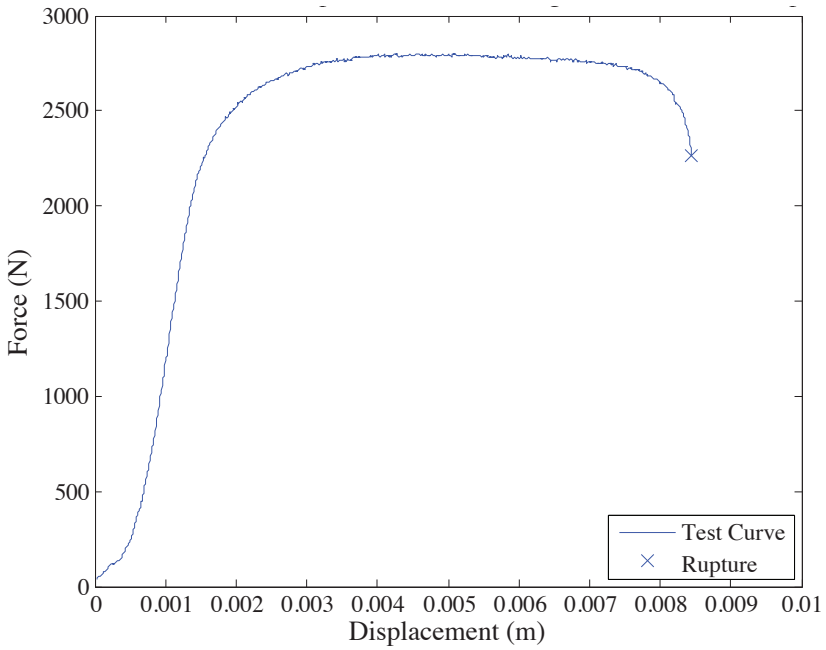

Figure 2.15: Force versus displacement plot longitudinal tensile Sample 4B (made with base plate).

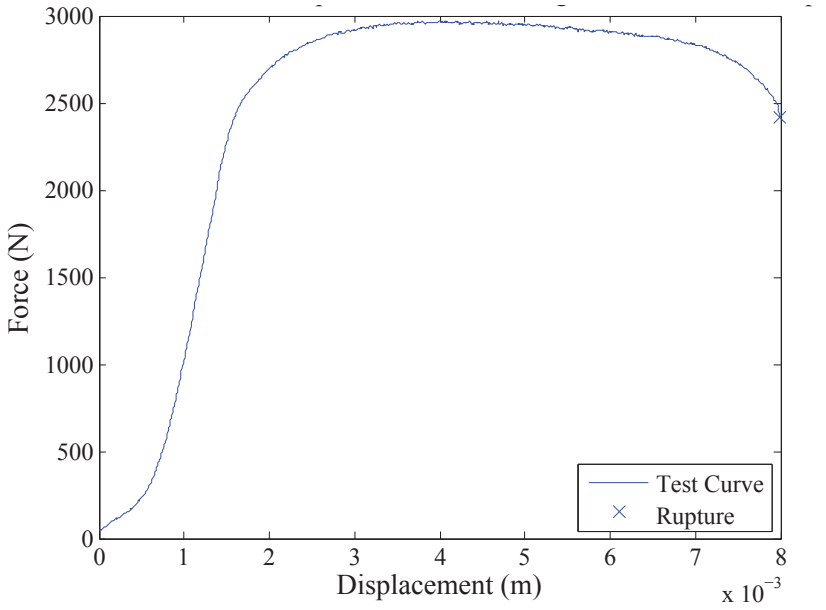

Figure 2.16: Force versus displacement plot longitudinal tensile Sample 4 (made without base plate).

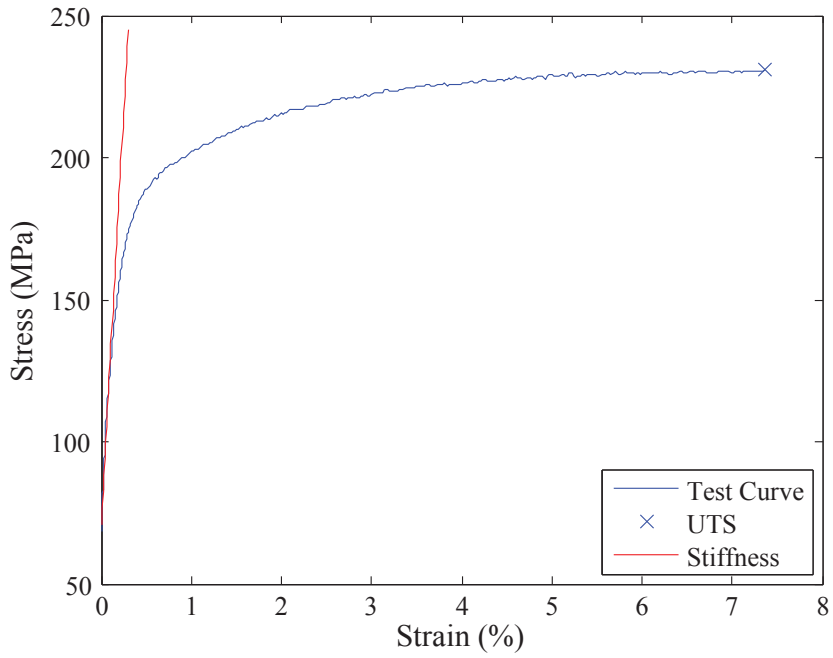

Figure 2.17: Stress-strain plot for longitudinal tensile Sample 4 (made without base plate).

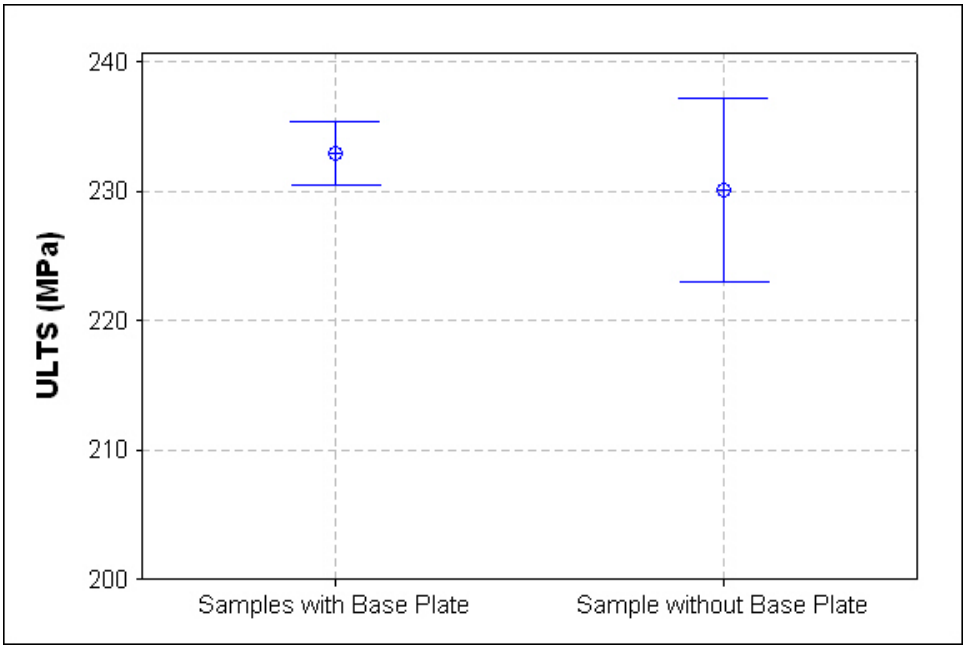

Figure 2.18: Interval plot showing ultimate longitudinal tensile strength (ULTS) for longitudinal tensile experiments–bars are one standard error from mean (crosshair).

2.3 Statistical Analysis of Mechanical Strength Tests

The USS and UTTS data were analyzed statistically by fitting ANOVA models. The adjusted Type I error probability, α, selected for this experiment was 0.05 for testing each of the model parameters, giving an overall error rate of at most 0.20 per mechanical test. The reason for allowing the overall alpha level to be 20% is that these experiments were explorative and designed to describe the overall relationships between USS or UTTS and the four factors. This means that for any given individual parameter there is a 5% probability of finding that a parameter has a significant effect on the strength when that is not the case. The α level is used as a threshold to determine significance of each variable in the model. The p-values represent the probability of obtaining a test at least as extreme as the one observed, assuming that the null hypothesis (of no trend, or no effect) is true. The lower the p-value, the less likely the result, assuming the null hypothesis. Thus, the null hypothesis is rejected in favor of the alternative hypothesis (there is a trend, or an effect) when the p-value is less than the selected α level.

The experimental runs that could not be tested were removed from the DOE. Padding the response matrices with zeros or other forms of data manipulation is not possible in this case as not enough is known about the USS and UTTS for these composites. Therefore, estimates for the outputs of the initial four-way ANOVA model for both the shear and transverse tensile tests could not be computed because of the reduced number of experimental runs and/or replicates (the ANOVA sum of squares for the parameters do not have a unique, linear, unbiased estimate, and therefore, have an infinite number of values [4]).

Based upon these results, the model was reduced so that only two parameters at a time were included in the generalized linear model. The GLM results of this reduced model are shown in Table 2.5 for the USS data and Table 2.6 for the UTTS data.

Table 2.5: ANOVA table for 2-factor GLMs for USS data.

Source of Variation	**Degrees of freedom**	**Type III Sum of Squares**	**Mean Square**	**F-Ratio**	**p-value**	**R^2-Value**
Normal Force	2	1769.56	884.78	9.9	0.0010	0.6144
Amplitude	2	1121.78	560.89	6.27	0.0077	
Weld Speed	3	2014.49	671.49	8.85	0.0007	0.6892
No. of Bilayers	3	2305.16	768.38	10.13	0.0003	
Amplitude	3	442.74	147.58	0.93	0.4452	0.3502
No. of Bilayers	3	544.42	181.47	1.14	0.3567	
Normal Force	3	1178.23	392.74	2.91	0.0615	0.4461
Weld Speed	3	341.46	113.82	0.84	0.4877	

Table 2.6: ANOVA table for 2-factor GLMs for UTTS data.

Source of Variation	**Degrees of freedom**	**Type III Sum of Squares**	**Mean Square**	**F-Ratio**	**p-value**	**R^2-Value**
Normal Force	2	1290.36	645.18	5.20	0.0283	0.5311
Amplitude	2	107.71	53.85	0.43	0.6593	
Weld Speed	3	1453.39	484.4647	6.33	0.0135	0.7394
No. of Bilayers	2	404.89	202.44	2.64	0.1249	
Amplitude	2	118.95	59.47	0.29	0.7515	0.2348
No. of Bilayers	2	506.75	253.37	1.25	0.3271	
Normal Force	2	404.89	202.44	2.64	0.1249	0.7394
Weld Speed	3	658.54	219.51	2.87	0.0962	

The results of the two-factor GLMs for the USS data show that the two best models (highest R^2 values) were the ones including normal force and amplitude ($R^2 = 0.6144$), and weld speed and number of bilayers ($R^2 = 0.6892$). Therefore, between 61% to 69% of the total variability in USS can be explained by these two linear combinations of factors, respectively. By examining the p-values it can be seen that each of the parameters is significant (p-values $< \alpha$ level of 0.05) in their respective models. Table 2.6 shows that the two best models are the ones including weld speed and number of bilayers ($R^2 = 0.7394$), and normal force and weld speed ($R^2 = 0.7394$). Therefore, 74% of the variability in UTTS is explained by either linear combination of two factors (weld speed and normal force or weld speed and number of bilayers). For these two models, weld speed is significant (p-value $< \alpha$ level of 0.05) when combined with number of bilayers, but not in the model with normal force. Despite this, this result is most likely an artifact of the limited UTTS data and is not consistent with the results from the USS data. It is noted that the GLM results correspond well with the surface plots of Figures 2.11 and 2.14.

In addition to understanding the significance of the parameters it is necessary to examine trends in the data. In order to visualize the way that the levels for each parameter affect the USS and UTTS, plots of relative averages are shown in Figures 2.19 and 2.20. The data points used in these plots represent the USS or UTTS for each parameter at each level averaged over all other levels and parameters.

The plots show functions that best-fit the data. The equations for the model fit lines are shown in Table 2.7 along with their corresponding R^2 values, which provide a quantitative measure of the ability of the regression lines to accurately represent the data points.

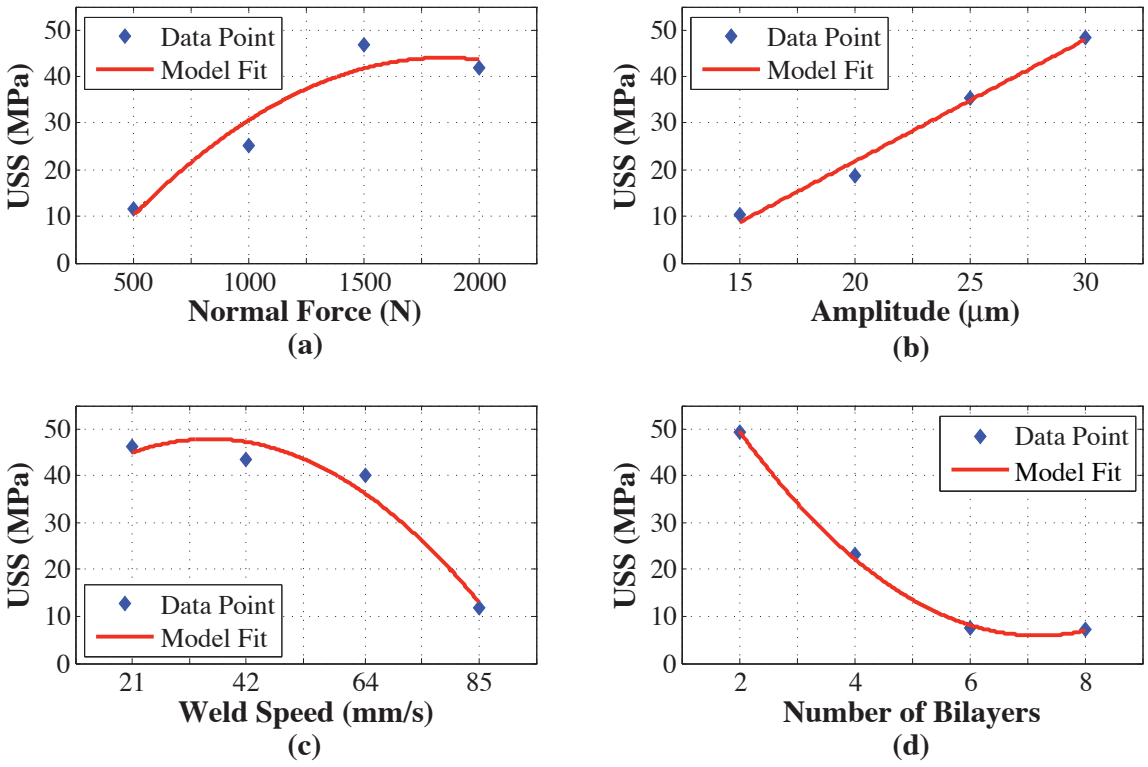

Figure 2.19: Deviation in average USS as a function of selected levels for each parameter: (a) USS vs. normal force, (b) USS vs. amplitude, (c) USS vs. weld speed, and (d) USS vs. number of bilayers.

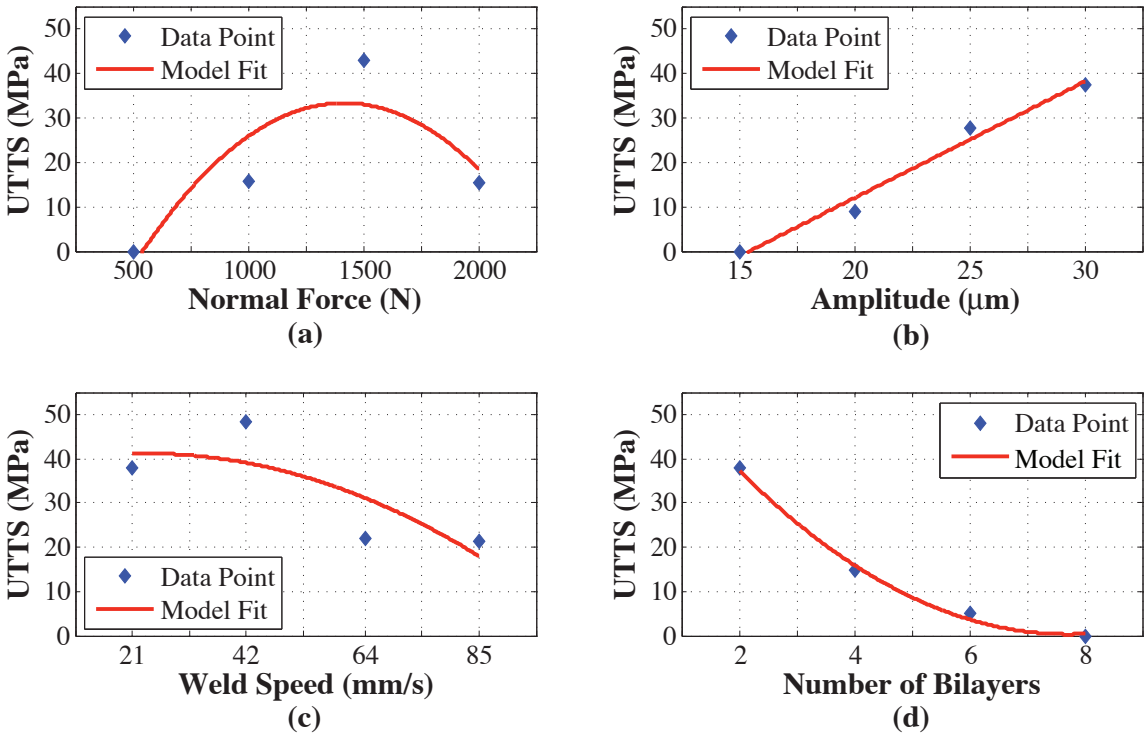

Figure 2.20: Deviation in average UTTS as a function of selected levels for each parameter: (a) UTTS vs. normal force, (b) UTTS vs. amplitude, (c) UTTS vs. weld speed, and (d) UTTS vs. number of bilayers.

Table 2.7: Equations of the linear model fits for trends in USS and UTTS data.

Mechanical Response	**Parameter**	**Model Fit Equation**	**R^2-Value**
USS	Normal Force	$y = -4.613x^2 + 34.316x$ - 19.797	0.9202
	Amplitude	$y = 13.058x$ - 4.367	0.9846
	Weld Speed	$y = -6.404x^2 + 21.327x + 30.062$	0.9616
	No. of Bilayers	$y = 6.453x^2$ - $46.459x + 89.503$	0.9989
UTTS	Normal Force	$y = -10.850x^2 + 61.569x$ - 54.053	0.7685
	Amplitude	$y = -40.413x + 2.618$	0.9808
	Weld Speed	$y = -2.769x^2$ $6.168x + 37.700$	0.6289
	No. of Bilayers	$y = 67.922x^2$ - $17.518x + 1.135$	0.9961

The given functions can be used for interpolation purposes within the data range, but not for extrapolation outside of the range of data because it is not known how the response variables are affected by the process parameters for any levels other than the ones studied in this research. Most of the R^2 values are all higher than 0.96 (and different from 1), which corroborates the goodness–of–fit of the model. The exceptions of normal force for the USS data, and normal force and weld speed for the UTTS data show that the trends shown by the model fits are good estimates, but they are not close enough to the actual data points for them to reflect a high R^2 value. In order to verify that the trends observed in the data are significant and that the linear model fits are reasonable, statistical hypothesis testing strategies for trend contrasts were employed. The analysis is done performing an ANOVA for trend contrasts in order to evaluate the probability that certain types of trends (straight-line, quadratic) are present in the data and that the model fits seen in Figures 2.19 and 2.20 are good estimates of the true data trends. Table 2.8 shows the results of this analysis.

Table 2.8: P-values for trend contrasts in USS and UTTS data as a function of UAM process parameters.

Mechanical Response	**Parameter**	**Straight-Line Trend p-value**	**Quadratic Trend p-value**
USS	Normal Force	<0.0001	0.0010
UTTS		0.0017	0.0002
USS	Amplitude	<0.0001	0.0059
UTTS		<0.0001	0.6786
USS	Weld Speed	<0.0001	<0.0001
UTTS		0.0006	0.1732
USS	No. of Bilayers	<0.0001	<0.0001
UTTS		<0.0001	<0.0001

The trend contrasts given in Table 2.8 show that there is a straight-line relation between the USS and UTTS data and all four parameters using a significance level of $\alpha = 0.01$ (all parameters have small p-values for the straight-line trend). Figures 2.19 and 2.20 illustrate that the straight-line effect results from the data sets have a rising trend in the cases of amplitude and normal force, or a falling trend, in the cases of weld speed and number of bilayers. For the USS, the SAS results demonstrate that amplitude has a slight quadratic trend (p-value: 0.0059), most likely due to the influence of the response at level 2. The number of bilayers and the weld speed for the USS data both have significant quadratic trends, and normal force has a significant quadratic trend present. The implication of these findings is that the model fit lines shown in Figure 2.19 can be used as good estimates of the true trends.

Table 2.8 indicates that for the UTTS there is no significant quadratic trend present in the amplitude plot (p-value: 0.6786), but both normal force and number of bilayers show a significant quadratic trend. The plot of weld speed does not reflect a

quadratic trend, which means that the estimated quadratic line is not a good estimate of the true trend. Overall, it is shown that the linear functions shown in Figure 2.20 can be used as good estimates of the true trends.

It should be noted though that because of the small amount of usable data, it is not known which of the process parameters, conditionally on all four others, actually do have a significant effect on the response variables, being either USS or UTTS. Experiments with a larger number of replicates are needed so that this can be determined even though bivariate models were able to be fitted and significance of terms in those models was determined. Further, it is still useful to detect, analyze and explain trends present in the data because such trends had not been previously developed for Ti/Al composites built by UAM and may turn out to be true indicators of the optimum combination of machine settings.

2.4 Micrographs of Bond Interface

The samples chosen for microstructural investigation correspond to Experiment #7, Sample 3 (Sample 7-3) and Experiment #12, Sample 1 (Sample 12-1). These specimens were selected because Sample 7-3 exhibits a relatively low USS and UTTS (28.675 MPa and 24.887 MPa, respectively) and Sample 12-1 exhibits a relatively high USS and UTTS (61.222 MPa and 32.794 MPa, respectively). We compare the microstructures of these two samples and seek to investigate differences between them that may explain the difference in mechanical strengths. Figures 2.21 and 2.22 are typical images of the tape layers at 100x magnification for Sample 7-3 and 12-1, respectively.

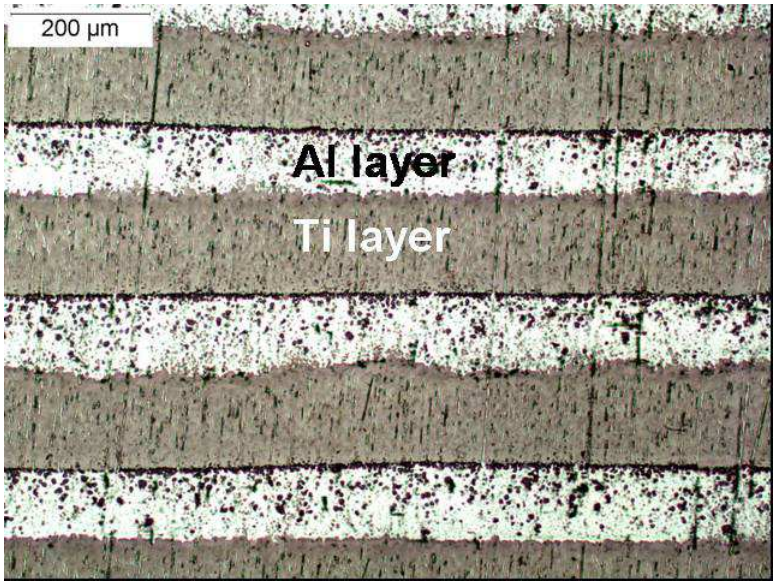

Figure 2.21: UAM built Ti/Al Sample 7-3 at 100x magnification.

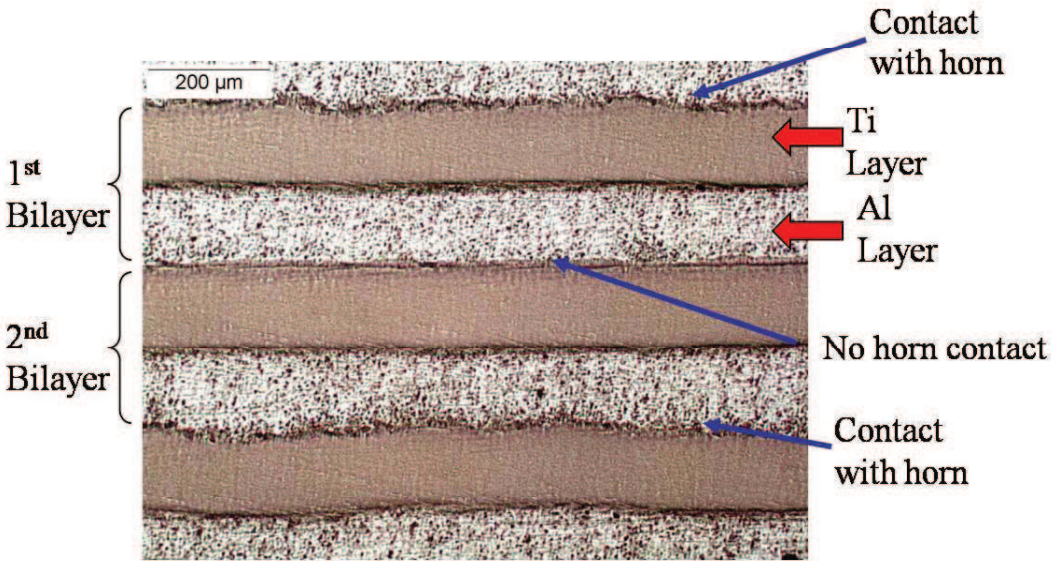

Figure 2.22: UAM built Ti/Al Sample 12-1 at 100x magnification.

Both of the samples were built using two bilayers with the titanium layer in contact with the sonotrode. Therefore, every four layers (aluminum on the bottom and titanium on the top) the sonotrode is in contact with the top titanium layer. Previous research has shown that there is a significant increase in roughness on the surfaces in contact with the sonotrode during the UAM process. This can be seen from Figure 2.21, but it is noted that while both Samples 7-3 and 12-1 were built using two bilayers, Sample 7-3 had 1000 N normal force, 25 μm amplitude, and 85 mm/s weld speed whereas Sample 12-1 had 1500 N normal force, 30 μm amplitude, and 42 mm/s weld speed. Consequently, the layers that were welded on Sample 7-3 are not expected to be as rough as layers welded in Sample 12-1, shown in Figure 2.22.

Figures 2.23 and 2.24 show closer views of Samples 7-3 and Sample 12-1, respectively. Similar observations can be made for both samples. The area labeled Region I shows foreign particles distributed throughout the aluminum tape layer. Evaluation of these particles and the immediate surrounding areas using a scanning electron microscope (SEM), energy dispersive X-ray spectroscopy, and backscatter electron SEM shows that these particles are composed of silicon originating from the SiC grit discs used for polishing the samples. The X-ray results for one of the particles tested is shown in Figure 2.25. The harder titanium breaks off pieces of the silicon disc during polishing, and the ensuing particles become lodged into the much softer aluminum layer. This is difficult to avoid because of the hardness mismatch between the titanium and 1100-O aluminum. The entire interface around Region I (bottom of Ti layer and top of Al layer) was checked using EDS and it was found that the post-process heat treatment did not induce any significant intermetallic compounds in this area.

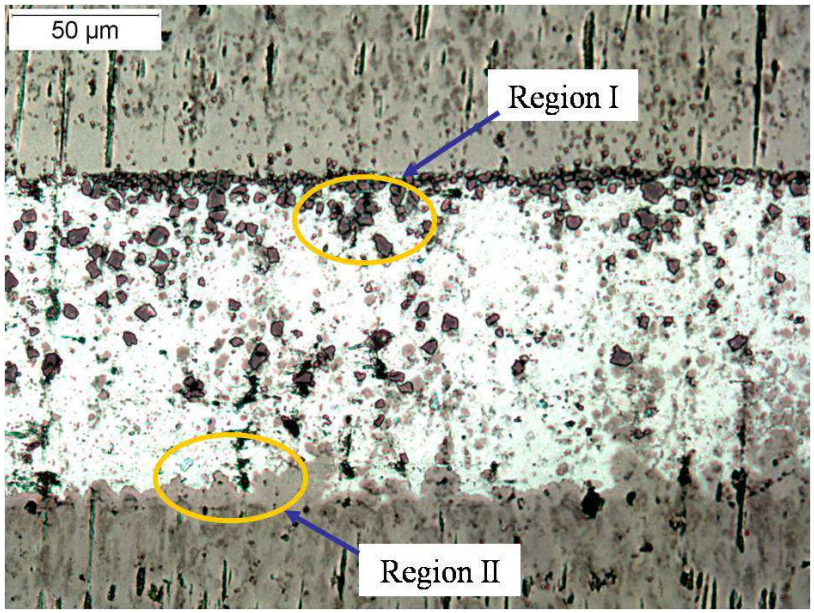

Figure 2.23: UAM built Ti/Al Sample 7-3 at 400x magnification.

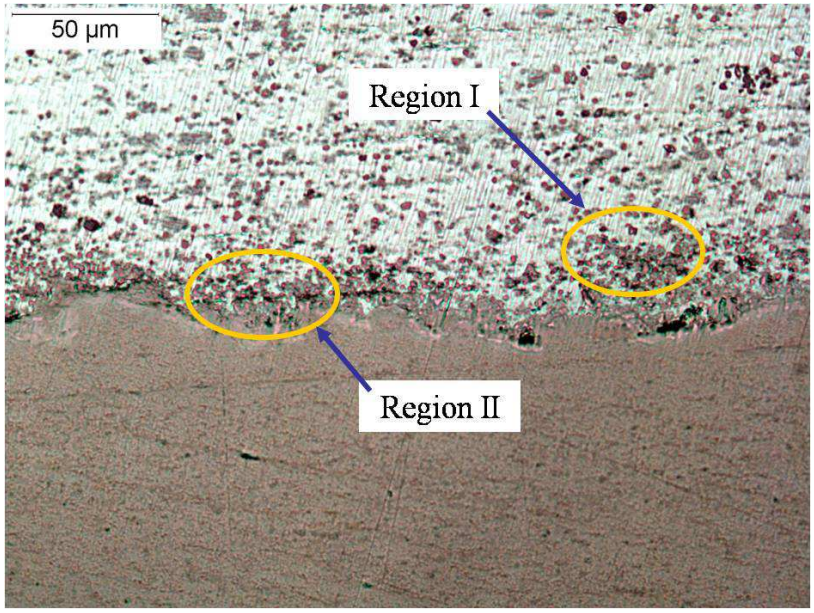

Figure 2.24: UAM built Ti/Al Sample 12-1 at 400x magnification.

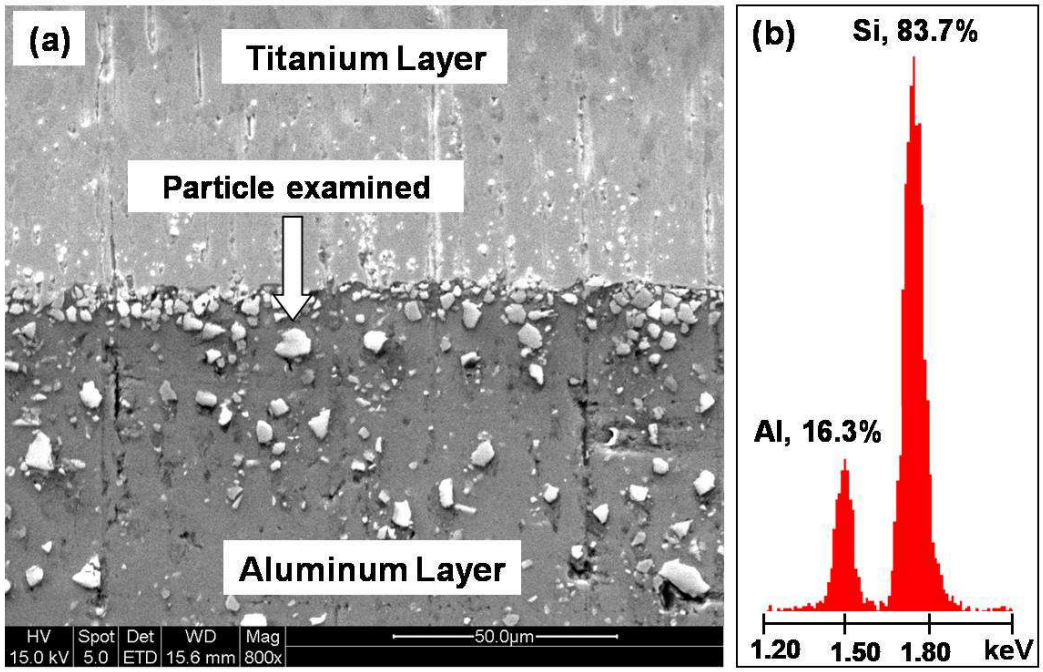

Figure 2.25: (a) SEM image showing location of a foreign particle examined; (b) the particles are composed of silicon originating from the SiC grit discs used for polishing.

In Region II the aluminum layer appears to have smeared into the crevasses of the titanium build below it. Because of the the discoloration in this region and in order to check for intermetallic compound formation along this interface, SEM was again utilized. Figure 2.26(a) shows a typical interface between the bottom of an aluminum layer and the top of a titanium layer that had ben in contact with the sonotrode. The region encircled is the area that is examined using EDS shown in Figure 2.26(b). The plus symbols represent points that were analyzed individually to determine their composition.

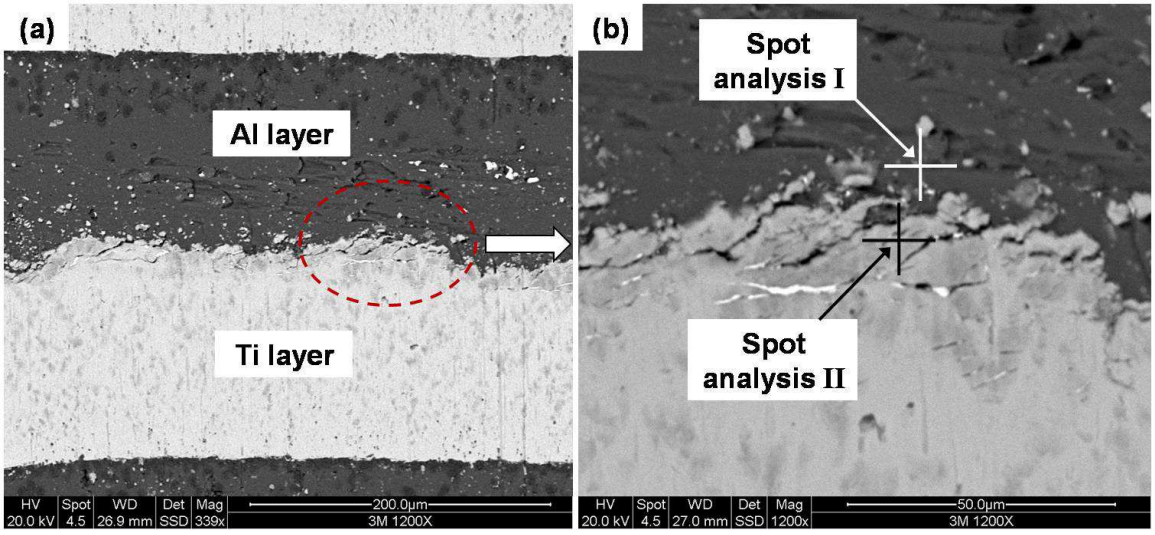

Figure 2.26: (a) SEM image of interface between bottom of Al layer and top of Ti layer in contact with sonotrode; (b) the area examined for EDS analysis and the specific spot points examined (+).

The results of the EDS analysis are shown in Figure 2.27 where (a) is the composition of the overall interface and (b) and (c) correspond to the spot points II and I, respectively. Finally, the lack of typical voids at the interface is quite noticeable and is explained in Section 2.5.5 by examining the ultrasonic welding process in general.

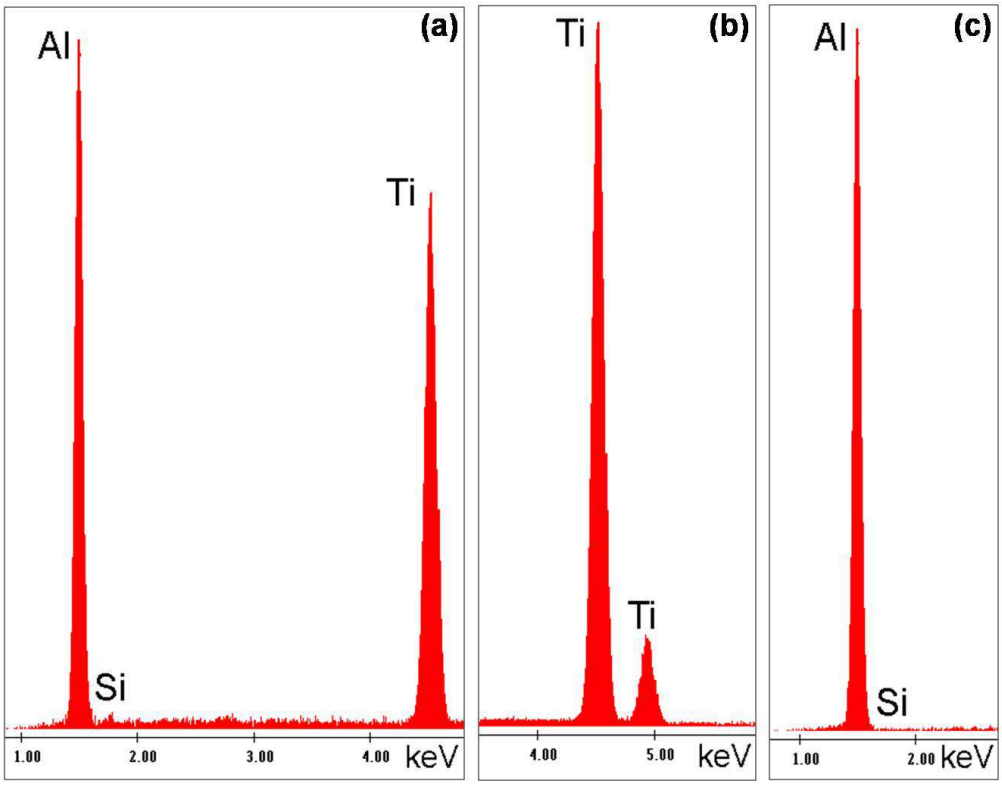

Figure 2.27: (a) EDS spectrum plots for (a) overall interface in Figure 2.26(b), (b) spot analysis II, and (c) spot analysis I.

2.5 Discussion

2.5.1 Mechanical Strength of Transverse Shear Specimens

Most of the samples display a predominantly linear force/displacement relationship. This indicates that samples failed in a macro-brittle fracture mode. Of course, at the microscopic level there would be regions of ductile failure and plastic deformation at the interface. Additionally, there is considerable deviation in USS with standard deviations ranging from 5.10 to 20.76 MPa between experiments. For Experiment #16 the average USS is 32.656 MPa with a standard deviation of 20.76 MPa,

which is 63% of the average value. This result highlights the inconsistency of the USS for Ti/Al shear samples made by UAM.

Experiment #12 produced the highest strengths with an average of 63.628 MPa and a standard deviation of 6.27 MPa. Therefore, the USS for a sample made under the parameters of Experiment #12 is about the same as the USS of solid 1100-O aluminum (62 MPa). Therefore, it can be implied that, under optimal welding parameters, the aluminum layer can fail before or at about the same time as the bonds, which causes a spike in the stress of the titanium layers leading to complete failure of the build. While this experiment produced strengths close to the failure strength of one of the parent materials, most of the other experiments had strengths up to 50% less than solid 1100-O aluminum.

2.5.2 Mechanical Strength of Transverse Tensile Specimens

All samples exhibit a predominantly linear force/displacement relationship, which indicates that samples failed in a macro-brittle fracture mode. Again, at the microscopic level there would be regions of ductile failure and plastic deformation at the interface. The samples all failed at a single weld interface and produced two separate pieces. There is substantial deviation in UTTS with standard deviations ranging from 3.37 to 11.22 MPa between experiments. For Experiment #8 the average UTTS is 12.546 MPa with a standard deviation of 6.62 MPa, which is 53% of the average value. Similar to the shear tests, Experiment #12 produced the highest strengths with an average of 48.254 MPa and a standard deviation of 11.22 MPa. This is only about 40% of the ultimate tensile strength of solid 1100-O aluminum. These results show

that UTTS is more consistent than USS, although UAM samples are much weaker in the transverse tensile direction than in shear.

2.5.3 Mechanical Strength of Longitudinal Tensile Specimens

All longitudinal tensile samples exhibited fairly consistent ultimate longitudinal tensile strengths as shown by the error bars in Figure 2.18. Also, all samples had an increase in tensile strength compared to that of solid 1100-O aluminum, but a decrease compared to that of cp Ti Grade 1. Table B.4 shows all relevant mechanical properties of solid 1100-O aluminum and cp Ti Grade 1, annealed. The ultimate tensile strength (UTS) of 1100-O aluminum is about 90 MPa and the UTS for cp Ti Grade 1 is 330 MPa [1, 2]. Therefore, the samples experienced a 59% increase in UTS over the UTS for solid Al 1100-O and about a 30% decrease in UTS below the UTS for solid cp Ti Grade 1.

A 50%-50% mix of the two parent materials' UTSs yields an ultimate tensile strength of 210 MPa for the overall composite. From this, it would appear that the ULTS for UAM built samples made under the process parameters given possess a 9.5% increase in ULTS over a composite made of equal amounts of titanium and aluminum. This may seem to be a sufficient benchmark for comparing the strength of the samples, but the mechanisms for stress distribution throughout the composite are more complex than this simplified approach presumes. It is also found that there appears to be an effect of increased tensile strength due to grain refinement or strain hardening based upon the Hall-Petch relation [3], although it is less than the 27% increase found in longitudinal tensile tests performed on UAM built 3003 aluminum samples [7].

Table 2.9: Mechanical properties of solid specimens of parent materials in Ti/Al UAM builds [1, 2].

Material	Yield Strength (MPa)	Ultimate Tensile Strength (MPa)	Modulus of Elasticity (GPa)	Percent Elongation at Failure
Al 1100-O	34.5	89.6	69	35
Cp Ti Grade 1, Annealed	240	330	100	30

The force versus displacement plots presented in Figures 2.15 and 2.16 display typical tensile test curves for metals and show the linear elastic region, the yield strength, plastic deformation, necking and finally failure points. The stress-strain curve shown by Figure 2.17 is slightly adjusted because the extensometer was not able to deflect the full amount needed to obtain data throughout the entire test. Therefore, it is cut off at the UTS, which is acceptable for the purpose of determining the UTS and the modulus of elasticity for the samples. In order to determine the modulus, the slope of the linear region of the stress-strain curve is calculated by choosing two representative points arbitrarily in that region and using regression to calculate the equation of the line that passes through the chosen points. Unfortunately, this can lead to some inconsistency when determining the points that lay in the most linear region and the points that do not. This may account for some of the variation in the moduli, but not a significant amount. The modulus of elasticity for solid Al 1100-O is about 69 GPa, and about 100 GPa for cp Ti, while it was found for these samples that the elastic modulus was on average 38 GPa. Therefore, it is conjectured that there are unbonded regions that decrease the stiffness. It seems as though the interfaces

may not be as stiff as the solid regions because of possible unbonded areas, thereby decreasing the overall stiffness of the specimen.

The results from this testing also demonstrate that there is not significant difference between longitudinal tensile strengths of samples made with the aluminum base plate and samples made without it. The average ULTS for samples made with the base plate was 233 MPa, while samples made without the base plate had an average ULTS of 230 MPa. This results in only a 1.3% difference between the tensile strengths. Based on these tests, it appears that the samples made without the base plate have a slightly less consistent ULTS (Figure 2.18), yet the standard error for these samples is still only ± 3.04% of the mean.

2.5.4 Effects of Manufacturing Parameters

It was shown through the bivariate models for USS and UTTS that there are several two-factor combinations that are significant. Mainly, the normal force - amplitude combination and the weld speed - number of bilayers combination for the USS data were found to have significant factors, and the weld speed - number of bilayers combination and the weld speed - normal force combination for the UTTS data were found to have significant factors. Therefore, more than 60% of the variability in the USS and UTTS data could be explained by these two-factor linear combinations. The significance of the factors when combined into a four-factor model is not known because of insufficient data. The effects of each process parameter on the shear strength and transverse tensile strength are discussed below in detail.

2.5.4.1 Effect of Normal Force

It can be seen from Figure 2.19(a) that the normal force has a relatively linear effect on the USS up to 1500 N, but further increases resulted in a drop in the observed USS. Resembling the shear tests, Figure 2.20(a) shows that the normal force has a relatively linear effect on the UTTS up to 1500 N, but further increases result in a drop in the UTTS. This is consistent with results found by Kong et al. [20], Yang et al. [31], and Ram et al. [13] for UAM builds. While the material tested in those studies was 3003 aluminum, it can be assumed that the same mechanism causing this trend in normal force is consistent in UAM Ti/Al composites as well. It is not known exactly why this occurs, but there are several plausible explanations. First, it is possible that too high of a normal force can result in excessive interfacial stresses causing breakage of previously formed bonds. Secondly, the increase in normal force leads to an increase in the sonotrode oscillatory force needed to maintain the set frequency. More specifically, the high normal force prevents the sonotrode from oscillating at the desired amplitude, thereby reducing the overall performance of the process [31]. This experiment does indicate that poor bonds are created at normal forces less than 1000 N simply shown from the lack of successful builds for treatment combinations containing a normal force level of 500 N. The optimal normal force for these builds is expected to be around 1500 N.

2.5.4.2 Effect of Oscillation Amplitude

Unlike normal force, the amplitude seems to linearly affect the USS and the UTTS across the chosen levels as shown in Figure 2.19(b) and Figure 2.20(b). As the oscillation amplitude increases, the relative USS and UTTS increase as well. By increasing

the amplitude, the total energy applied to the system is increased, thereby causing greater alternating shear forces at the weld interface. This leads to better removal of any oxide films or other contaminants on the surface of the layers. The break-up of these surface impurities permits better metal-to-metal contact of the faying surfaces, which allows for elastic-plastic deformation and atomic diffusion to take place at the interface [20].

2.5.4.3 Effect of Weld Speed

As shown in Figure 2.19(c), the USS declined relatively linearly when the welding speed increased from 21 mm/s to 64 mm/s, but then dropped dramatically when increased further. Based upon the results of this experiment it seems that a slower weld speed produces a higher USS in Ti/Al specimens. Figure 2.20(c) shows that the UTTS jumped up from 40 to almost 50 MPa between 21 mm/s and 42 mm/s, then dropped drastically back down at speeds of 64 mm/s and 85 mm/s. This trend is slightly different from the one found for the shear tests. The spike in the UTTS at 42 mm/s occurs because the values used for calculating that point were all from the same treatment combination (Experiment #12), which produced very high tensile strengths because of the other parameter settings. Overall, for the weld speeds used in this experiment, it seems that a slower weld speed produces a higher UTTS in UAM Ti/Al specimens. Welding speed determines the amount of energy input per unit length. The slower the sonotrode moves across the build plate the more time is allowed for contact between the oscillating sonotrode and the material, thereby increasing the total energy put into the build. Conversely, by increasing the welding speed the sonotrode resident time reduces, leading to inadequate oxide layer removal and less plastic deformation at the interface [20, 31].

2.5.4.4 Effect of Number of Bilayers

The number of bilayers that are stacked between welds seems to have a very significant effect on the build. The data in Figure 2.19(d) and Figure 2.20(d) shows that there is a negative linear trend of the USS and UTTS as the number of bilayers is increased. This is intuitive because for increasing number of bilayers the same energy imparted by the sonotrode needs to be dispersed through a larger volume of material. Also, as the height of the build increases the part becomes more compliant, thus resulting in greater deflection of the part. In turn, there is an increase in the relative motion between the part and the horn, which means that energy is being used to deflect the part, so there is less available for the scrubbing action of the sonotrode on the material.

This idea can be used to describe the negative effect of an increased number of bilayers. As bilayers are added, the height is increased, thereby decreasing the stiffness of the build under the sonotrode. The described phenomenon is more prominent in the case of bilayers because there is no welding in between so the layers are free to slide relative to each other. Even though increasing the number of bilayers may decrease production time, it is at the cost of losing a large amount of bonding between lamina. It may be possible in the future to increase the operating range of the machine and find that the number of bilayers can be increased because the total amount of available energy is higher, but this is not optimal under the present machine capabilities. This experiment shows that the fewer the bilayers the better the chance of building a solid part because of superior bonding between layers.

2.5.5 Examination of Bond Interface Microstructure

The results of the EDS analyses of the top and bottom Ti/Al interfaces (Figures 2.25 and 2.27) indicate that there are no significant intermetallic compounds present due to the heat treatment. The two spot regions examined are all titanium (spot analysis II) or all aluminum (spot analysis I) with some silicon from the polishing. Several interfaces were checked as such and all showed similar compositions. In region II of the optical micrograph shown in Figure 2.24 it appears that in some places the bottom layer is encroaching into the aluminum tape layer above it by as much as 50 μm. This was not evident in the SEM images nor in other micrographs of the interface. The SEM images show that the titanium layers in contact with the sonotrode appear to have no more of an average roughness than about 20 μm. The sonotrode texture has an average roughness of 14 μ. This observation combined with the EDS analysis leads to the conclusion that there is no substantial (if any) amount of intermetallic compounds formed at the Ti/Al interface.

It has been shown that in ultrasonic welding of two dissimilar metals there is extensive mechanical interlocking and deformation [16]. The softer of the two materials flows around the surface topography of the harder material [16]. Because aluminum is much softer than titanium, the asperities on the titanium surface do not undergo sufficient deformation to allow for nascent surface creation. The aluminum tape simply conforms to the shape of the titanium faying surface, which prevents solid state metallurgical bonding from occurring. As a result, the strength of the build is based mainly on mechanical interlocking of the materials. The span of strengths exhibited

by the samples in this DOE is then due to the amount and severity of roughness imposed by the sonotrode on the titanium layer, which creates the surface profile that the aluminum deforms into.

As stated, surfaces in contact with the textured sonotrode are generally rougher than surfaces not in contact. Because in our study the layer in contact with the sonotrode is always made of titanium, the titanium layers have a rougher topography than layers that do not come in contact with the sonotrode. Hence, when the aluminum tape is placed on top there are more significant peaks and valleys for the aluminum to flow into causing greater mechanical interlocking at these layers. This explains the fact that builds with more bilayers exhibit much lower strengths compared to builds with fewer bilayers. In the builds with four, six, and eight bilayers there are fewer total layers that are in contact with the sonotrode. In turn, there are fewer layers where a large amount of mechanical interlocking could occur, which is key to these specimen's mechanical strength. The fracture locations for transverse tensile samples were measured and are displayed in Table B.3. By examining the layer number where the sample broke and correlating it to the number of bilayers for a given sample, it is found that out of 18 samples only three fractured at a layer that had been in contact with the sonotrode. All other samples fractured at layers in between the sonotrode contact layers. This reinforces the hypothesis that the layers that were rolled over by the sonotrode would exhibit higher strength than non-contact layers.

It is difficult to fully assess effects of the process parameters on the bond formation because of the post-process heat treatment that all samples underwent. Therefore, without conducting testing on Ti/Al samples that have not been heat treated, it is

hard to know how much of an effect the UAM process had on the strength of the samples versus the effect of the heat treatment. It is recommended that another DOE with similar parameters and levels be performed on Ti/Al samples without the additional heat treatment step.

CHAPTER 3

3003 ALUMINUM DOE

3.1 Experimental Methods

3.1.1 Sample Fabrication and Statistical Procedures

For this DOE, 0.006" (152.4 μm) thick tapes of 3003 H-18 aluminum were used as the composite material. All samples were built by Edison Welding Institute (EWI) using their Solidica, Inc. Beta machine. Six 0.75" tall by 1.00" wide and 8.00" long (19 mm by 25.4 mm by 203.2 mm) strips were created per build plate (Figure 3.1). From each strip two transverse shear samples and two transverse tensile samples were machined according to the geometries needed for testing. Since it was predetermined that four samples of each geometry were needed per treatment combination, every two adjacent strips were built under the same process parameters as each other. This resulted in a total of 36 strips divided amongst six build plates in order to create the required number of samples and treatment combinations. The final listing of the build order, treatment combination and mechanical test results can be seen in Appendix B.

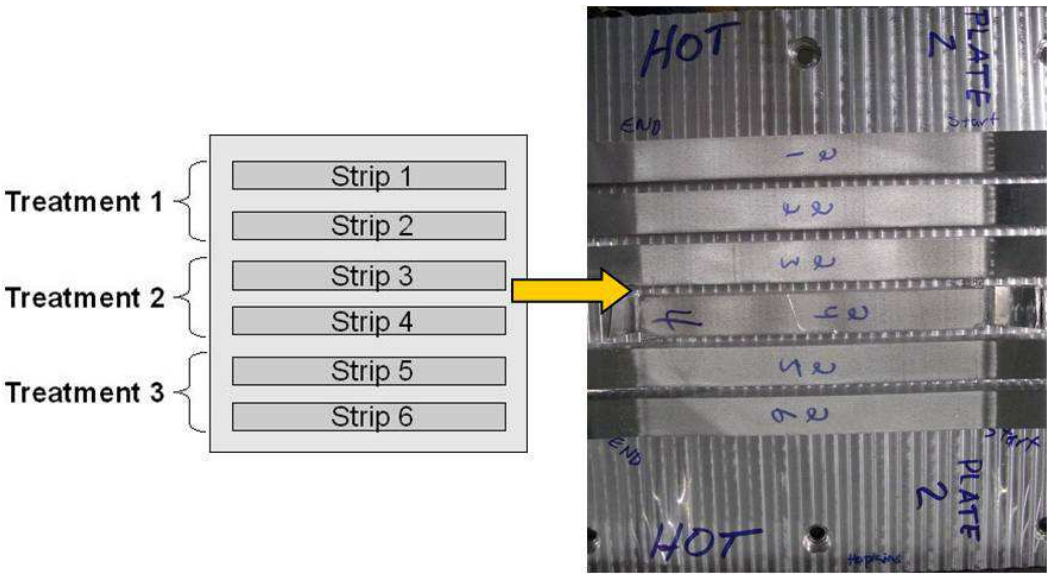

Figure 3.1: Schematic of build plate configuration (left) and photograph of resulting build plate (right).

A Taguchi L18 orthogonal array was employed for the experimental design. The Taguchi array is a statistically robust design that reduces the number of treatment combinations from 54 to 18 for a design consisting of three parameters at three levels each and one parameter at two levels [23]. The process parameters and their corresponding levels are shown in Table 3.1. The levels for each of the manufacturing parameters were selected because they represent an even distribution across the range of operation limits (not machine capabilities) for each setting based upon pilot experiments. The tack force refers to the normal force that is applied during the tack pass, and likewise, the weld force is the normal force applied during the weld pass. Both parameters oscillation amplitude and weld rate refer to those settings used in

the weld pass. Table 3.2 summarizes all other sources of variation that were held constant during the experiment.

Table 3.1: Process parameters and levels used for Al 3003 DOE.

Parameter	**Level 1**	**Level 2**	**Level 3**
Tack Force (N)	200	350	–
Weld Force (N)	600	800	1000
Oscillation Amplitude (μm)	18	22	26
Weld Rate[a] (in/min)	100	125	150
	(42 mm/sec)	(53 mm/sec)	(64 mm/sec)

[a]Default machine input unit is in/min. Values in mm/sec are rounded off to nearest integer.

Table 3.2: Other sources of variation identified in Al 3003 DOE.

Process Variable	**Set Value**
Tack Rate (in/min)	120
Tack Amplitude (μm)	9
Spot Time (sec)	0
Base Plate Temperature (°F)	300
Horn Texture (μm)	7

The unsuccessful treatment combinations from the pilot experiments are shown in Table 3.3. For pilot experiments 1, 2, 3, and 4b the builds could not be created because of nugget formation on the sonotrode. In UAM, a nugget is a piece or chunk of the tape material that breaks off from the rest of the tape layer and becomes welded to the sonotrode. This disrupts the build process because, if left on, it will cause undesirable features on subsequent layers, as well as attract more nuggets to the sonotrode. The sonotrode needs to be chemically etched in hydrochloric acid for

several hours in order to remove the nugget. Pilot experiment 4a could not be created because the parameter combination would not allow the first tape layer to weld to the base plate. The parameter levels in Table 3.1 are from the last iteration of pilot experiments (after pilot experiment 4) and combinations of those levels were able to successfully begin the build process. The unsuccessful parameter combinations provide some important information about the UAM process (at least in regards to 3003 aluminum and the UAM Beta machine). It is evident from Table 3.3 that there is an upper and lower threshold to combinations of weld force and oscillation amplitude. If the amplitude and weld force are too high then the tape layer welds to the sonotrode and nuggets are formed. In contrast, if the weld force and oscillation amplitude are too low, no bonding occurs.

Table 3.3: Treatment combinations from pilot experiments that were unsuccessful in creating builds.

Pilot Experiment	**Tack Force (N)**	**Weld Force (N)**	**Amplitude (μm)**	**Weld Rate (mm/s)**
1	350	1500	32	53
2	350	1500	30	53
3	350	1500	26	53
4a	350	500	22	42
4b	350	1100	26	53

Table 3.4 shows the Taguchi orthogonal array with the coded parameter levels. The treatment combinations were randomized and were built and tested in that randomized order to avoid any bias due to build order. The Experiment Number corresponds to this randomized order that the samples were built and tested in. The original statistical model used for this DOE was a generalized linear model (GLM) with four main effects, and the standard analysis of the data using this model, a four-way analysis of variance (ANOVA), was implemented. The linear model equation is

$$Y_{ijklt} = \mu + \alpha_i + \beta_j + \gamma_k + \delta_l + \epsilon_{ijklt}, \tag{3.1}$$

where it is assumed that ϵ_{ijklt} is of a normal distribution about zero, and all ϵ_{ijklt} are mutually independent with $i = 1, 2; \quad j = k = l = 1, 2, 3; \quad t = 1, 2, 3, 4.$

The model equation summarizes the dependence of the response variable (USS or UTTS), Y_{ijklt}, upon the levels of the treatment factors [4]. In equation (3.1), μ denotes the overall mean of the response variable. The effects of each of the process parameters on the mean response are represented by α_i, β_j, γ_k, and δ_l, where α_i is the effect of tack force at the ith level on the response while the other three factors are fixed. Similarly, β_j, γ_k, and δ_l represent the effects of weld force, amplitude, and weld rate at the jth, kth, and lth levels, respectively, while the other factors are fixed. The error variable, ϵ_{ijklt} is a random variable with zero mean which denotes any nuisance variation in the response. In this model it is assumed that the error variables are independent and that they have a normal distribution with zero mean and constant variance. These assumptions were checked and verified to be proper assumptions for the data. This is the most appropriate model to be used initially because there are

no known interactions between the process parameters and it was not known if there would be enough statistical degrees of freedom to add more terms to the model.

After sample production and testing it was found that the p-value for the overall model could be reduced by adding a two-factor interaction to the model. Thus, an interaction factor between tack force and weld force, $(\alpha\beta)_{ij}$, was added to the model equation with response variable USS. Likewise, an interaction factor between tack force and amplitude, $(\alpha\gamma)_{ik}$, was added to the model equation with response variable UTTS. These model equations were found to produce the most useful information about the process parameters and their effects on the response variables.

Table 3.4: Coded Taguchi L18 orthogonal array.

Experiment Number	**Treatment Combination**	**Tack Force**	**Weld Force**	**Amplitude**	**Weld Rate**
3	1	1	1	1	1
11	2	1	1	2	2
8	3	1	1	3	3
14	4	1	2	1	1
15	5	1	2	2	2
10	6	1	2	3	3
13	7	1	3	1	2
9	8	1	3	2	3
6	9	1	3	3	1
17	10	2	1	1	3
1	11	2	1	2	1
16	12	2	1	3	2
12	13	2	2	1	2
5	14	2	2	2	3
7	15	2	2	3	1
18	16	2	3	1	3
4	17	2	3	2	1
2	18	2	3	3	2

Four shear and four transverse tensile samples were created and tested per treatment combination. All mechanical tests were run on a 20 kip (89 kN) Interlaken load frame fitted with a ± 5000 lb (22.2 kN) load cell in series with the load train. The load frame was connected to an MTS 458.20 Micro Console controller that was coupled to a data acquisition system comprising a Data Physics Mobilyzer and PC. All tests were run under displacement control with a ramp (average rate of 0.01 in/sec) and hold input program. During testing, displacement was measured using the linear variable differential transformer (LVDT) integrated into the load frame. Because the LVDT measures the load frame's hydraulic ram displacement, all displacement data includes displacement generated with the load train as well as the specimen. Due to this, the shape of the force-displacement plots can only be used to determine if a given sample failed in brittle or ductile mode through qualitative analysis [28]. Further, this data cannot be used to calculate specimen strain or related properties such as elastic modulus. Finally, the statistical analyses were performed using SAS 9.1 statistical software.

3.1.2 Transverse Shear Testing

UAM shear specimens were built based upon ASTM Standard Test Method for Lap Shear Strength of Sealants (ASTM C 961-06) [10]. The specimens were designed such that a tape layer was along the shear plane as shown by Figure 2.1 in Chapter 2. The samples were machined out of the build strips down to nominal dimensions (Figure 2.1). Final design dimensions are the same as those in Appendix A. The samples were tested by placing them in a shear jig where one leg is supported and the other leg is loaded from the top again shown in Figure 2.2. Figure 2.3 shows

a sample in the shear jig just prior to being tested in the load frame. Loading was applied until sample failure while measuring force and hydraulic ram displacement.

3.1.3 Transverse Tensile Testing

UAM transverse tensile specimens were built such that the tape layers were perpendicular to the applied axial loading (Figure 2.4). The samples were machined out of the build strips down to the nominal dimensions. Final design dimensions are the same as those found in Appendix A. Control tests had previously found that this configuration does not bias the ultimate tensile strength and is repeatable (Table 2.3). In turn, the geometry shown was used for the transverse tensile testing of the 3003 aluminum samples in this research. Tensile strength of the bonding between the layers was tested by placing the samples into specially designed grips. Figure 2.5 shows the configuration of the grips and the samples. The samples were placed under a tensile stress by being axially loaded until failure while the force and hydraulic ram displacement were measured.

3.1.4 Micrograph Preparation

After mechanical testing, certain samples were selected in order to examine the bond interface at a microscopic level and to determine if there is a correlation between macroscopic mechanical strength and micro-structure. Samples were cross-sectioned (perpendicular to weld direction) and hot mounted in a clear polymer matrix. Samples were polished using 120C, 400C, 600C, 800C grit paper, and 3μm diamond cloth, successively, followed by 45 minutes of vibratory polishing. Observations were conducted on as-polished samples using an inverted (metallurgical) optical microscope under various magnifications.

3.1.5 UAM Bond Characterization

Optical micrographs of UAM cross sections were analyzed using the image analysis software ImageJ [24] to assist in calculating the linear weld density (LWD). Various other studies have examined the LWD of UAM built samples to try and quantitatively characterize the amount of bonding present at the interfaces [14, 21, 20]. LWD is defined as

$$\%LWD = \frac{\text{Bonded interface length}}{\text{Total interface length}} \times 100. \tag{3.2}$$

Microstructural observations were conducted using an optical light microscope at 25x and 100x magnifications, the latter being used for LWD calculations. A five by five grid of micrographs were taken across the entire sample cross sectional face resulting in 25 pictures per sample. Linear weld density was measured per photograph, each photograph showing about five interfaces (six tape layers). Therefore, a total of 125 to 130 LWD measurements were taken and averaged to find the LWD per sample.

For finding the bonded interface length, areas that are deemed to be voids or unbonded regions are marked by creating a large black box underneath of them as shown by Figure 3.2. In ImageJ, the length of these boxes is measured and a resulting ratio of the total length minus the boxes' length over the total length per line is calculated. When plotted, these boxes, representing the interfaces, appear as large spikes on the graph and the peak of these spikes is recorded as the LWD at each interface. This procedure is repeated for all pictures of a given sample and the average of the measured LWD values is given as the total LWD for that given sample.

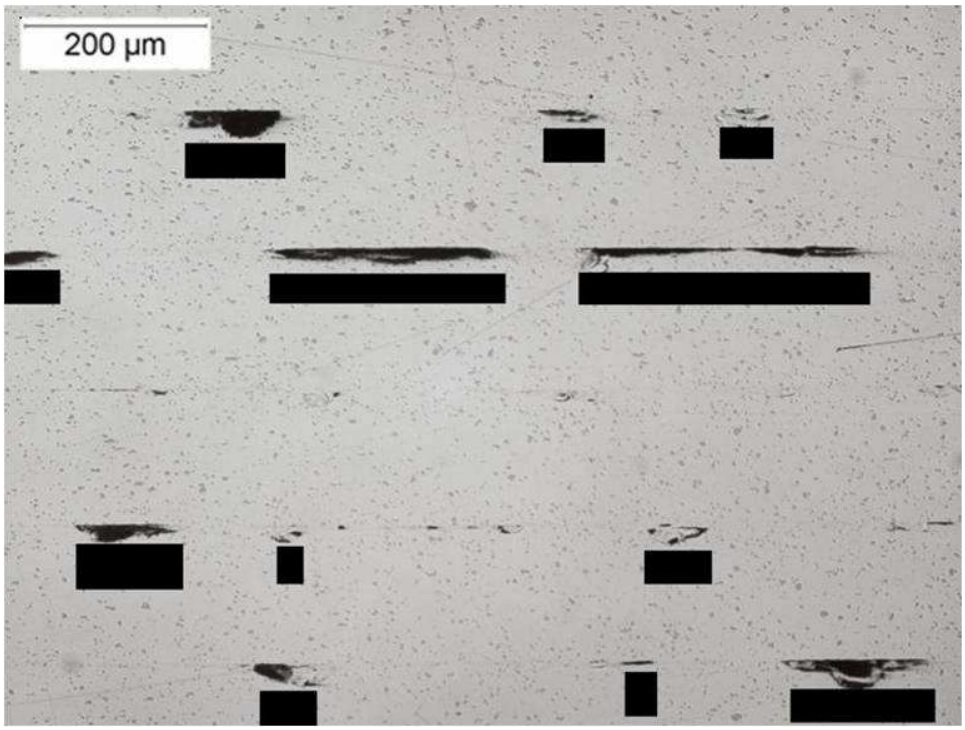

Figure 3.2: Black boxes represent voids and unbonded areas for calculating LWD using image analysis software.

In addition to calculating the LWD, the amount of bonding was characterized by examining optical micrographs of UAM fracture surfaces. Fracture surface micrographs were taken of various shear fracture surfaces and transverse tensile fracture surfaces at 25x and 52x magnifications, respectively. Only the top surfaces of the interfaces were used. This is because the bottom surface has been textured by the horn while the top surface is only textured where there was intimate contact and subsequent bonding to the mating tape. Five images were taken per shear fracture surface and three were taken per transverse tensile fracture surface. A common nominal threshold was applied to all images and results were used to determine the

percentage of bonded area with respect to total sample area. The reported percentage bonded area for a given sample is the percentage bonded area per image averaged across the total number of images for that sample.

3.2 Mechanical Test Results

3.2.1 Transverse Shear Tests

Four treatment combinations did not produce samples that could be tested. All four of the treatment combinations that were not built had an oscillation amplitude of 18 μm and varying levels of tack force, weld force, and weld rate. These samples could not be built due to delamination of the strip during the building process. This is caused by a combination of reaching the critical height to width ratio (0.7-1:1) that has been found to exist for parts built by UAM [27], and a lack of overall power (due to low oscillation amplitude) necessary to create sufficiently clean faying surfaces. Other samples are missing because of breakage during post-process machining. Overall, 14 of the 18 treatment combinations could be built with at least one sample per combination.

The breaking force varied considerably between samples within individual experiments and between experiments. A typical force versus displacement plot for UAM 3003 aluminum composites tested in shear can be seen by Figure 3.3. All shear test results are tabulated and displayed in Appendix B. Figure 3.4 shows the USS averages over the sample replicates and the standard error. The standard error is defined as in section 2.2.1. The recorded breaking force was the point at which the specimen underwent complete failure such that the force dropped off significantly.

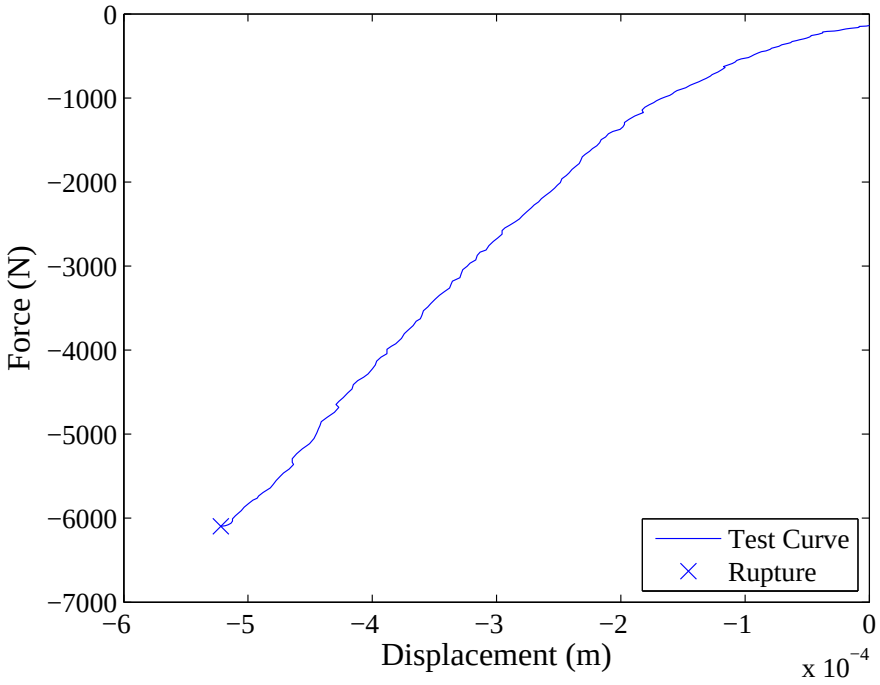

Figure 3.3: Force versus displacement plot from shear test for Expt. #6, Sample 4.

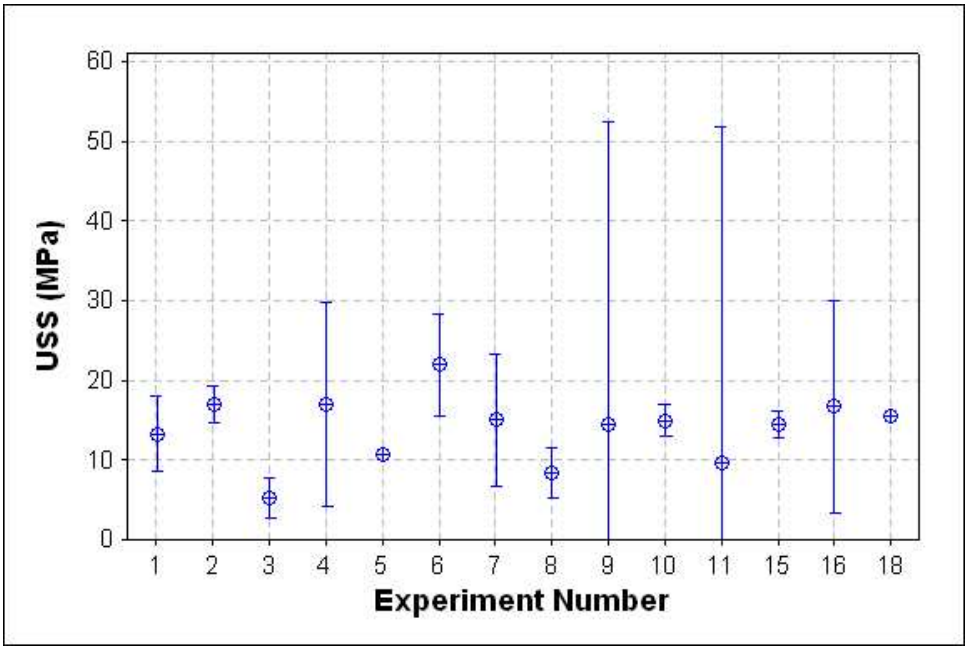

Figure 3.4: Interval plot showing ultimate shear strength (USS) for shear experiments — bars are one standard error from mean (crosshair).

3.2.2 Transverse Tensile Tests

Four treatment combinations did not produce samples that could be tested. All four of the treatment combinations that were not built had an oscillation amplitude of 18 μm and varying levels of tack force, weld force, and weld rate. These samples could not be built due to delamination of the part during the building process. This is caused by a combination of reaching the critical height to width ratio (0.7-1:1) that has been found to exist for parts built by UAM [27], and a lack of overall power (due to low oscillation amplitude) necessary to create sufficiently clean faying surfaces. Other samples are missing because of breakage during post-process machining. Overall, 14 of the 18 treatment combinations could be built with at least one sample per combination.

The breaking force varied considerably between samples within individual experiments and between experiments. A typical force versus displacement plot for UAM 3003 aluminum composites tested in transverse tension can be seen by Figure 3.5. All transverse tensile test results are tabulated and displayed in Appendix B. Figure 3.6 shows UTTS averages over the sample replicates and the standard error. The standard error is defined the same as in section 2.2.1. The recorded breaking force was the point at which the specimen underwent complete failure such that the force dropped off significantly.

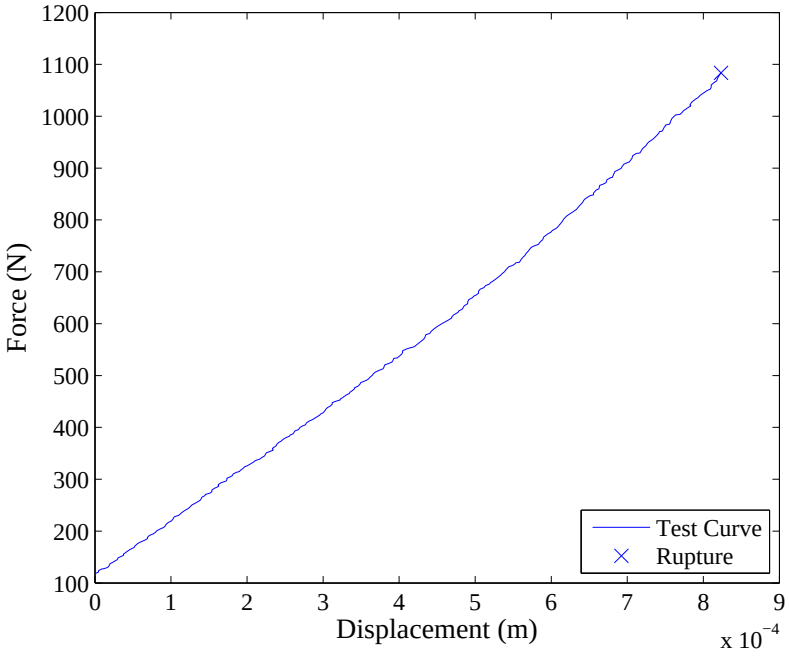

Figure 3.5: Force versus displacement plot from transverse tensile test for Expt. #6, Sample 2.

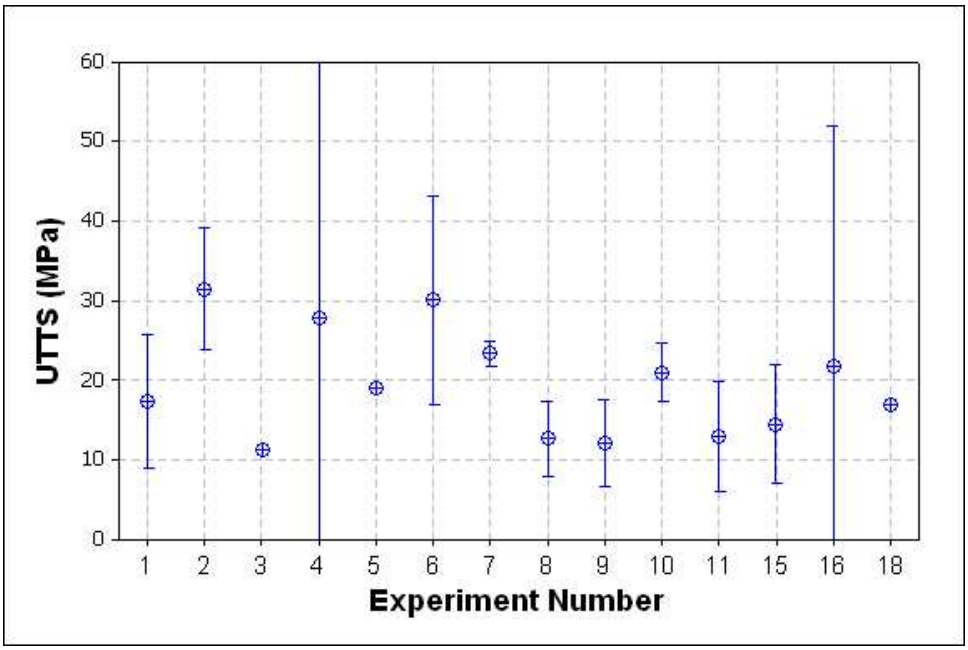

Figure 3.6: Interval plot showing ultimate transverse tensile strength (UTTS) for transverse tensile experiments — bars are one standard error from mean (crosshair).

3.3 Statistical Analysis of Mechanical Strength Tests

3.3.1 ANOVA Results

The USS and UTTS data were analyzed statistically by fitting ANOVA models. The adjusted Type I error probability, α, selected for this experiment was 0.05 for testing each of the model parameters, giving an overall error rate of at most 0.20 per mechanical test. The reason for allowing the overall alpha level to be 20% is that these experiments were explorative and designed to describe the overall relationships between USS or UTTS and the four factors. This means that for any given individual parameter there is a 5% probability of finding that a parameter has a significant effect on the strength when that is not the case. The α level is used as a threshold to determine significance of each variable in the model. The p-values represent the probability of obtaining a test at least as extreme as the one observed, assuming that the null hypothesis (of no trend, or no effect) is true. The lower the p-value, the less likely the result, assuming the null hypothesis. Thus, the null hypothesis is rejected in favor of the alternative hypothesis (there is a trend, or an effect) when the p-value is less than the selected α level.

The experimental runs that could not be tested were removed from the DOE. Padding the response matrices with zeros or other forms of data manipulation is not possible in this case as not enough is known about the USS and UTTS for these composites. The ANOVA was then performed on the remaining USS and UTTS data based upon the model given by equation 3.1 with the corresponding interaction term added to the model equation. The resulting ANOVA tables are given by Tables 3.5 and 3.6.

Table 3.5: ANOVA table for USS data.

Source of Variation	**Degrees of freedom**	**Type III Sum of Squares**	**Mean Square**	**F-Ratio**	**p-value**
Tack Force	1	2.92	2.92	0.38	0.5506
Weld Force	2	163.34	81.67	10.52	0.0019
Amplitude	2	33.16	16.58	2.14	0.1578
Weld Rate	2	17.46	8.73	1.12	0.3546
Tack Force, Weld Force Interaction	2	69.52	34.76	4.48	0.0332
Model Total	9	336.91	37.43	4.82	0.0055
Error	13	100.97	7.77		
Total	22	437.87			

Table 3.6: ANOVA table for UTTS data.

Source of Variation	**Degrees of freedom**	**Type III Sum of Squares**	**Mean Square**	**F-Ratio**	**p-value**
Tack Force	1	38.36	38.36	1.98	0.1826
Weld Force	2	311.91	155.95	8.06	0.0053
Amplitude	2	211.85	105.92	5.47	0.0189
Weld Rate	2	100.07	50.04	2.59	0.1134
Tack Force, Amplitude Interaction	2	82.16	41.08	2.12	0.1593
Model Total	9	911.10	101.23	5.23	0.0039
Error	13	251.60	19.36		
Total	22	1162.70			

The results from the ANOVA indicated in Table 3.5 show that the p-value for treatment factors tack force and weld rate are greater than $\alpha = 0.05$. Thus, the null hypotheses cannot be rejected for these effects. In turn, it is said that the different levels of these factors in this model do not have a significant effect on the USS of UAM built samples. In contrast, treatment factor weld force has a p-value less than

0.05, thus the null hypothesis can be rejected in favor of the alternative. Therefore, it is concluded that there is a significant effect of different levels of weld force on the response variable, USS.

Table 3.5 shows that, statistically, amplitude cannot be found to be significant, but the p-value here does not reflect that four of the six treatment combinations of amplitude at its lowest level (18 μm) could not be tested. It is incorrect to represent these experimental runs as having zero shear strength, but it is also incorrect to ignore these treatment combinations and base a conclusion solely on the ANOVA table results. Therefore, it is said that it is likely that an effect of different levels of amplitude on the response variable exists, but it cannot be shown solely from the ANOVA table p-value. Confidence levels will be used to further explore the effects of each parameter and will help to explain how amplitude affects ultimate shear strength of builds.

It was found that there is an interaction between weld force and tack force (p-value $< \alpha$ level of 0.05). In order to further investigate this effect, an interaction plot (Figure 3.8) was created to visualize the relationship between these two effects and provide further evidence for the conclusion that an interaction between tack force and weld force exists as discussed in section 3.3.2.

Table 3.6 illustrates that tack force and weld rate both have p-values greater than the selected significance level of 0.05. Therefore, the null hypotheses cannot be rejected and it is concluded that there is not a significant effect of different levels of these factors on the response variable, UTTS. Weld force and amplitude both have p-values less than 0.05, hence it is said that varying levels of weld force and amplitude have a significant effect on the UTTS of UAM built samples.

It was found that by adding the interaction between amplitude and tack force the overall error could be reduced, thus the interaction was kept in the model. The p-value is higher than 0.05 indicating that this interaction is not significant, but this will be further investigated by examining an interaction plot for these two factors.

3.3.2 Interaction Plots

Previous studies have shown that there is an interaction between weld force (normal force) and amplitude, and that this interaction has an effect on LWD [21]. This interaction was placed into the ANOVA model for the shear data, but it was found to be insignificant. Thus, it was replaced by the interaction of weld force and tack force in order to conserve degrees of freedom and decrease the model error. In order to be sure of this lack of interaction, an interaction plot was created of amplitude and weld force as seen by Figure 3.7. The plot shows that the lines do not cross and are relatively parallel. This plot supports the conclusion from the ANOVA that the interaction between weld force and amplitude does not have any significance with regards to USS as found in this DOE. It can be concluded that for increasing levels of weld force and amplitude there is an increase in USS. All other interactions with USS as the response variable were checked in this manner, and no others showed a significant interaction, with the exception of weld force and tack force.

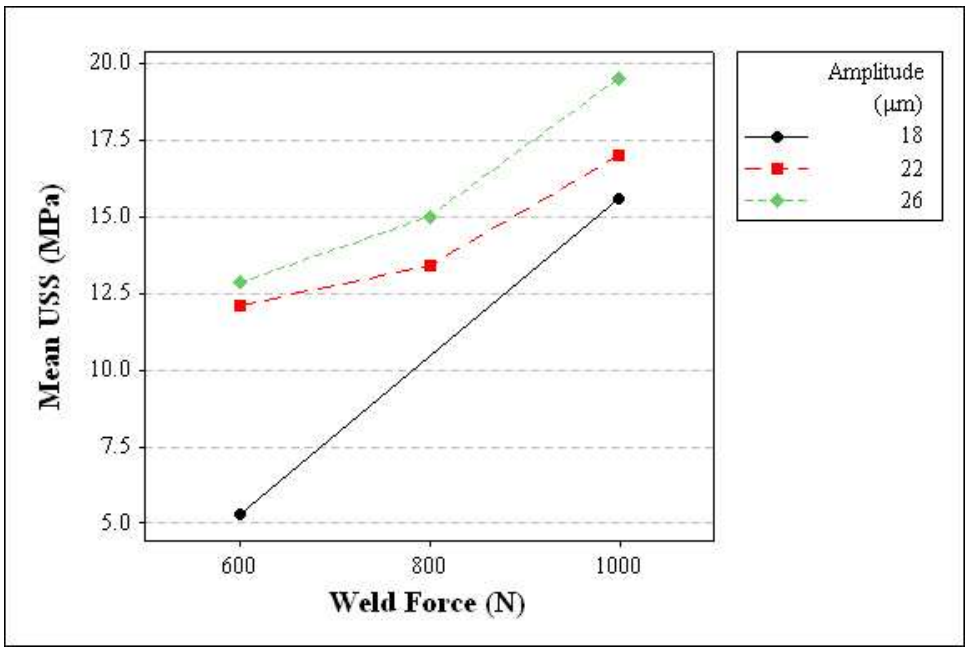

Figure 3.7: Interaction plot between parameters weld force and amplitude for USS data.

The interaction plot for tack force and weld force is shown in Figure 3.8. For a 600 N weld force, a 350 N tack force produces a higher USS. Then, at 800 N weld force, a slightly higher USS is produced with a 200 N tack force. This is again shown at 1000 N weld force with a tack force of 200 N producing a higher USS. The standard error was calculated for each of the data points shown on the plot in order to determine if there could be an overlap between the range of values at each data point. From this it was found that it is very likely that a difference between the levels of tack force at the 600 N level of weld force exists, but there is very little, if any, difference between levels of tack force at 800 N and 1000 N weld force.

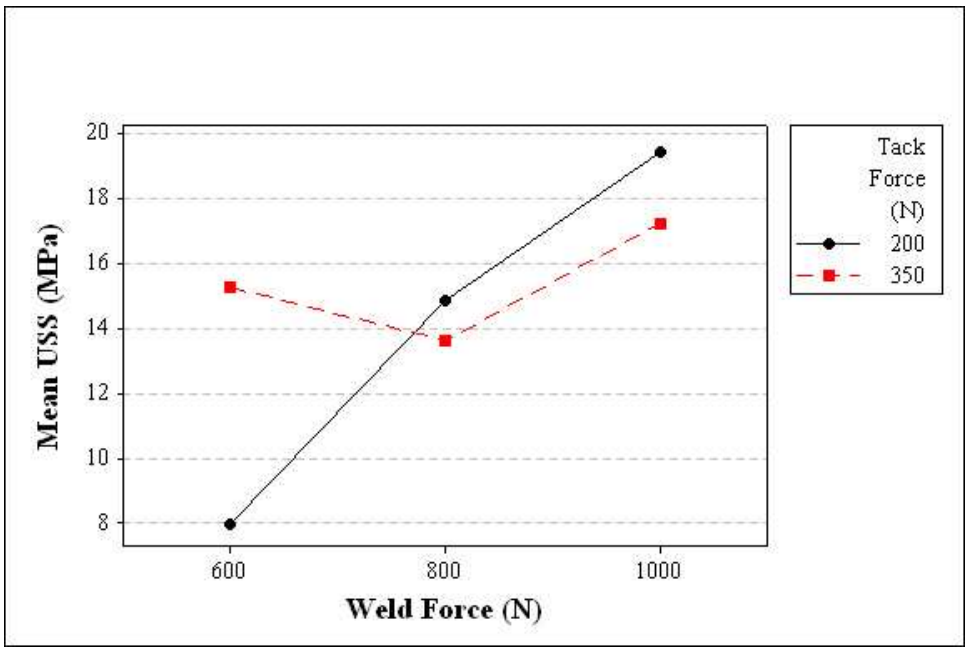

Figure 3.8: Interaction plot between parameters tack force and weld force for USS data.

For UTTS as the response variable, the interaction between weld force and amplitude was again checked graphically (Figure 3.9). The plot shows that the lines do not cross and are somewhat parallel. Thus, this plot supports the conclusion from the ANOVA that the interaction between weld force and amplitude does not have any significance with regards to UTTS as found in this DOE. It was found that for the transverse shear tests there was an interaction between tack force and weld force. Therefore, this interaction was checked for these tests. The ANOVA model did not show any significance and so it was removed because the error was higher for that model than for the one reflected by Table 3.6. The interaction plot of these factors was examined so as to verify this conclusion.

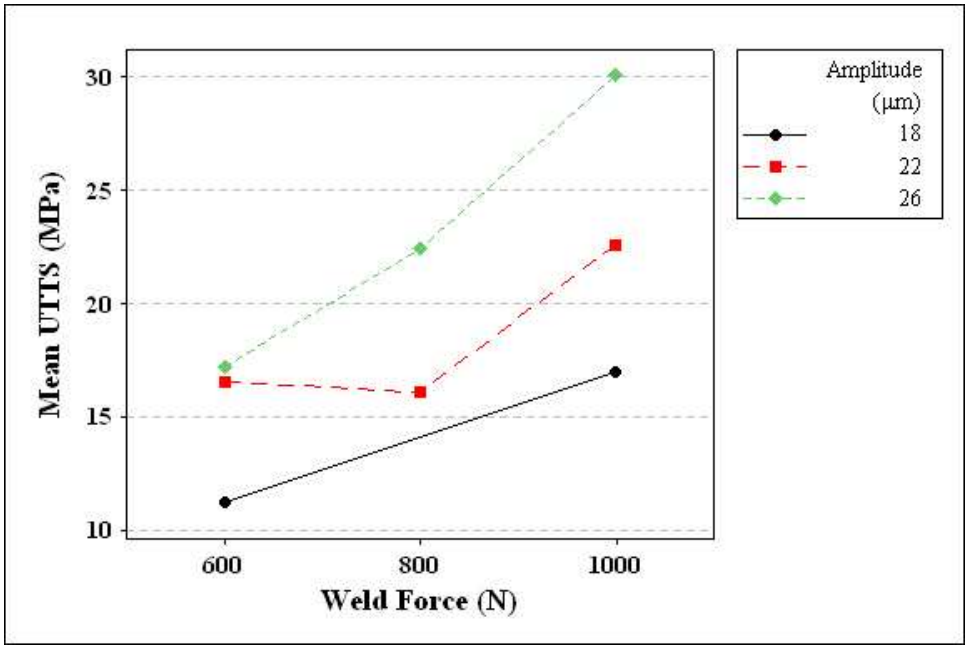

Figure 3.9: Interaction plot between parameters weld force and amplitude for UTTS data.

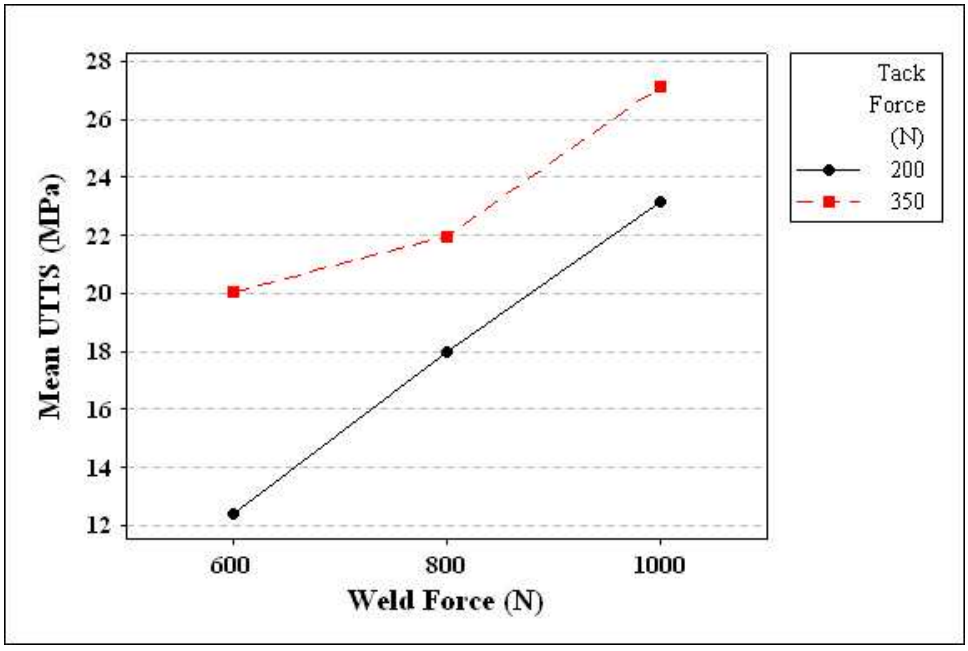

Figure 3.10: Interaction plot between parameters tack force and weld force for UTTS data.

Figure 3.10 shows that there is no interaction between weld force and tack force in regards to their effect on UTTS and that a tack force of 350 N may consistently produce a higher UTTS. Finally, Figure 3.11 shows that a higher level of tack force consistently produces a higher response paired with increasing levels of amplitude, and therefore, there is no interaction between these two parameters. This supports the conclusion based on the ANOVA table p-values for the UTTS data.

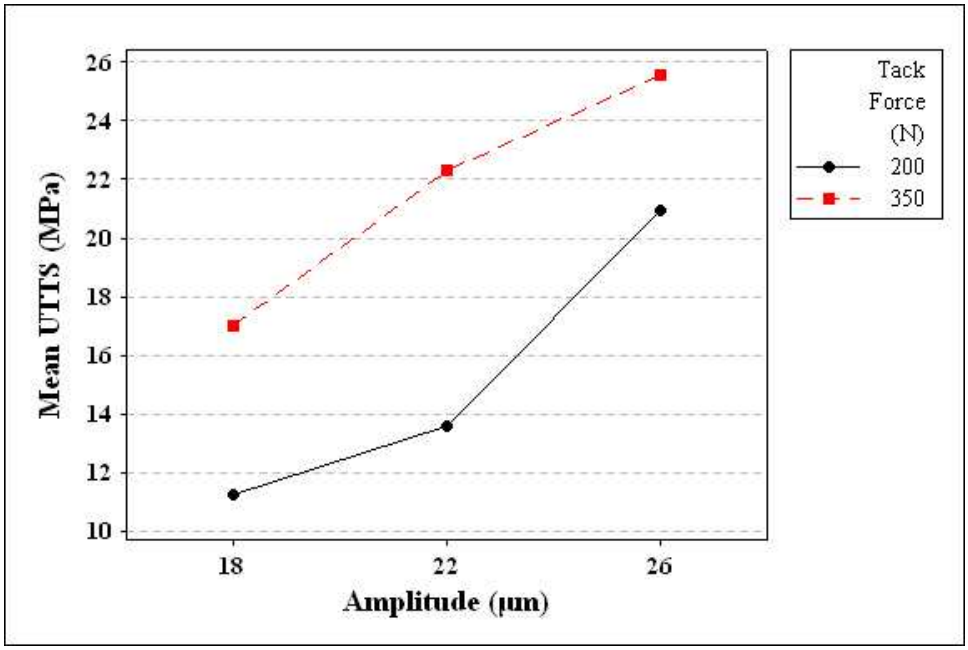

Figure 3.11: Interaction plot between parameters amplitude and tack force for UTTS data.

3.3.3 Confidence Intervals

Confidence intervals were examined at the 90% ($\alpha = 0.1$) level to further investigate the effects of the parameters on the USS and UTTS. Tukey's Method for multiple pair-wise comparisons was employed with the aid of SAS computer software and the

results are displayed in Tables 3.7 and 3.8. Confidence intervals give a range where it is known with a 90% probability that the difference between the means at each level exists within that range.

Table 3.7: Confidence intervals of main effects for USS as response variable.

	Level		Difference	Simultaneous 90% Confidence Limits for	
Parameter	**i**	**j**	**Between Means**	**LSMean(i)-LSMean(j)**	
Tack Force	1	2	-0.761	-2.961	1.439
Weld Force	1	2	-2.587	-5.978	0.804
	1	3	-6.599	-9.854	-3.344
	2	3	-4.012	-7.416	-0.608
Amplitude	1	2	-1.265	-6.703	4.172
	1	3	-3.499	-8.874	1.875
	2	3	-2.234	-5.072	0.604
Weld Rate	1	2	0.432	-3.278	4.142
	1	3	2.241	-1.290	5.772
	2	3	1.809	-1.925	5.542

Table 3.7 shows that there is no effect on the USS for different levels of tack force. This occurs because the confidence limits contain zero about half-way across the range of values implying that the difference between level 1 and level 2 of tack force could be positive or negative. This means that either the higher level of tack force or the lower level could produce a higher USS and therefore, it does not have a significant effect.

Weld force shows that there is most likely a difference between levels 1 (600 N) and 2 (800 N), and there is conclusively a difference between levels 2 and 3, and levels 1 and 3. This is known because both ends of the confidence limits are negative

suggesting that there is a 90% probability that level 3 will produce a higher USS than both levels 1 and 2. The confidence levels for amplitude show that there is no difference between levels 1 and 2, but there is a very strong likelihood that level 3 produces a higher USS than both levels 1 and 2. This can be concluded because, even though the confidence intervals for levels 1 and 3, and levels 2 and 3 contain zero, they are highly skewed negative. Between levels 1 and 3, 83% of the confidence interval is negative, and between levels 2 and 3, 89% of the confidence interval is negative. Thus, it is concluded that a higher level of amplitude causes a positive increase in its effect on the USS of the builds.

For weld rate, there may be a difference between level 3 and levels 1 and 2 because for both of these confidence intervals, the range contains zero but is skewed positive. This implies that a slower weld rate produces a higher USS, at least compared to the fastest level. It should be noted that weld rate was not found to be a significant factor at these levels, and so it is not highly important as to which level is selected.

Table 3.8 shows that there may be a slight effect on the UTTS for different levels of tack force. Despite containing zero within the range for the confidence limits, the range is skewed negative implying that when tack force is set at 350 N there tends to be a higher UTTS. Since tack force was not found to be significant the tack force could be set at either level.

The confidence interval for weld force and UTTS shows that there is most likely a difference between levels 1 (600 N) and 2 (800 N), and levels 2 (800 N) and 3 (1000 N), and there is conclusively a difference between levels 1 and 3. This is known because both ends of the confidence limits are negative implying that there is a 90% probability

that level 3 will produce a higher UTTS than both levels 1 and 2. This result agrees with that found for weld force and its effect on USS.

The confidence intervals for amplitude show that there is no difference between levels 1 and 2, but there is a very strong likelihood that level 3 produces a higher UTTS than both levels 1 and 2. This can be concluded because between levels 2 and 3 the confidence interval does not contain zero and is fully in the negative range. Also, even though the confidence interval for the least square mean difference between levels 1 and 3 contain zero they are highly skewed negative. Between levels 1 and 3, 92% of the confidence interval is negative. Hence, a higher level of amplitude results in a higher UTTS just as found for amplitude and USS.

Similar to the USS results, there may be a difference between level 3 and levels 1 and 2 of weld rate because for both of these confidence intervals the range contains zero but is skewed positive. This implies that a slower weld rate produces a higher

Table 3.8: Confidence intervals of main effects for UTTS as response variable.

	Level			**Simultaneous 90% Confidence Limits for**	
Parameter	**i**	**j**	**Difference Between Means**	**LSMean(i)-LSMean(j)**	
Tack Force	1	2	-3.688	-8.327	0.951
Weld Force	1	2	-5.589	-11.291	0.113
	1	3	-9.846	-15.371	-4.320
	2	3	-4.257	-9.923	1.409
Amplitude	1	2	-0.932	-9.558	7.695
	1	3	-6.891	-15.146	1.365
	2	3	-5.959	-10.391	-1.527
Weld Rate	1	2	-3.768	-11.356	3.820
	1	3	4.475	-1.934	10.883
	2	3	8.242	-0.141	16.626

UTTS at least compared to the fastest level. It should be noted though that weld rate was not found to be a significant factor at these levels.

3.3.4 Scatter Plots and Trend Contrasts

Scatter plots of the USS and UTTS data for each factor were created in order to detect any trends that may be present. The plots shown in Figures 3.12 and 3.13 reflect this data and show several interesting characteristics. Figure 3.12(a) does not reflect any trend in levels of tack force as supported by the ANOVA table results and confidence intervals of USS data. There does appear to be linear and possible quadratic trends in factors normal force, amplitude, and weld rate (Figures 3.12(b), (c), and (d), respectively).

Figure 3.13(a) shows that there is a slight positive trend in the levels of tack force as reflected by the ANOVA table and confidence intervals of UTTS data. Yet, tack force was found to be an insignificant factor so it was excluded from further trend analyses. All three other factors have trends similar to that found in the USS data. Based upon these observations, straight-line and quadratic trend contrasts for weld force, amplitude, and weld rate were examined to determine if these trends are truly present or not.

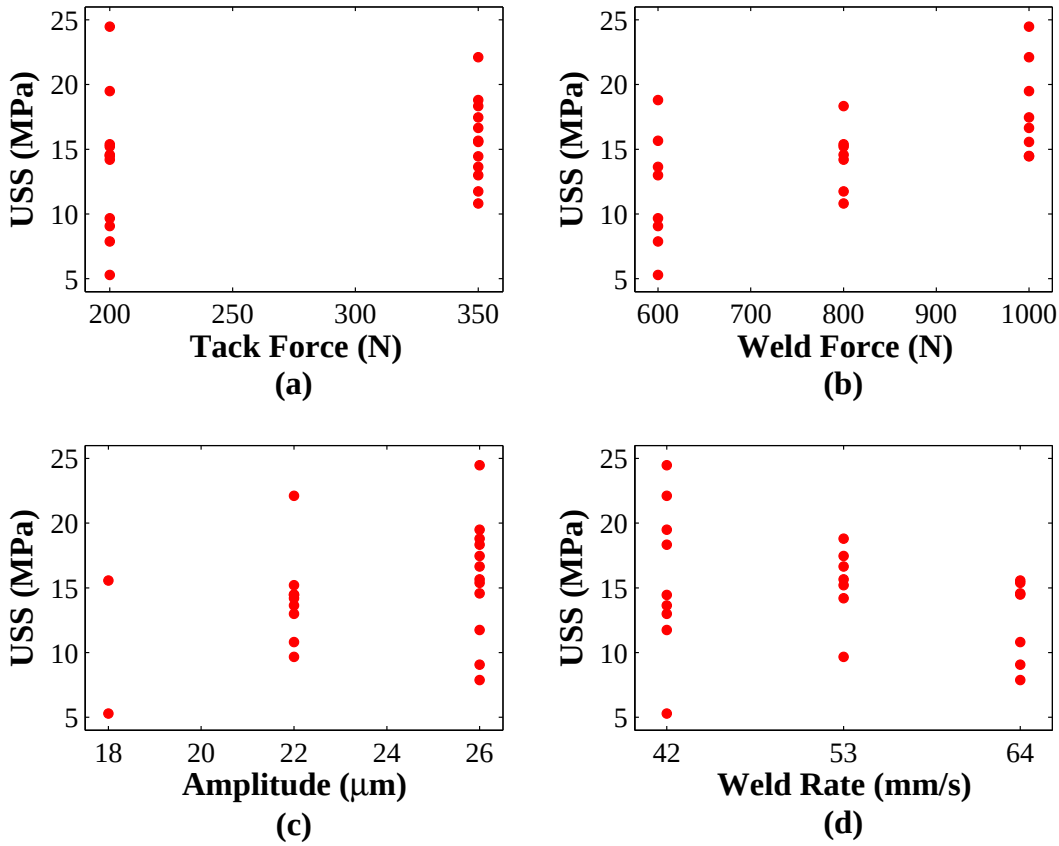

Figure 3.12: Scatter plot of USS data as a function of selected levels for each parameter: (a) USS vs. tack force, (b) USS vs. weld force, (c) USS vs. amplitude, and (d) USS vs. weld rate.

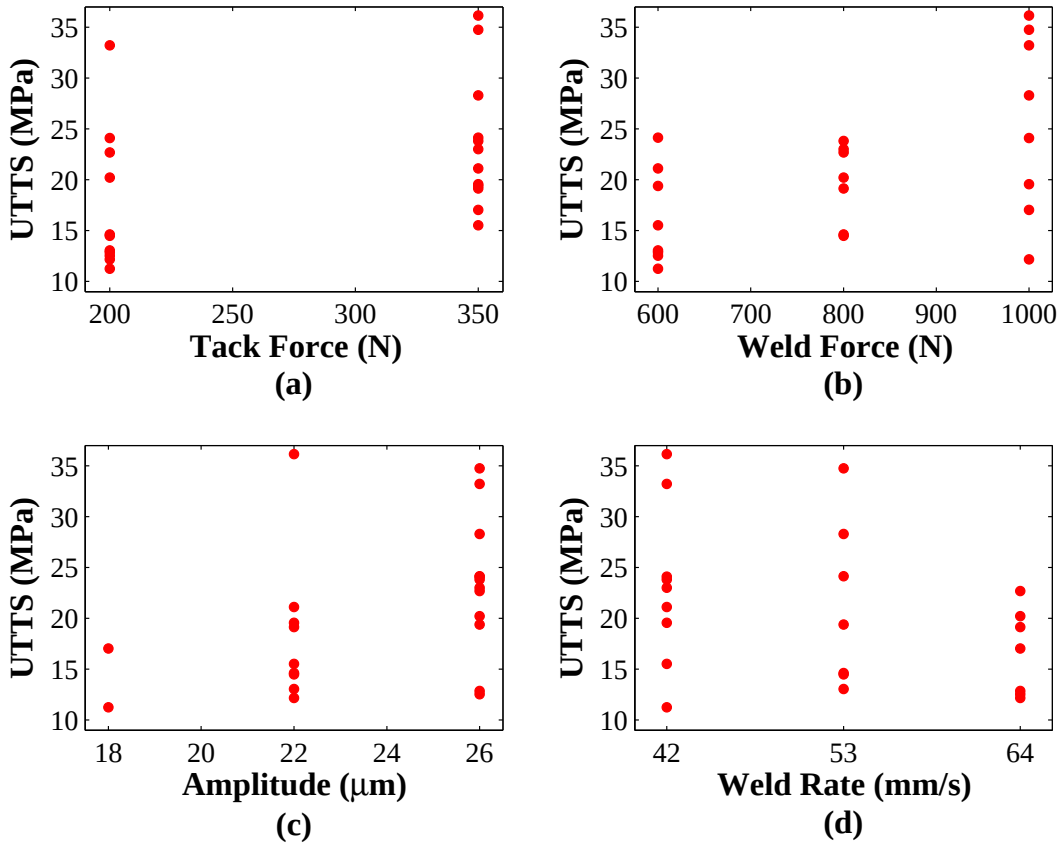

Figure 3.13: Scatter plot of UTTS data as a function of selected levels for each parameter: (a) UTTS vs. tack force, (b) UTTS vs. weld force, (c) UTTS vs. amplitude, and (d) UTTS vs. weld rate.

Table 3.9 shows the results of investigating the contrasts. Using a significance level of $\alpha = 0.01$ it is found that there is a straight-line trend present in the data for weld force (both USS and UTTS). There are no other significant trends reflected by the p-values for any of the other parameters. It should be noted though that because of the few number of samples for amplitude at 18 μm the trend contrasts are most likely incorrect for this parameter.

Table 3.9: P-values for trend contrasts in USS and UTTS data as a function of UAM process parameters.

Mechanical Response	**Parameter**	**Straight-Line Trend p-value**	**Quadratic Trend p-value**
USS	Weld Force	0.0005	0.6003
UTTS		0.0015	0.7679
USS	Amplitude	0.1671	0.7542
UTTS		0.0832	0.321
USS	Weld Rate	0.1773	0.6445
UTTS		0.1405	0.0883

Consequently, it is more accurate to observe the trends based on the scatter plot for amplitude, in which there is an observable positive linear trend for both the USS and UTTS data.

For each parameter, the USS and UTTS data was averaged over the replicate number at the individual levels so that any overall trends could be more readily distinguishable. Figure 3.14 plots the averaged trends for each parameter for USS and UTTS data and shows basic model-fits (black lines) for the data.

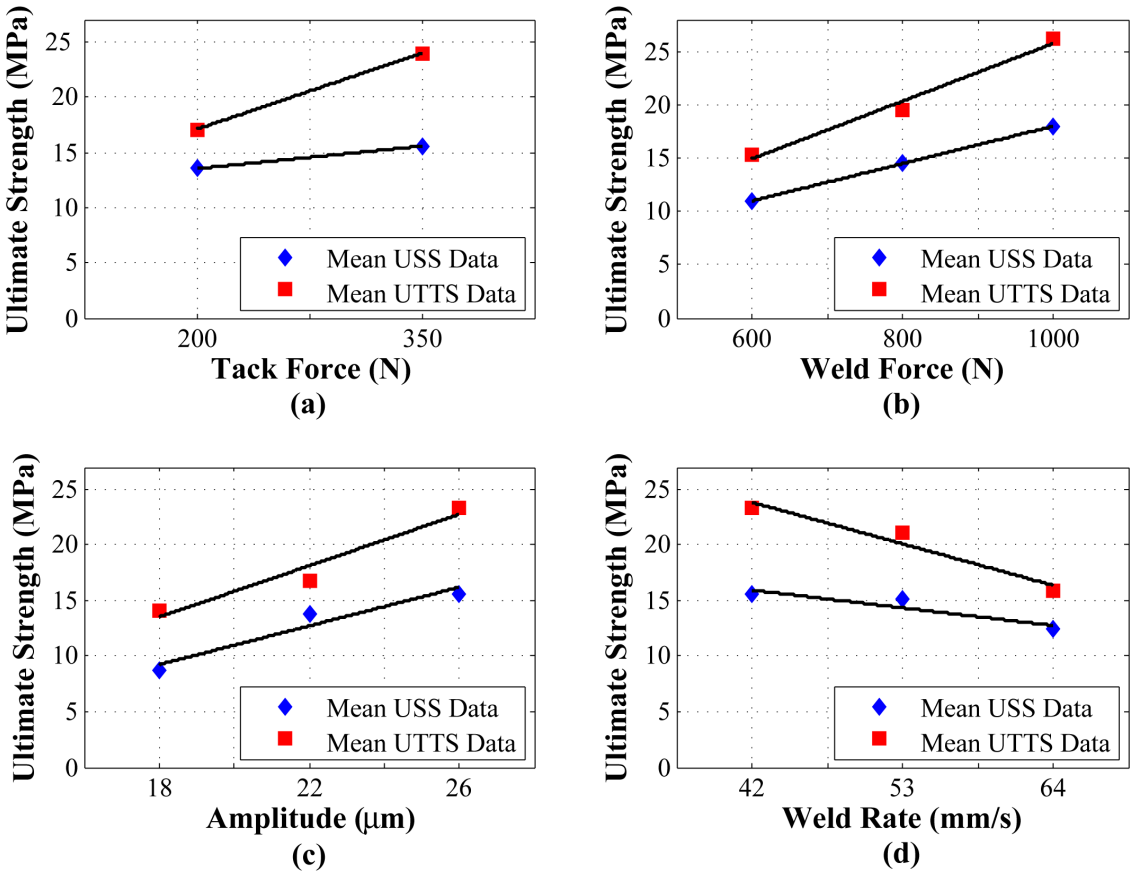

Figure 3.14: Deviation in average USS and UTTS as a function of selected levels for each parameter: (a) Ultimate strength vs. tack force, (b) ultimate strength vs. weld force, (c) ultimate strength vs. amplitude, and (d) ultimate strength vs. weld rate.

It can be seen that for both USS and UTTS, the two significant parameters (weld force and amplitude) have a positive linear trend and produce their highest response at the highest level of each parameter. Therefore, for the levels of each parameter given in this DOE and based upon the combined results of the statistical analyses, a specimen with maximized USS and UTTS would be built under the following parameter combination:

- Tack Force: 350 N

- Weld Force: 1000 N
- Amplitude: 26 μm
- Weld Rate: 100 or 125 IPM (42 or 53 mm/s).

3.4 Results of Microstructural Analysis

Linear weld density (LWD) was first examined for several samples. Samples were chosen that represented high, medium, and low USS and UTTS. Table 3.10 summarizes the process parameter combinations for each experiment examined and the corresponding average mechanical strength. Typical images used for calculating LWD are shown in Figures 3.15 and 3.16.

Table 3.10: Summary of experiments from which samples were viewed microscopically.

Experiment Number	**Tack Force (N)**	**Weld Force (N)**	**Amplitude (μm)**	**Weld Rate (mm/s)**	**USS (MPa)**	**UTTS (MPa)**
1	350	600	22	42	13.3	17.4
2	350	1000	26	53	16.5	31.5
3	200	600	18	42	5.2	11.2
6	200	1000	26	42	20.0	30.2
8	200	600	26	64	8.1	12.7
10	200	800	26	64	14.6	21.0

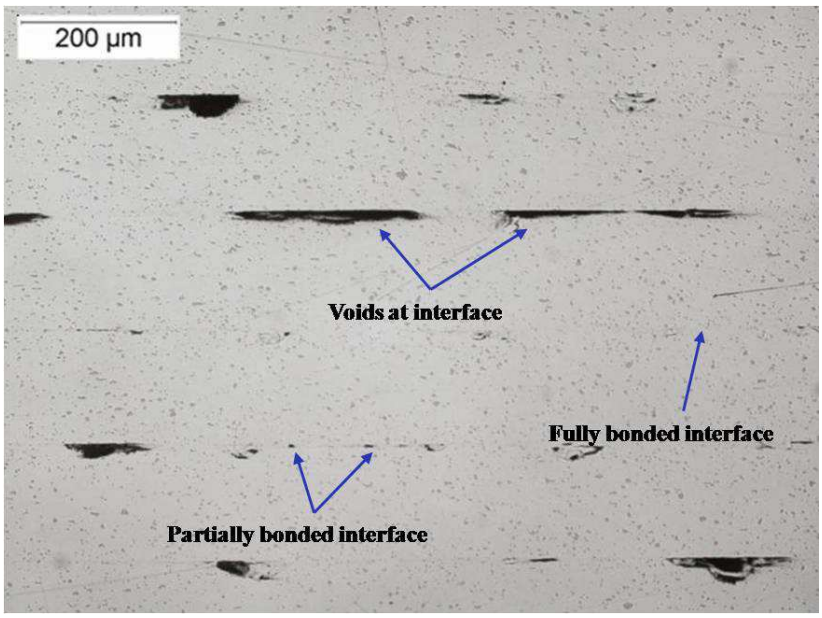

Figure 3.15: Micrograph of Experiment 6, Sample 2 at 100x magnification used in calculating total LWD – sample is from experiment with high USS and UTTS.

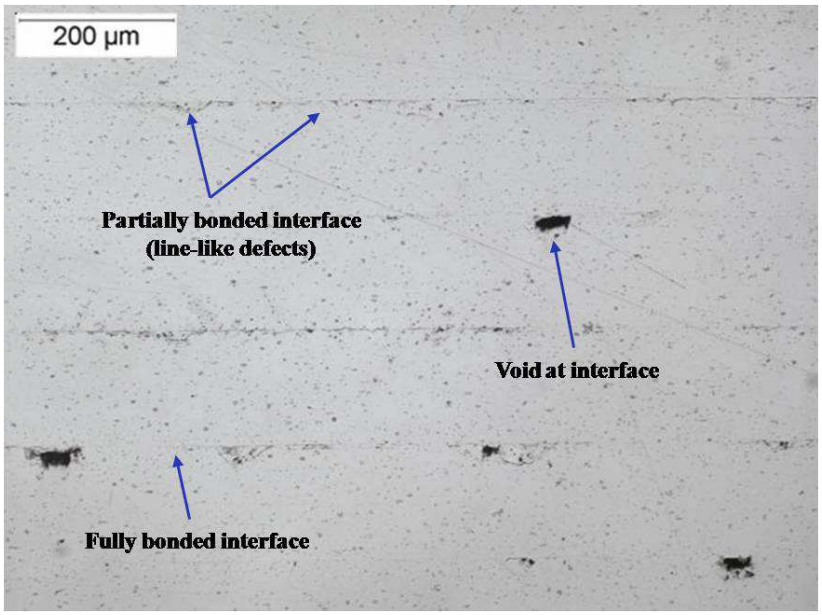

Figure 3.16: Micrograph of Experiment 8, Sample 2 at 100x magnification used in calculating total LWD – sample is from experiment with low USS and UTTS.

It can be seen that there are three regions of bonding at the interface. There are areas where large voids exist, areas where there are small crack-like voids and partial bonding, and finally where there is full bonding and no interface is visible. From Figure 3.16, note that there are fewer large voids compared to the sample from Experiment 6 (Figure 3.15), but there are still visible interfaces with smaller, line shaped voids and defects. Figure 3.17 shows the full results of the LWD analysis performed for this DOE.

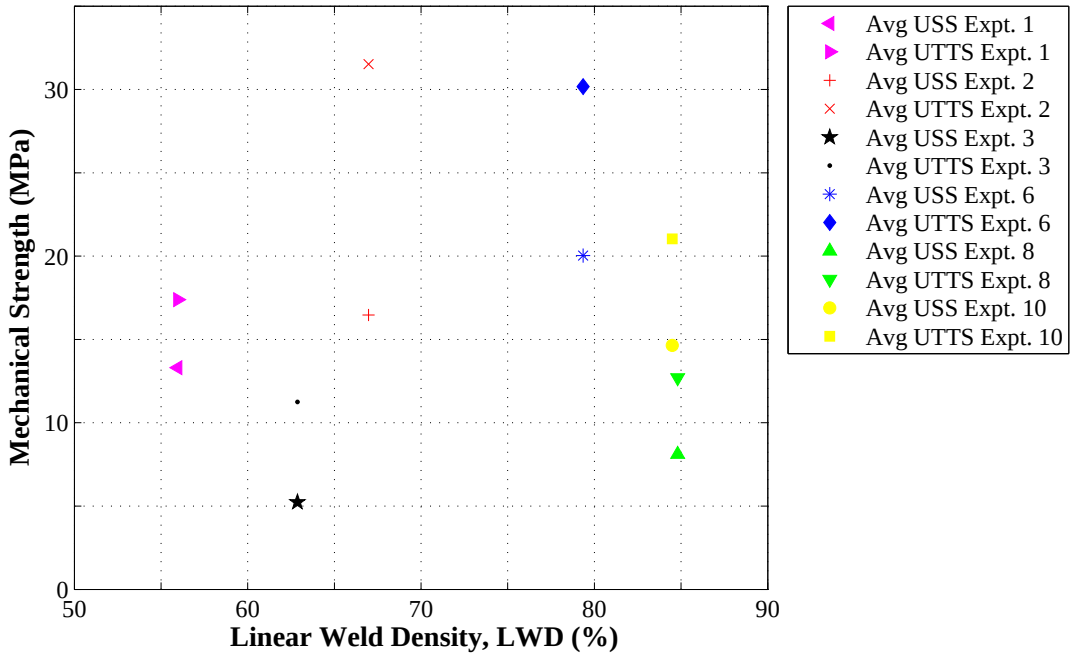

Figure 3.17: Linear weld density (LWD) versus average mechanical strength (USS and UTTS) of UAM built specimens.

It can be seen that there is an unexpected drop in mechanical strength with increasing LWD. There appears to be either an optimum value or a limiting threshold between 70% and 80% LWD. It is unsure why this occurs, but several possible explanations will be put forth in section 3.5.4. Due to the subjective nature of calculating LWD, other, more objective methods for characterizing the bonding microstructurally were employed.

Fracture surfaces were examined for both USS and UTTS samples. This method of characterizing the bonding at the interfaces has been found to be useful and informative in previous studies [7, 32]. A sample micrograph before and after applying the image analysis threshold can be seen in Figures 3.18 and 3.19, respectively.

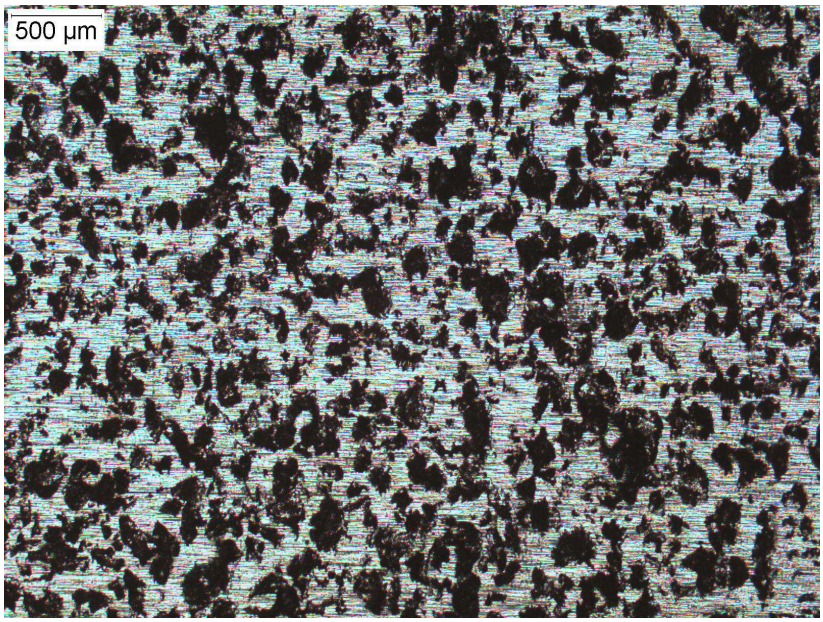

Figure 3.18: Fracture surface of sample from Experiment #2 before image processing – dark regions are previously bonded regions.

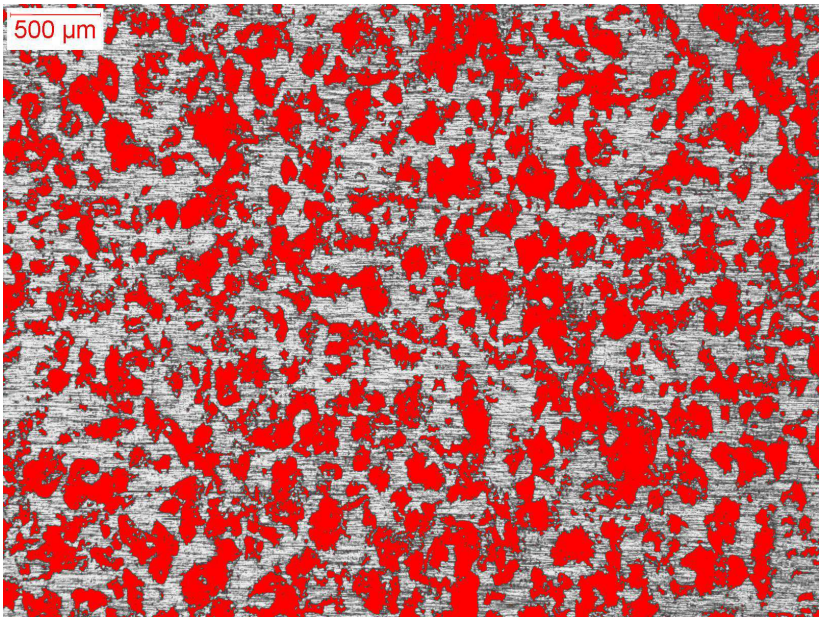

Figure 3.19: Fracture surface of sample from Experiment #2 after threshold adjustment.

It was visually verified that the dark regions seen by the micrographs of fracture surface were, in fact, suspected bonded regions by observing a fracture surface using a confocal laser scanning microscope (Figures 3.20 and 3.21). This instrument has the capability of providing a three-dimensional optical image of a surface as well as the ability to measure the height of features on the surface. It is known that bonded areas will be regions of greater height and deformation than unbonded regions because they would be in contact with the surface above. The images show that there is a definitive height difference and that the dark regions seen in the fracture surface images are higher than the lighter, unbonded regions.

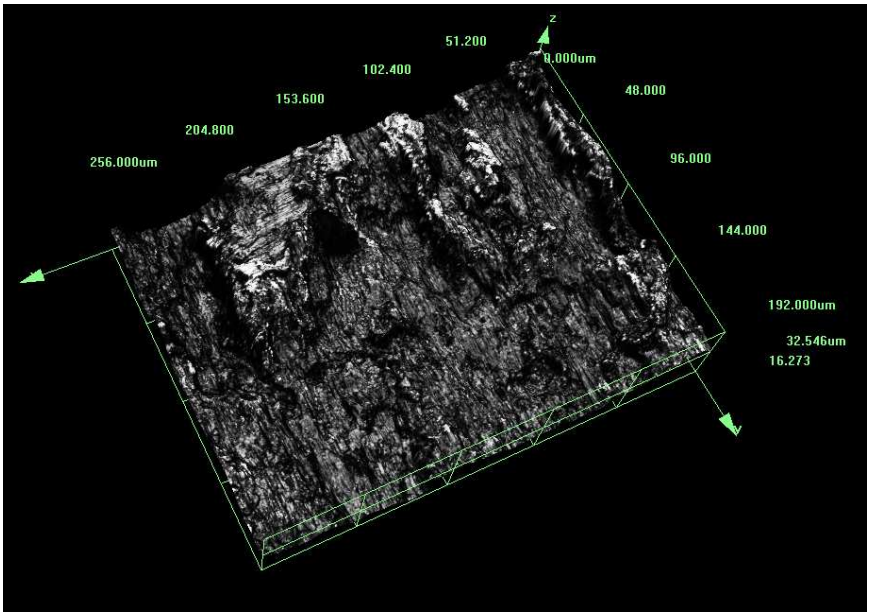

Figure 3.20: Three-dimensional view of fracture surface from shear test sample.

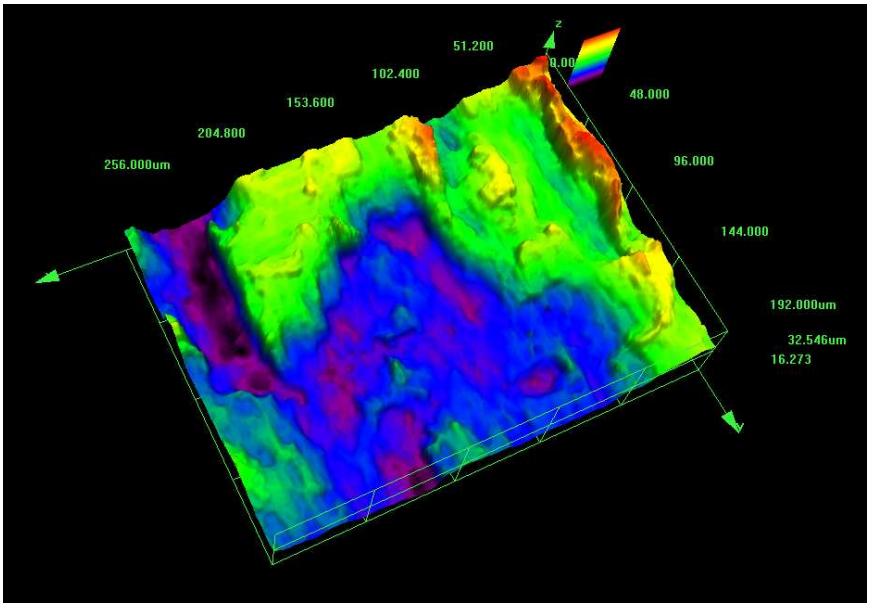

Figure 3.21: Three-dimensional view of fracture surface from shear test sample with height gradient processing applied.

Using the ImageJ analysis software on images with an applied threshold, the percentage of the detected bonded areas (red) to the overall area could be calculated. The results are displayed in Figures 3.22 and 3.23. Both plots show that all of the samples have a relatively similar percentage bonded area. The range for the UTTS samples is between 35% and 45% bonded area, and between 30% and 50% for the USS samples. The range is slightly larger for the USS samples because of smearing of the bonded regions that can occur during testing, which increases the perceived ratio of dark areas to light areas seen in the images.

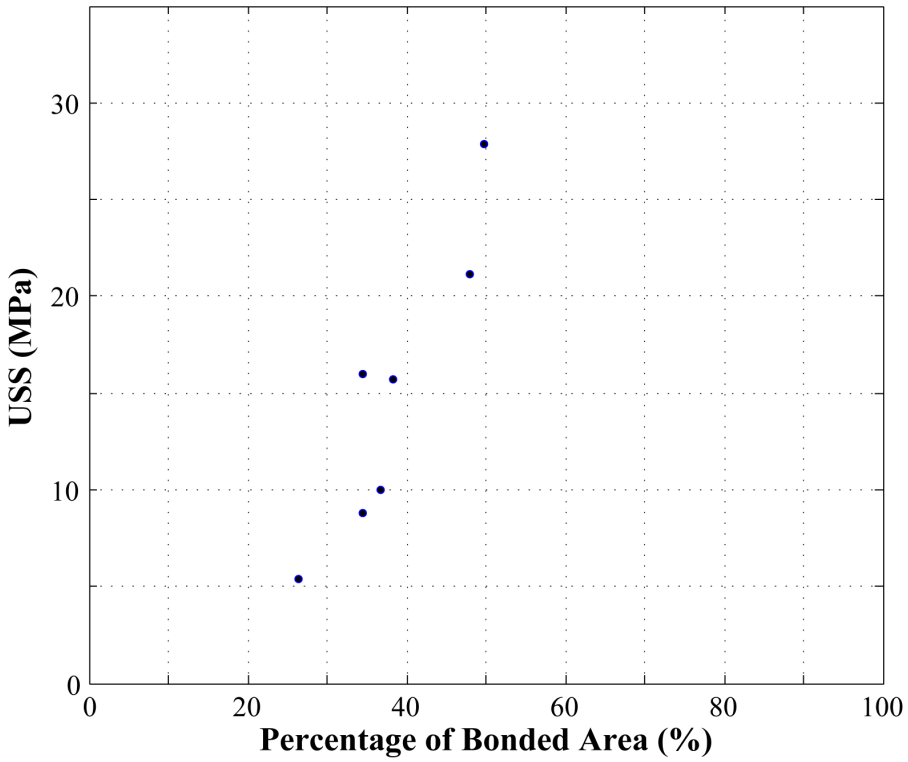

Figure 3.22: Percentage of bonded area on USS fracture surfaces versus USS of sample.

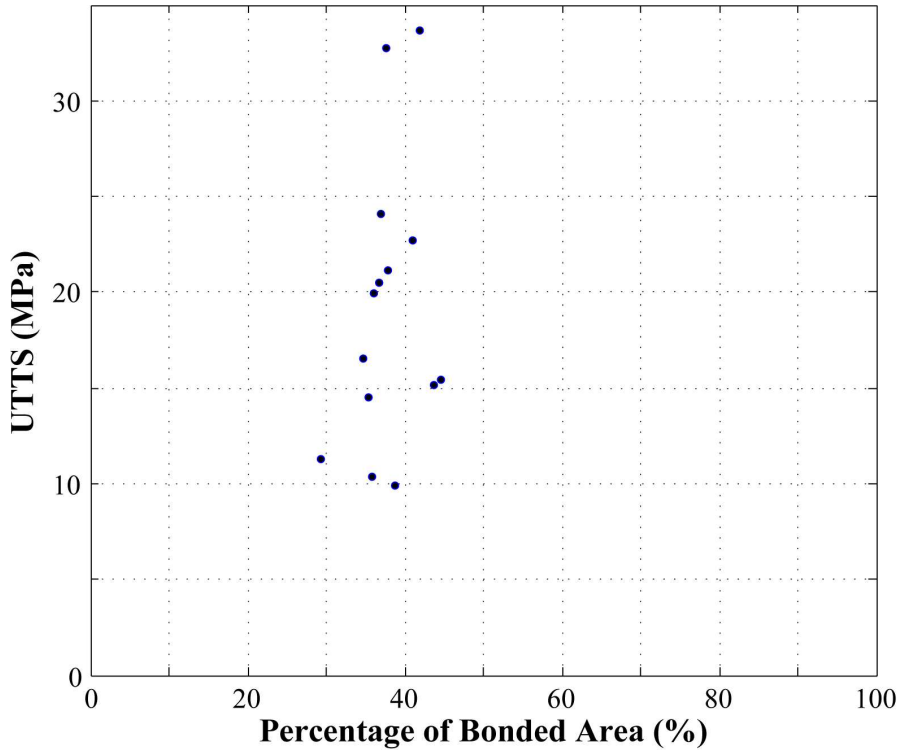

Figure 3.23: Percentage of bonded area on UTTS fracture surfaces versus UTTS of sample.

It would be expected that as the percentage of bonded area increases then the mechanical strength (USS and UTTS) of the specimen would increase as well (or vice versa). Figures 3.22 and 3.23 show that all of the samples tested in this DOE had an average percent bond area of 38% with a standard error of 1.2%. A possible explanation of this unanticipated result is given in section 3.5.4. While this result is unexpected, it is consistent with prior research. It had been found previously that the percentage of bonded area on 3003 aluminum fracture surfaces for specimens tested in shear and tension with varying mechanical strengths was consistently around 66% [7]. The reason for the discrepancy between this earlier result and the value found

in the current study is that those samples were made under a different combination of processing parameters than any of the combniations found in this DOE.

3.5 Discussion

3.5.1 Mechanical Strength of Transverse Shear Specimens

Samples mainly displayed a predominantly linear force/displacement relationship. This indicates that the bulk samples failed in a brittle fracture mode, but the locally bonded regions at microscopic level would be ductile. There is substantial variability between samples within a given experiment. The highest standard deviation is 5.24 MPa for Experiment #7, which is 34% of the average USS for that experiment. While this inconsistency is not optimal it is dramatically less than the variation between shear samples in the Ti/Al DOE (section 2.5.1).

Experiment #6 produced the highest strengths with an average of 20.030 MPa and a standard deviation of 4.01 MPa. This is still only about 18% of the USS of solid 3003 aluminum (110 MPa). Therefore, it can be implied that the total energy available for bonding in this DOE was not sufficiently high enough to create builds with ultimate shear strengths comparable to that of the solid 3003 aluminum.

3.5.2 Mechanical Strength of Transverse Tensile Specimens

All samples exhibit a predominantly linear force/displacement relationship, which again indicates that samples failed in a brittle fracture mode, but the locally bonded regions at microscopic level would be ductile. The samples all failed at a single weld interface and produced two separate pieces. There is substantial deviation in UTTS with the highest standard deviation being 11.73 MPa (42% of average value for Experiment #4). Experiment #2 produced the highest strengths with an average

of 31.523 MPa and a standard deviation of 4.78 MPa. This is only about 16% of the ultimate tensile strength of solid 3003 aluminum (200 MPa).

The discrepancy between the experiment with the highest mechanical strength (Experiment #6 for shear tests; Experiment #2 for tension tests) can be explained by examining the combination of process parameters for each experiment. Both experiments had a weld force of 1000 N and amplitude of 26 μm, but the tack forces and weld rates were different. This result agrees with the conclusions of the statistical analysis in that normal force and amplitude are significant parameters, but tack force and weld rate are not. The percent difference between the USS of Experiment #2 and Experiment #6 is only 19%. The percent difference between the UTTS of Experiment #2 and Experiment #6 is only 4%. Therefore, the key to a specimen with high mechanical strength is to have the highest level of weld force and highest level of amplitude in this DOE, while weld rate and tack force could be at any of their levels in this study.

3.5.3 Effects of Manufacturing Parameters

The results of the ANOVA including the interaction plots, confidence intervals and statistical trend analyses lead to the conclusion that weld force and amplitude have a significant effect on the USS and UTTS of UAM built samples. The physical explanation for the effects of these two parameters is discussed below in detail. While tack force and weld rate were not found to have a significant effect on the outcome measures (USS and UTTS) they too are examined.

3.5.3.1 Effect of Tack Force

From the statistical analyses, tack force was not found to affect the USS or the UTTS. The tack force is needed for the operation of the machine, but the force needed for this step does not change the overall strength of the build because the levels used are too low to induce bonding. The tack force is just enough to imprint the horn texture onto the metallic tape and create a roughness. The added roughness increases the friction between the tape layers and thus prevents the tape from becoming misaligned during the subsequent weld pass.

3.5.3.2 Effect of Weld Force

The mechanical strength in terms of USS and UTTS, increases as the level of weld force increases as shown by Figure 3.14(b). In this study, there was no drop-off in mechanical strength with increasing levels of normal force as in the Ti/Al DOE. This is because the maximum level of weld force used in the current DOE is significantly less than the highest levels used in the Ti/Al DOE. It is possible that a drop in the USS and UTTS would be observed for samples made of 3003 aluminum if the levels employed were similar to those used in the Ti/Al DOE.

Solid state bonds are formed due to metallic bonding when oxide and contaminant free metal surfaces are brought into intimate contact [22]. Metallic bonding occurs because valence electrons (outermost electrons) in metals are not bound to any particular atom [17]. Therefore, they are able to drift throughout the metal resulting in atomic nuclei with ionic cores. These drifting electrons bind the ion cores together in a lattice structure [17]. Therefore, metallic bonds can be created between two metal pieces by establishing intimate contact between oxide and contaminant free areas

without the formation of a liquid phase. In order to achieve the necessary closeness of the metal atoms, a high normal force is required. As normal force is increased surface asperities are crushed and the faying surfaces are brought into closer contact so that the valence electrons can jump between the atoms of one faying surface to the atoms of the other creating the metallic bond [26]. Further, an increase in applied normal force increases the magnitude of the resultant interfacial shear stresses which aids in bond formation [14]. Therefore, for a maximized USS and UTTS of 3003 aluminum specimens a weld force of 1000 N should be employed.

3.5.3.3 Effect of Oscillation Amplitude

Like weld force, oscillation amplitude was found to have a positive linear effect on the USS and UTTS (Figure 3.14(c)). The higher the oscillation amplitude, the higher the amount of applied ultrasonic energy. This energy combined with the static applied normal force (weld force) determines the total energy available for bond formation during the welding process [14]. The amplitude aids in the destruction of the oxide layer and contaminant film which allows for clean metal-to-metal contact between the mating surfaces [22]. Furthermore, an increase in amplitude increases the magnitude of the shear forces and the resulting amount of local plastic deformation of surface asperities. Both of these factors are favorable for the formation of intimate nascent metal and subsequent strong metallic bonds. Further studies are necessary to fully asses the effect of oscillation amplitude, but the present research shows that an amplitude of 26 μm produces the best results.

3.5.3.4 Effect of Weld Rate

While not being significant, weld rate still has an effect on the USS and UTTS of the specimens. Weld rate was found to have a relatively negative linear effect on the USS and UTTS over the parameter range, as can be seen in Figure 3.14(d). The USS and UTTS decreased with an increase in weld rate. Weld rate determines the amount of energy per unit length or, alternatively, the amount of time over which energy is applied to a given point during the welding process [14]. An increase in the weld rate, decreases the amount of time that energy input can occur, resulting in insufficient interfacial stresses causing inadequate oxide layer removal and nascent surface formation. Hence, the overall strength of the specimen decreases as well. For this DOE, there was not a great enough difference between the levels of weld rate in order for there to be a significant decrease in strength between levels. It is presumed that over a larger range of weld rates, a substantial difference in mechanical strength would be observed. Therefore, in order to decrease manufacturing time yet retain a relatively high level of mechanical strength, it is recommended that a weld rate of 125 IPM be used based upon the results of this research.

3.5.4 UAM Bond Characterization

As noted previously, the results of the microstructure analysis are somewhat unconventional. It would be expected that as the normal force (weld force) and amplitude increase (at least to a certain point) greater deformation and oxide layer removal would occur, consequently increasing the LWD and mechanical strength as well. It has been found that while an increase in mechanical strength occurs with increased weld force and amplitude, LWD does not increase beyond a certain value. The results

of the LWD analysis shown in Figure 3.17 suggest that in order to maximize relative mechanical strength an optimum LWD between 70% and 80% should be realized. It should be noted that the standard errors for the LWD data points were between 1% and 3%, indicating that they are fairly accurate representations of the LWD for those samples.

Presently, it is unclear why there is an optimum at a value other than 100% LWD, but it could possibly be due to hot working of the material at the interface when a low normal force and high amplitude is used. In this scenario, high sliding frictional forces may exist that excessively heat the part at the interface thereby reducing the overall strength, yet giving the appearance of high LWD. This is reflected by Experiments #8 and #10 both of which are on the higher end of observed LWD, but have lower mechanical strengths. These experiments were built using the highest level of oscillation amplitude, and the lowest and middle levels of weld force, respectively (Table 3.10). Further investigation is needed to evaluate in greater detail the cross-sectional interface microstructure of these samples.

From examination of the fracture surfaces it is found that the majority of transverse tensile samples have between 35% and 45% bonded area and the shear samples have between 30% to 50% bonded area. As stated previously, the shear samples have a slightly larger range because of smearing that occurs during testing giving the appearance of a greater bonded area. It is hypothesized that all of the samples in this DOE have approximately the same percent bond area because of a lack of total energy. Elaborating on this point, each process parameter combination results in a certain amount of energy input to the material during the weld cycle. If this energy is not enough to break up the oxide layer and plastically deform the surface asperities

then a remaining texture will be left and little bonding will occur. The energy for a given cycle needs to be greater than the elastic strain energy associated with the parent material in order to have large-scale plastic deformation of surface asperities.

It is believed that for any given parameter combination used in this DOE there was not enough energy to greatly deform the asperities and promote formation of a large contact area between the mating surfaces. Therefore, the percent bonded area for all samples would be relatively the same because, even for the optimal combination of process parameters, the energy was still below the elastic strain energy for 3003 aluminum. The difference in mechanical strengths is due to the situation that at the contact points between the faying surfaces there was a given energy input. So, for the parameter combinations that resulted in greater energy availability (high weld force, high amplitude) there was localized metallic bonding occurring at the contact points, resulting in a greater mechanical strength than a build with less available energy per contact point. It is possible that if more energy were available from the system (i.e. the VHP-UAM system with 10 kW of power as opposed to 2 kW for the Beta) then large deformation of surface asperities could occur, and the percent bond area would increase towards 100%. Presumably, this would result in a USS and UTTS close to that of the parent material.

In order to determine whether this theory is reasonable, the elastic strain energy was calculated for a typical 3003 aluminum surface asperity. The elastic strain energy for an applied normal stress (tension) is given by

$$U_i = \int_V \frac{{\sigma_Y}^2}{2E} dV, \tag{3.3}$$

where σ_Y is the yield strength of the parent material, and E is the modulus of elasticity of the parent material integrated over V, volume [8]. A yield strength of

186 MPa and a modulus of elasticity of 68.9 GPa were used in the calculations and are given in [1] for aluminum 3003 H-18. In order to avoid the integration, a strain energy density was calculated (strain energy per unit volume) and was found to be 0.2512 J/cm^3. It was desired to compare this value to the applied machine energy during a given welding cycle, but this is a non-trivial calculation. Currently, the power cannot be tracked during a weld cycle on the Beta machine (it is possible on the VHP-UAM machine). For this reason, the mechanical energy applied would need to be calculated. This value was attempted to be calculated using

$$U = \frac{(\text{Machine Power})\,(\text{Contact Length})}{\text{Weld Rate}}, \tag{3.4}$$

where the machine power was the maximum power output from the Beta machine, the contact length was estimated based upon contact stress analyses, and the weld rate was the slowest weld rate used in the DOE.

Difficulties arise when one tries to determine a control volume that the energy would dissipate through. As the tape layers are welded the overall build volume increases making the use of the bulk part volume invalid. Further, it is not known how the energy dissipates through the overall build and how it is coupled to the base plate and possibly the anvil below. Using the volume of a tape layer produces a very large amount of energy that would be available for welding, but again, the tape layers are coupled together and the energy would travel through the entire part so this would result in an overestimate of the energy. At this time, the hypothesis put forth cannot be validated without further testing and/or better computational methods.

CHAPTER 4

FATIGUE LIFE

4.1 Experimental Methods

4.1.1 Specimen Geometry

Fatigue samples were built using EWI's Beta machine using 3003 aluminum H-18 in accordance to the geometry recommendations of ASTM Standard Practice for Conducting Force Controlled Constant Amplitude Axial Fatigue Tests of Metallic Materials [11]. In order to avoid creating a build higher than necessary, the grip length of the specimens was reduced. Steel inserts were used to make-up for the loss in length when the specimens were inserted into the collets of the fatigue testing machine. These were necessary in order to ensure that the gauge length of the specimen was perfectly aligned with the edges of the grips. The samples were cut from the build in the vertical direction by electrical discharge machining (EDM) such that the tapes layers are transverse to the applied loading. The gauge section was machined on a lathe following the machining practices outlined in ASTM E 466. Figure 4.1 below shows the specimen with overall dimensions and tape layout. Final dimensions can be seen in Appendix A.

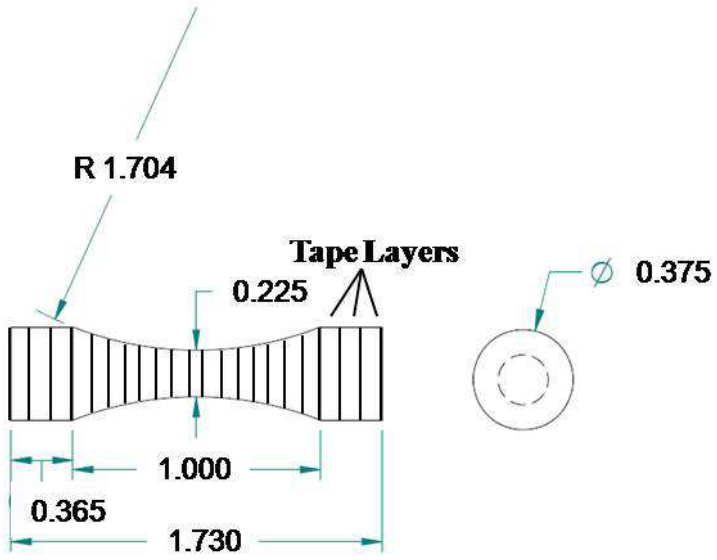

Figure 4.1: Geometry and tape diagram of fatigue specimens.

4.1.2 Manufacture Procedure

In order to build the specimens to the desired height, blocks that were 2" wide by 4" long by 1.25" tall (50.8 mm by 101.6 mm by 31.8 mm) (0.25" of the build plate will be used in the grip section) were constructed using EWI's UAM Beta machine. Two 3003 aluminum blocks of this size were created using parameter combinations based upon mechanical testing results of the 3003 aluminum DOE (Figure 4.2). The first block was created using a 200 N tack force, 1000 N weld force, 26 μm amplitude, and 100 in/min (42 mm/sec) weld rate. This combination produced samples with a high USS and UTTS from the 3003 aluminum DOE and corresponds to the treatment combination for Experiment #6. The second block was created using a 350 N tack force, 800 N weld force, 22 μm amplitude, and 125 in/min (53 mm/sec) weld rate. This combination produced samples with a medium USS and UTTS from the 3003

aluminum DOE and corresponds to the treatment combination for Experiment #5, with the exception of the weld rate which was originally 150 in/min (64 mm/sec), but was slowed down slightly in order to avoid manufacturing complications. Originally, there was a third block that had a low end parameter combination (350 N tack force, 600 N weld force, 18 μm amplitude, and 150 in/min weld rate), but this was discarded because of repeated manufacturing issues.

The 3003 aluminum tapes were laid in a brick wall-like stacking fashion such that the builds alternated between three side-by-side tapes (with a 0.060" overlap) and two side-by-side tapes on the next layer (Figure 4.3). Periodic machining was necessary to trim off the excess tape to avoid entanglement in the machine during subsequent passes. The samples were then machined out of the large blocks as cylinders with a 0.375" diameter.

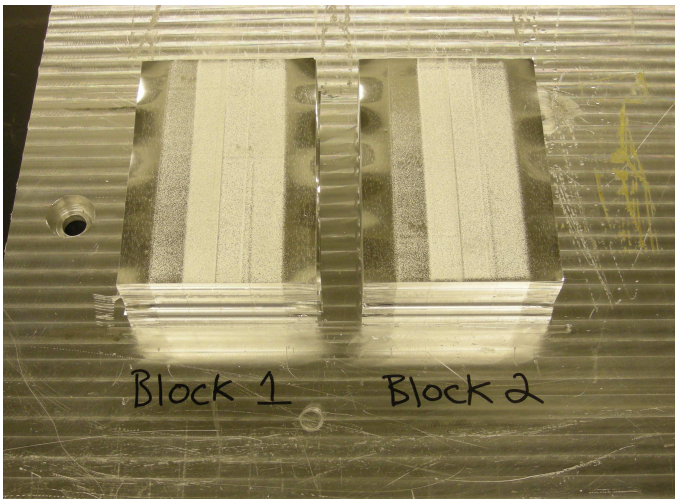

Figure 4.2: Photograph of UAM built blocks of aluminum that fatigue samples were machined from.

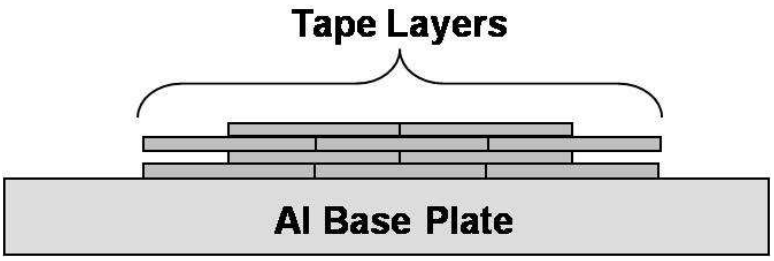

Figure 4.3: Schematic of tape layout for UAM fatigue builds.

4.1.3 Testing Procedure

A total of 20 samples were created and tested (10 from each parameter combination) using a Rotating Beam Fatigue Testing Machine that applies fully reversible axial bending loads to un-threaded specimens as shown by Figure 4.4. Five different moments were applied to the 20 specimens such that the resulting stress in the samples would be evenly spaced below the yield strength of 3003-H18 aluminum (186 MPa). Table 4.1 below shows the bending moments and resulting stresses used. The samples were loaded into the collet with zero load applied, the machine was brought up to speed and the poise weight was quickly adjusted to the desired bending moment value. A digital counter recorded the number of cycles to failure. The loading was applied at a frequency of 1000 rpm (16,667 Hz).

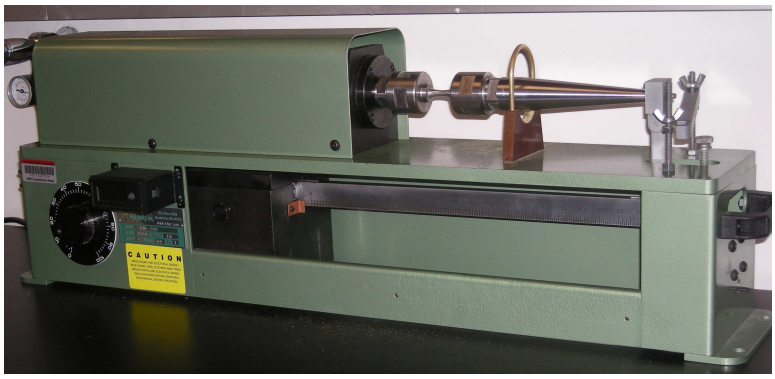

Figure 4.4: Photograph of Rotating Beam Fatigue Testing Machine used for UAM fatigue tests.

Table 4.1: Moments and resulting stresses applied to fatigue samples.

	Sample Number				
	1	**2**	**3**	**4**	**5**
Nominal Bending Stress (MPa)	55	76	97	118	139
Calculated Bending Stress (MPa)	55.5	74.0	98.6	117.1	135.6
Moment (Posie Wt.) (in-lb)[a]	9	12	16	19	22

[a]Machine input is in in-lb.

4.2 Results

The bonds of the fatigue samples were much weaker than anticipated. None of the tests could be carried out to completion using the rotating beam fatigue testing machine because the weight of the free-end collet was enough to break samples from both Blocks I and II without any additional applied moment and without an cycles. The collet weighs about 2 lb (0.907 kg), which results in an extra 0.9 in-lb (0.102 N-m) of moment applied to the specimen in the gauge region. Under normal operating conditions, for the materials used in this machine this extra moment would have an

insignificant effect on the specimen, but for these UAM samples this moment proved to be catastrophic. The calculated moment was then used in the normal bending stress equation,

$$\sigma_b = \frac{Mc}{I}, \tag{4.1}$$

where M is the applied moment (0.9 in-lb), c is the maximum distance from the neutral axis to the edge of the specimen (0.1125 in), and I is the moment of inertia for a circular cross-section (1.258×10^{-4} in^4). The resulting bending stress is 805 psi (5.55 MPa). This is significantly lower than the average experimentally found transverse tensile stress for the samples from Experiment #6 in the 3003 aluminum DOE. Those samples were experiencing a tensile stress of about 30 MPa (4351 psi) before failing. Therefore, further investigation was needed to explain the dramatically lower stress that the fatigue samples were failing at.

Fracture surfaces were microscopically examined and characterized following the same procedures outlined in section 3.1.5. Figure 4.5 shows several micrographs of a typical fracture surface from the fatigue samples.

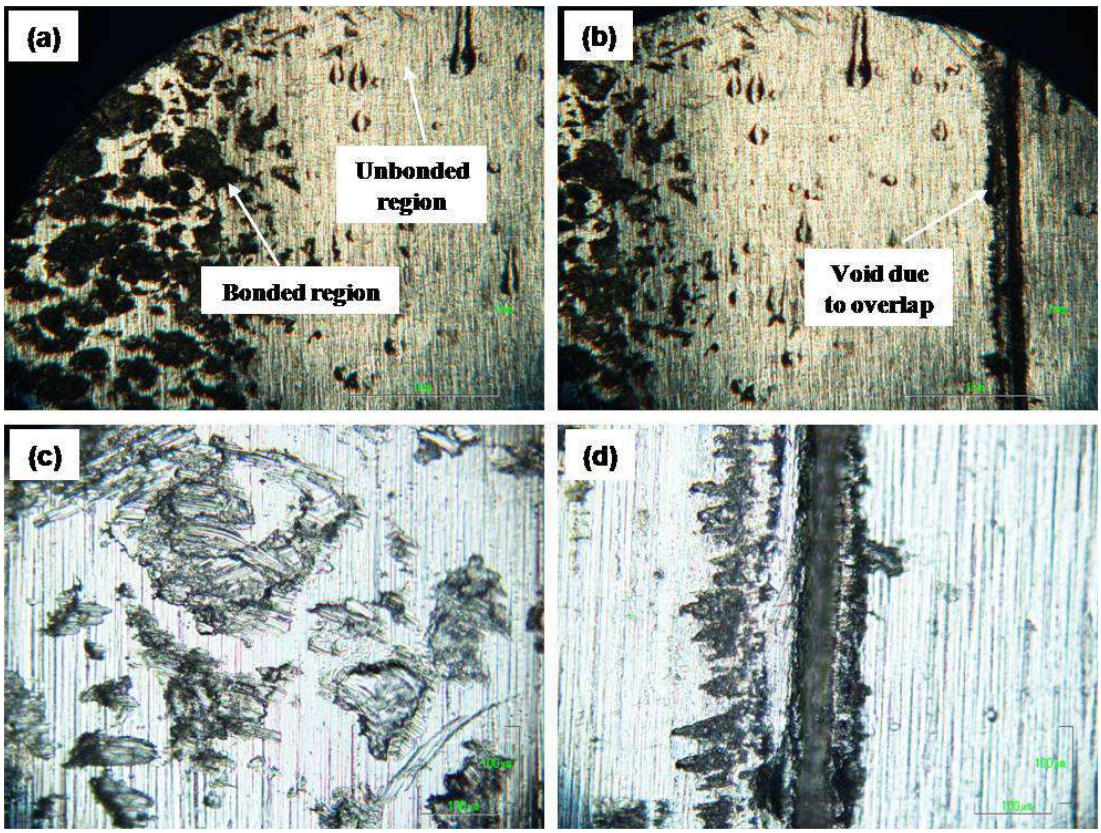

Figure 4.5: Micrographs of fatigue sample fracture surface (a),(b) at 40x, (c) at 200x focused on bonded regions, and (d) at 200x focused on gap produced by overlapping of tapes during manufacture.

As highlighted by Figure 4.5(b) and (d) all of the samples had a valley-like region that was produced during manufacture. This area exists because every few tapes that were supposed to have been slightly overlapped became misaligned during the weld cycle producing a gap, which is essentially a large, continuous void through the sample as shown by Figure 4.6(a) and (b).

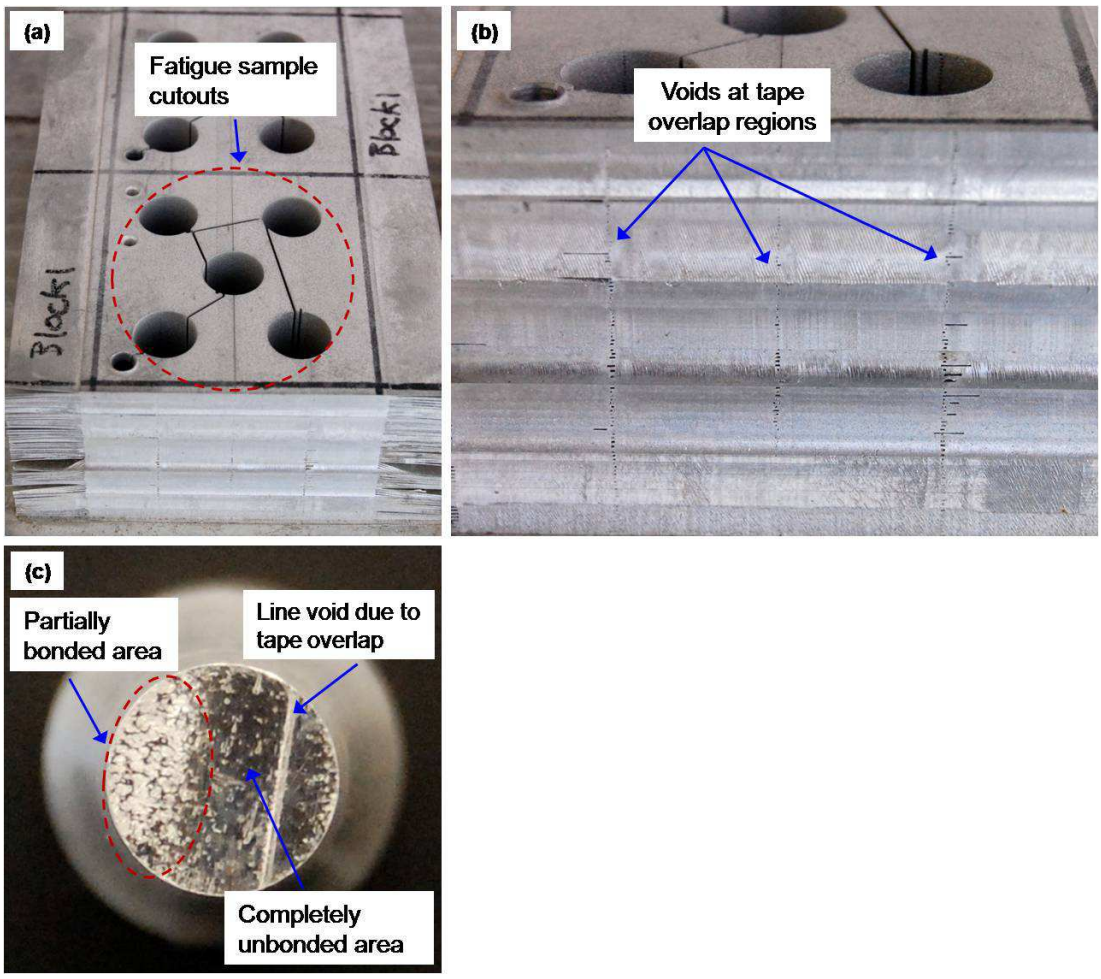

Figure 4.6: Photographs showing (a) the overall block from which fatigue samples were machined from (holes), (b) close-up of tape layer interfaces showing the voids at the overlap regions, and (c) typical fatigue sample fracture surface on macro scale.

The percent bonded area was calculated for several of the specimens and the average was found to be 18%. This is quite clearly displayed through the micrographs where it can be seen that only a small area is more fully bonded and similar to that seen in the micrographs of the transverse tensile samples, and a large portion of the surface has very little to no bonding. Micrographs of the areas that visually seemed to have a relatively high amount of bonding reported a percent bonded area of between

40% to 60%, while the rest of the sample fracture surface micrographs had between 6% to 12%. Calculations showed that on average the area that appeared to have a decent amount of bonding covered only 37% of the entire fracture surface as shown by Figure 4.6(c).

4.3 Discussion

While the tests were unsuccessful with regards to determining the fatigue life of the specimens, they were useful in that it was found that the overlapping system is not beneficial to the strength of the builds. It is possible that due to the overlap of the layers, when the sonotrode comes in contact with the tape it applies uneven pressure across the tape causing some areas to be well-bonded and others to be left untouched as depicted by Figure 4.7.

In the future, care should be taken to avoid removing the specimens from areas where the overlap occurs. Moreover, the overlap should try to be removed when producing larger builds by using sheets of metal instead of tapes, in which case there would not be a need for overlapping of layers. Alternatively, when the overlapping layers manufacturing scheme is unavoidable, higher normal force could be employed in order to overcome the unevenness in the sonotrode contract pressure. Further investigation is necessary to determine the fatigue life of 3003 aluminum UAM built specimens.

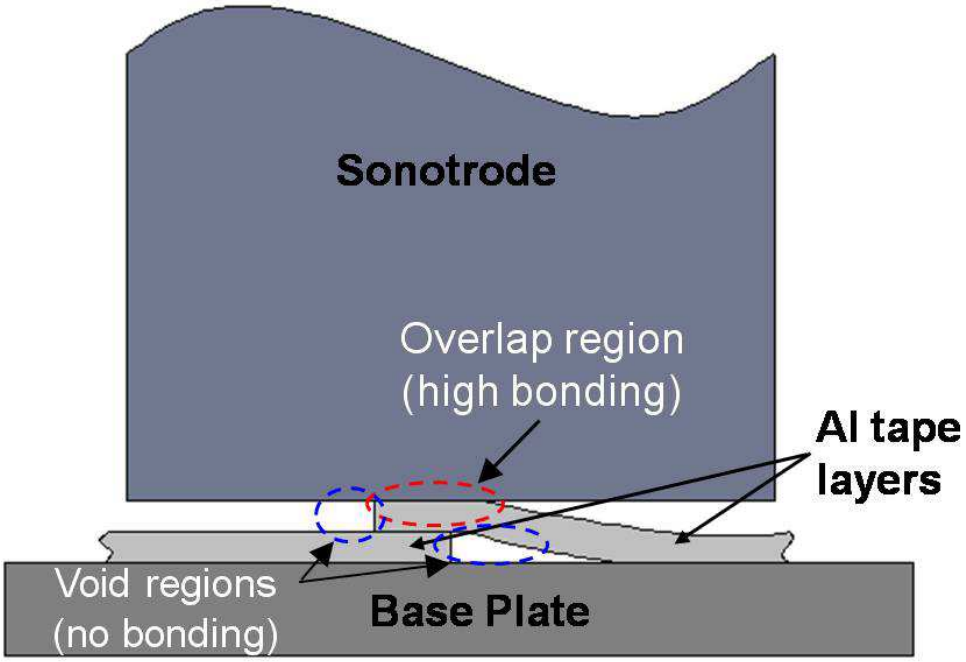

Figure 4.7: Schematic of situation caused by overlapping of tapes and resulting void/unbonded area creation.

CHAPTER 5

CONCLUDING REMARKS

The goal of this research was to develop and characterize a combination of manufacture parameters that optimize the mechanical strength of metallic composites made by ultrasonic consolidation. The specific focus involved a statistical analysis of the results of transverse shear and transverse tension tests of Ti/Al builds and 3003 aluminum builds. Additional effort was given to the development of a correlation between the observed mechanical strength of the specimens and their interface microstructure and fracture surface microstructure.

The overall approach of this investigation is as follows. Chapter 1 provided background on the UAM process and reviewed the fundamental concepts behind the design and analysis of a statistical experiments. The second chapter worked through the development, statistical analysis, and physical explanation of the results for an experiment involving Ti/Al composites. In Chapter 3, a new DOE was created and statistically analyzed for 3003 aluminum builds. The linear weld density and fracture surface percent bonded area of certain samples were calculated and compared to the mechanical strength of those samples and a hypothesis was proposed to explain the results. Fatigue samples were built using a set of parameters from the 3003 aluminum DOE and a procedure for testing was established in Chapter 4. Testing was

unsuccessful and fatigue life data for an S-N plot was not acquired due to unforeseen manufacturing issues.

5.1 Conclusions

This research has accomplished several key goals. Standardized methods of mechanical testing (shear and transverse tensile) were established and verified. A design of experiment utilizing a Taguchi mixed array was carried out on Ti/Al composites for four process parameters at four levels each. Due to delamination during UAM or during the post-processing machining, many of of the treatment combinations could not be tested. There was great variability between all samples in both shear and tensile tests, and samples mainly broke in a macro-brittle fracture mode between layers. The greatest shear strength observed is about 68 MPa (Experiment #12), which is close to the shear strength of solid 1100-O aluminum. The transverse tensile strengths are all much less than the ultimate tensile strength of both parent materials, with the greatest average UTTS still being 53% less than that of solid 1100-O aluminum.

Generalized linear models were used to study the relations of the four factors (normal force, amplitude, weld speed, number of bilayers) and USS or UTTS. Models including two of these factors at a time were investigated. In addition, linear contrasts and linear regression models were studied to further explore these relations. Larger sample sizes are needed in order to fit models with all four factors and possible interactions among these factors. While further investigation is needed to fully assess the effects of the parameters in this study, the trends indicate that the following combination of levels of process parameters examined in this DOE produce the highest strengths: normal force of 1500 N, oscillation amplitude of 30 μm, weld

speed between 21 mm/s (50 in/min) and 42 mm/s (100 in/min), and two bilayers. By examining the microstructure of the samples it is concluded that little to no metallurgical bonding occurred at the interface. The softer aluminum is believed to flow around the topography of the harder titanium, which in turn does not allow for deformation of asperities thereby limiting nascent surface contact area which is necessary for solid-state bonding. The strength of the builds is derived from the severity of the mechanical interlocking of the two metals at the interface due to the imprinting of a roughness from the sonotrode. SEM images and EDS analysis showed that the heat treatment did not induce the formation of any significant amount (if any) of intermetallic compounds at the Ti-Al interfaces.

The 3003 aluminum DOE provided a number of important insights as well. A design of experiment utilizing a Taguchi mixed array was carried out on 3003 aluminum composites for four process parameters – one at 2 levels (tack force), and the other three at three levels each. The results of pilot experiments showed combinations of parameter levels do not work. Mainly, upper and lower bounds were determined for combinations of weld force and amplitude. Transverse shear and transverse tensile samples were created and tested and samples failed mainly in a macro-brittle fracture mode. An analysis of variance, interaction plots, confidence intervals, and trend contrasts were all utilized for examining the USS and UTTS data.

The results of these analyses show that the parameters weld force and oscillation amplitude have a significant influence (at a 95% level) on the resulting mechanical strength (USS and UTTS) of the specimens. Furthermore, there is no evidence of any interaction existing between parameters. Thus, it is put-forth that the following combination of levels of process parameters examined in this DOE produce the

highest strengths: tack force of 350 N, weld force of 1000 N, oscillation amplitude of 26 μm, and weld rate between 42 mm/s (100 in/min) and 53 mm/s (125 in/min). Interface microstructure analyses including LWD and percent bond area characterizations suggest that these UAM builds all exhibit relatively the same amount of bonded area regardless of strength for a given parameter combination in this DOE. A hypothesis was established that states that there is insufficient power available to produce extensive plastic deformation of surface asperities and that the difference in specimen strength is due to localized bonding because of increased energy input at certain contact points.

Investigation of fatigue strength was unsuccessful with regards to determining the fatigue life, but an extremely important practical discovery was made. It was found that the overlapping of tape layers for manufacturing taller builds leads to large voids in the overlap regions and results in a very low percent bonded area and severely depressed strengths.

5.2 Future Work

Despite the advances made in this research, there are still numerous challenges in characterizing the strength of UAM specimens. Electron back-scatter diffraction (EBSD) and possibly orientation imaging microscopy (OIM) could be applied to current 3003 aluminum samples to see if the theory that localized bonding is occurring at a few contact points (i.e. recrystallization, grain growth, subgrain refinement) is correct. Previous studies have found that recrystallization does occur at the interface between 3003 aluminum layers [5, 15]. However, this should be examined for the specific samples from the 3003 aluminum DOE in this research. This would allow for

a correlation to be made between the mechanical strength of the build and the grain structure at the interfaces.

A mechanics of materials/energy model should be completed for the strain energy criteria. This would provide fundamental insights into the UAM process and possibly allow for the creation of a constituent relationship or model with predictive capabilities. Lastly, new fatigue samples should be created that do not include a tape overlap region, thereby allowing for an S-N plot to be established for 3003 aluminum built by UC.

The following studies are recommended:

- A mechanical strength study should be established that pushes up the machine energy curve and allows for an investigation of the percent bonded area and LWD at higher machine energies.
- Determine if increased bonded area results in increased strength eventually leading to builds with strengths close to that of the parent material.
- Fill in points on possible energy curve (using VHP-UAM machine).

APPENDIX A

DRAFTS OF SAMPLES CREATED FOR UAM MECHANICAL TESTING

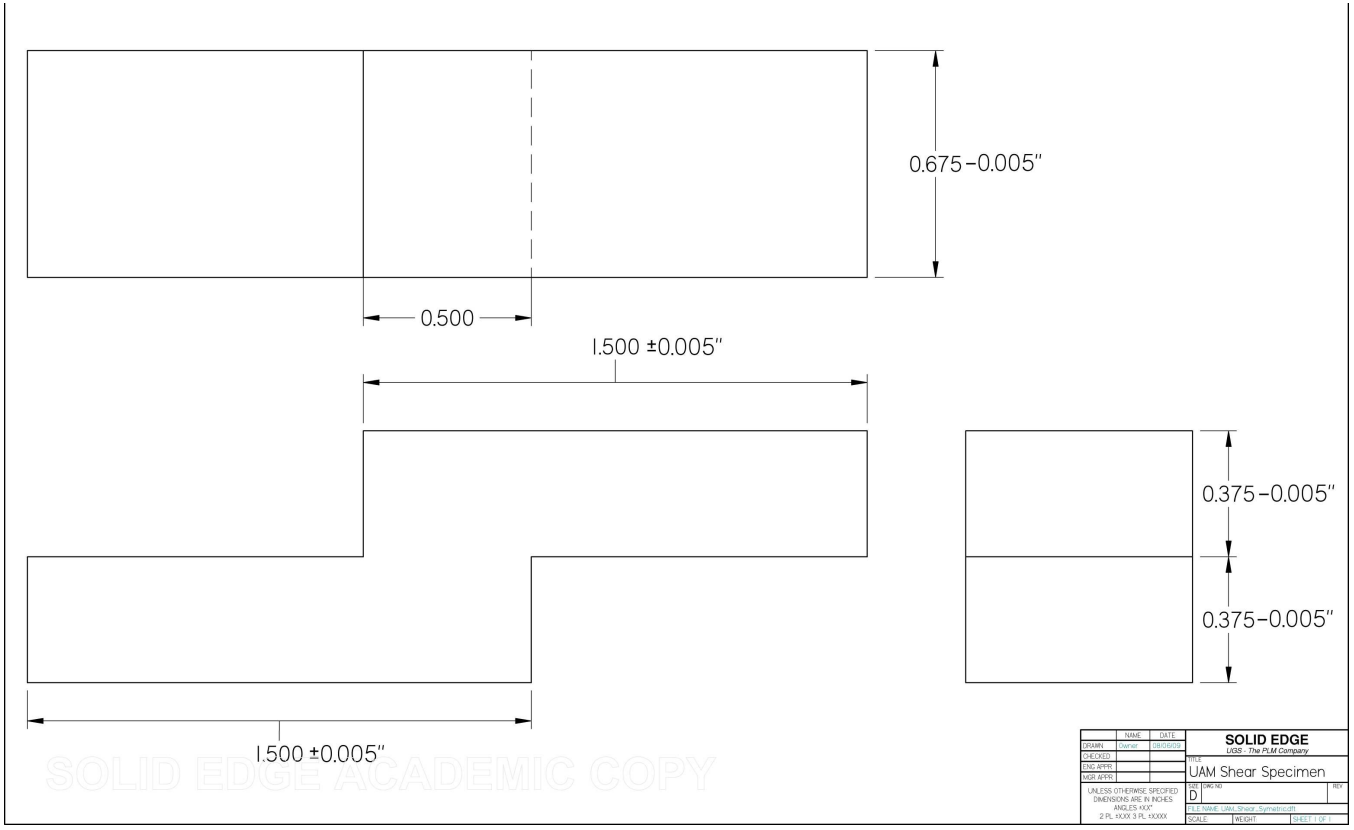

Figure A.1: Nominal dimensions for bulk shear samples. All dimensions in inches.

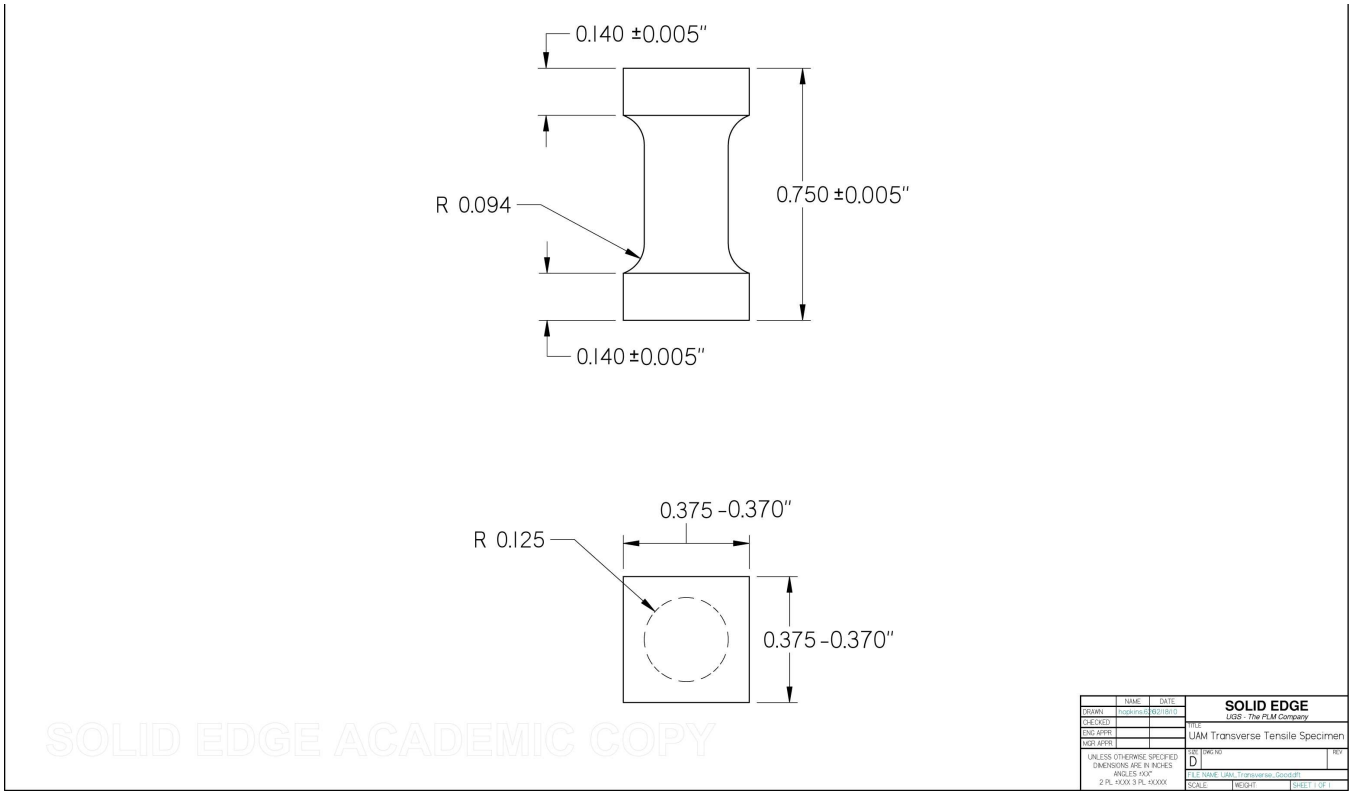

Figure A.2: Nominal dimensions for bulk transverse tensile samples. All dimensions in inches.

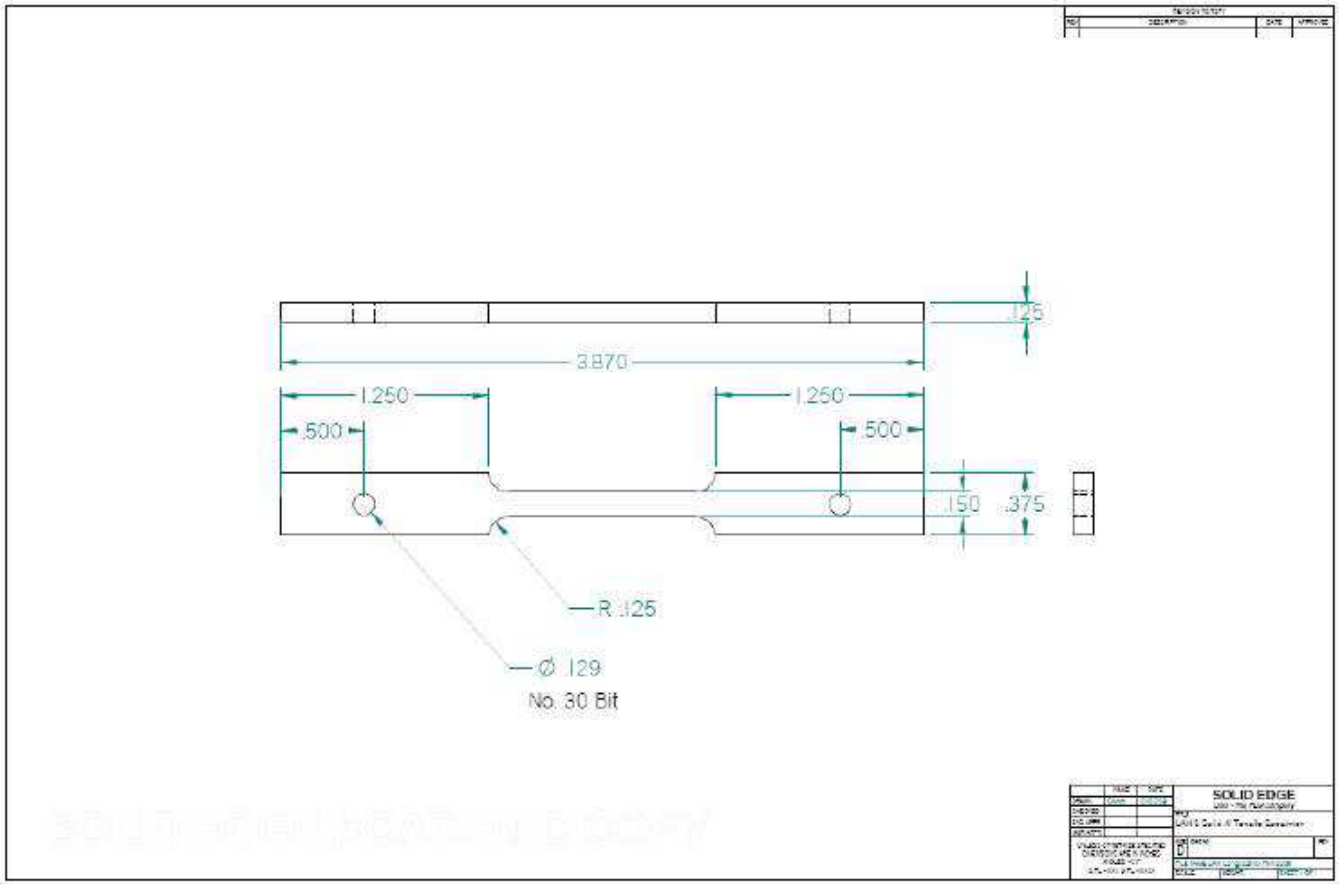

Figure A.3: Nominal dimensions for bulk longitudinal tensile samples. All dimensions in inches.

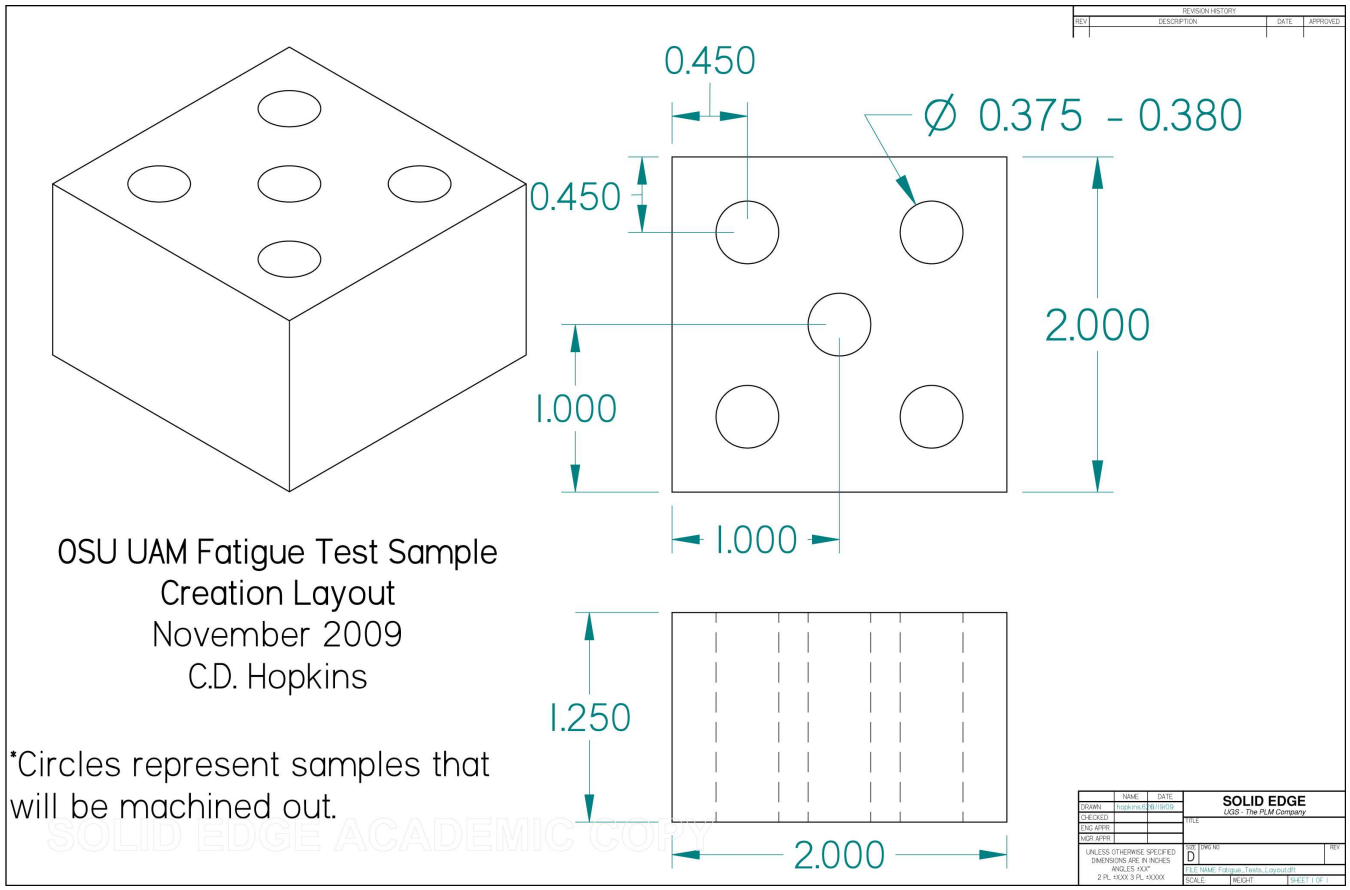

Figure A.4: Nominal dimensions for blocks created for fatigue tests with holes representing location of sample extraction. All dimensions in inches.

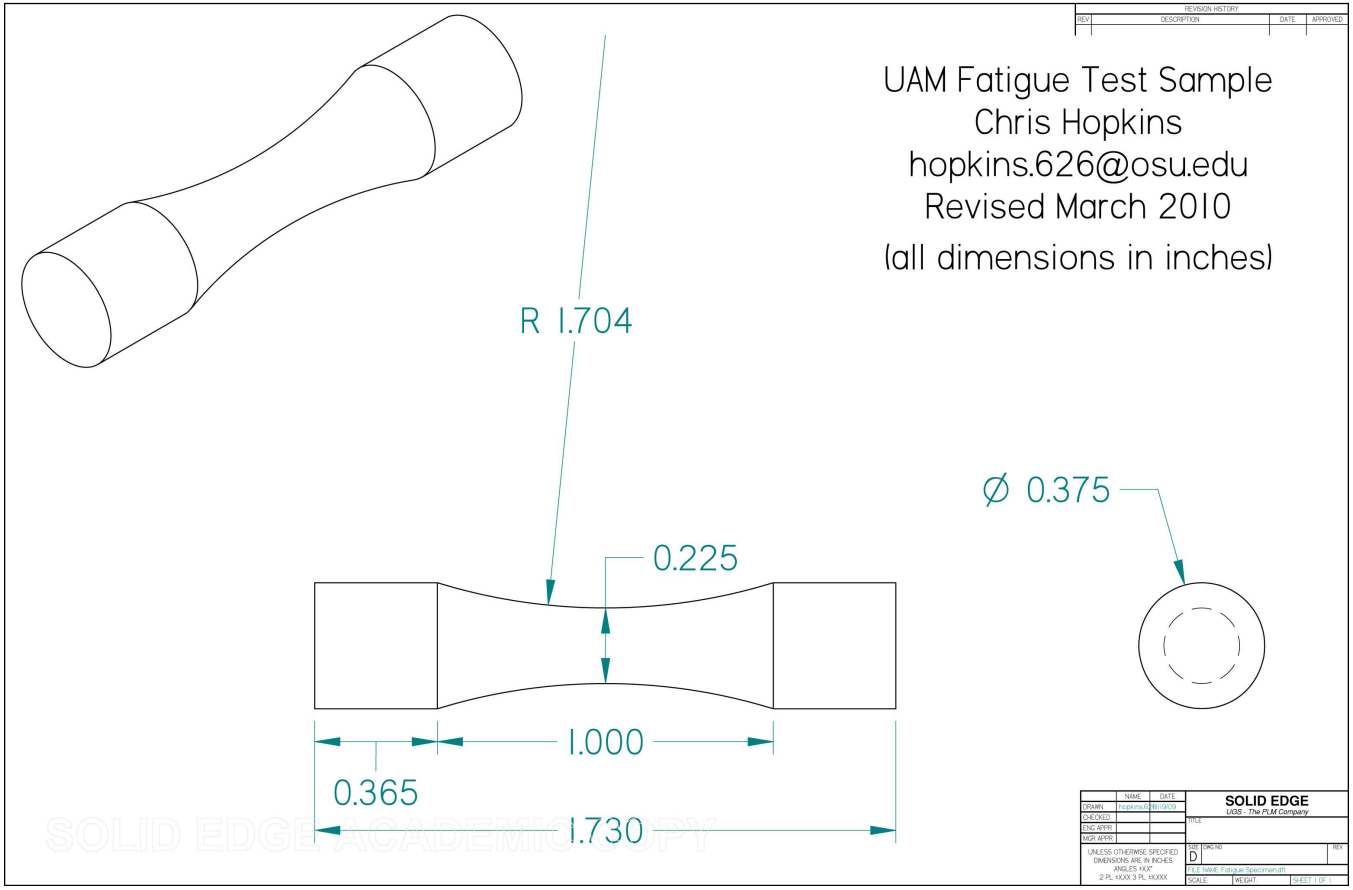

Figure A.5: Nominal dimensions for fatigue samples. All dimensions in inches.

APPENDIX B

SUPPLEMENTARY DOE MECHANICAL STRENGTH RESULTS

Table B.1: Complete results from Ti/Al DOE transverse shear tests.

Experiment Number	**Breaking Force (N)**	**Shear Area (10^{-4} m^2)**	**USS (MPa)**	**Average USS (MPa)**	**Standard Deviation**
1	10427	2.1818	47.792	51.518	5.27
	9767	1.7681	55.243		
7	7697	2.0990	36.671	30.845	5.10
	5746	2.1133	27.188		
	6106	2.1295	28.675		
8	8052	2.1121	38.125	33.314	7.25
	4924	2.1524	22.877		
	7246	2.1370	33.908		
	7977	2.0803	38.345		
11	10776	2.0716	52.016	41.954	8.31
	9630	2.1164	45.502		
	7509	2.1077	35.627		
	7500	2.1632	34.669		
12	12816	2.0934	61.222	63.628	6.17
	14625	2.1152	69.143		
	14431	2.1184	68.126		
	11874	2.1196	56.020		
14	8648	2.0581	42.019	46.769	12.46
	12240	2.1077	58.070		
	11656	2.0959	55.615		
	6595	2.1021	31.372		
15	7378	2.1115	34.941	31.065	7.66
	7493	2.0808	36.008		
	4684	2.1052	22.247		
16	7613	2.0934	36.366	48.362	20.76
	12551	2.0795	60.358		
	4288	2.1465	19.975		
	2905	2.0865	13.923		

Table B.2: Complete results from Ti/Al DOE transverse tensile tests.

Experiment Number	**Breaking Force (N)**	**Gauge Area (10^{-5} m^2)**	**UTTS (MPa)**	**Average UTTS (MPa)**	**Standard Deviation**
7	98.18	3.1669	3.100*	28.216	7.50
	1156	3.1416	36.809		
	788.2	3.1669	24.887		
	726.9	3.1669	22.952		
8	249.2	3.1669	7.863	12.546	6.62
	545.7	3.1669	17.230		
11	17.88	3.1416	0.569*	35.988	8.47
	860.1	3.1416	27.377		
	1139	3.1416	36.269		
	1392	3.1416	44.319		
12	1039	3.1669	32.794	48.254	11.22
	2046	4.1447	49.371		
	1887	3.1416	59.577		
	1611	3.1416	51.272		
14	1071	3.1669	33.808	31.424	3.37
	912.3	3.1416	29.039		
	326.9	3.4782	9.398*		
16	1406	3.1923	44.034	44.034	-

*Not included in statistical calculations.

Table B.3: Fracture location measurements for Ti/Al DOE transverse tensile samples.

Experiment Number	Distance from Bottom[a] (in)	Layers from Bottom[b]	Average Distance from Bottom (in)	Average Layer Number	Standard Deviation of Layers
7	0.473	95*	0.359	72	32
	0.348	70			
	0.522	104			
	0.206	41			
8	0.120	24	0.335	67	61
	0.549	110			
11	0.270	54*	0.370	74	30
	0.547	109			
	0.274	55			
	0.288	58			
12	0.245	49	0.370	74	34
	0.579	116			
	0.224	45			
	0.433	87			
14	0.230	46	0.396	79	47
	0.562	112			
	0.561	112*			
16	0.253	51	0.253	51	-

[a]The distance is from the bottom of the Al baseplate to the fracture surface minus the 0.060" thickness of the baseplate.

[b]Each layer of Ti and Al is 0.005".

*Not included in statistical calculations.

Table B.4: Ti/Al longitudinal tensile testing results for samples made with base plate.

Sample	Breaking Force (N)	Gauge Area (10^{-5} m^2)	Ultimate Longitudinal Tensile Stress (MPa)	Percent Elongation at Failure
1B[a]	2673	1.1554	231.36	-
2B	2916	1.2600	231.41	22.68
3B	2750	1.1806	232.89	25.54
4B	2803	1.2016	233.23	22.14
5B	2952	1.2497	236.23	25.27
		Average =	233.02	23.91
		Stand. Dev. =	1.98	1.75

[a]Did not fully break, therefore fifth sample used.

Table B.5: Ti/Al longitudinal tensile testing results for samples made without base plate.

Sample	Breaking Force (N)	Gauge Area (10^{-5} m^2)	Ultimate Longitudinal Tensile Stress (MPa)	Modulus of Elasticity (GPa)	Percent Elongation at Failure
1	2694	1.2016	224.23	22.8	19.29
2	2869	1.2194	235.16	61.6	24.55
3	2676	1.1613	230.43	6.1	18.13
4	2969	1.2864	230.80	58.2	22.50
		Average =	230.16	37.18	21.12
		Stand. Dev. =	4.50	27.15	2.94

Table B.6: Complete results from 3003 aluminum DOE transverse shear tests.

Build Order	Treatment Combination	Tack Force (N)	Weld Force (N)	Amplitude (μm)	Weld Rate (mm/s)	Ultimate Shear Strength (MPa) Sample 1	Sample 2	Sample 3	Sample 4
1	11	350	600	22	42	13.928	14.780	11.206	-
2	18	350	1000	26	53	17.656	15.505	16.227	18.686
3	1	200	600	18	42	-	-	5.032	5.426
4	17	350	1000	22	42	11.879	17.010	22.117	-
5	14	350	800	22	64	10.763	-	-	-
6	9	200	1000	26	42	18.846	20.126	21.118	27.831
7	15	350	800	26	42	14.433	22.219	9.670	13.808
8	3	200	600	26	64	9.952	5.525	8.842	9.296
9	8	200	1000	22	64	11.490	17.469	-	-
10	6	200	800	26	64	15.720	15.046	13.158	15.980
11	2	200	600	22	53	6.306	12.953	-	-
12	13	350	800	18	53	-	-	-	-
13	7	200	1000	18	53	-	-	-	-
14	4	200	800	18	42	-	-	-	-
15	5	200	800	22	53	13.910	14.395	15.208	-
16	12	350	600	26	53	20.674	10.632	18.762	-
17	10	350	600	18	64	-	-	-	-
18	16	350	1000	18	64	15.571	-	-	-

Table B.7: Complete results from 3003 aluminum DOE transverse tensile tests.

Build Order	Treatment Combination	Tack Force (N)	Weld Force (N)	Amplitude (μm)	Weld Rate (mm/s)	Ultimate Transverse Tensile Strength (MPa) Sample 1	Sample 2	Sample 3	Sample 4
1	11	350	600	22	42	14.517	16.538	-	21.118
2	18	350	1000	26	53	24.749	31.837	33.818	35.687
3	1	200	600	18	42	-	-	-	11.247
4	17	350	1000	22	42	-	36.154	9.580*	19.565
5	14	350	800	22	64	19.149	-	-	-
6	9	200	1000	26	42	32.743	33.678	15.416*	24.099
7	15	350	800	26	42	22.963	24.650	22.431	23.587
8	3	200	600	26	64	10.343	15.393	15.151	9.906
9	8	200	1000	22	64	12.608	11.741	-	-
10	6	200	800	26	64	19.935	20.480	13.336*	22.689
11	2	200	600	22	53	12.496	13.591	-	-
12	13	350	800	18	53	-	-	-	-
13	7	200	1000	18	53	-	-	-	-
14	4	200	800	18	42	-	-	-	-
15	5	200	800	22	53	9.615	19.375	11.533	17.720
16	12	350	600	26	53	24.145	-	9.207*	19.392
17	10	350	600	18	64	-	-	-	-
18	16	350	1000	18	64	-	-	17.025	-

*Not included in statistical calculations

BIBLIOGRAPHY

[1] The Aluminum Association. *Aluminum Standards and Data*. 6th edition, 1979.

[2] R. Boyer, G. Welsch, and eds. Collings, E. W. *Materials Properties Handbook: Titanium Alloys*. ASM International, Materials Park, OH, 1994.

[3] T. Clyne and P. Withers. *An Introduction to Metal Matrix Composites*. Cambridge University Press, 1993.

[4] A. Dean and D. Voss. *Design and Analysis of Experiments*. Springer, New York, 1999.

[5] R.R. Dehoff and S.S. Babu. Characterization of interfacial microstructures in 3003 aluminum alloy blocks fabricated by ultrasonic additive manufacturing. *Acta Materialia*, pages 1–12, March 2010.

[6] K. Graff. *New Developments in Advanced Welding*. Woodhead Publishing Limited, 2005.

[7] R.M. Hahnlen. Development and characterization of NiTi joining methods and metal matrix composite transducers with embedded NiTi by ultrasonic consolidation. Master's thesis, The Ohio State University, Columbus, OH, 2009.

[8] R.C. Hibbeler. *Mechanics of Materials*. Pearson Prentice Hall, Upper Saddle River, NJ, 6th edition, 2005.

[9] SAS Institute Inc. Sas 9.1 copyright (c), 2002-2003.

[10] ASTM International. C 961-06: Standard test method for lap shear strength of sealants, 2006.

[11] ASTM International. E 466-07: Standard practice for conducting force controlled constant amplitude axial fatigue tests of metallic materials, 2007.

[12] ASTM International. E 8/e 8m-08: Standard test method for tension testing of metallic materials, 2008.

[13] G.D. Janaki Ram, Y. Yang, J. George, C. Robinson, and B. Stucker. Improving linear weld density in ultrasonically consolidated parts. In *Proceedings of the 17th Solid Freeform Fabrication Symposium, Austin, Texas*, 2006.

[14] G.D. Janaki Ram, Y. Yang, and B.E. Stucker. Effect of Process Parameters on Bond Formation During Ultrasonic Consolidation of Aluminum Alloy 3003. *Journal of Manufacturing Systems*, 25(3):221, 2006.

[15] K. Johnson. *Interlaminar Subgrain Refinement in Ultrasonic Consolidation*. PhD thesis, Loughborough University, Loughborough, UK, 2008.

[16] K.C. Joshi. The formation of ultrasonic bonds between metals. *Welding Journal*, 50(12):840–848, 1971.

[17] C. Kittel. *Introduction to Solid State Physics*. John Wiley & Sons, Canada, 7th edition, 1995.

[18] C.Y. Kong and R.C. Soar. Fabrication of metal–matrix composites and adaptive composites using ultrasonic consolidation process. *Materials Science & Engineering A*, 412(1-2):12–18, 2005.

[19] C.Y. Kong, R.C. Soar, and P.M. Dickens. Characterisation of aluminum alloy 6061 for the ultrasonic consolidation process. *Materials Science & Engineering A*, 363(1-2):99–106, 2003.

[20] C.Y. Kong, R.C. Soar, and P.M. Dickens. Optimum process parameters for ultrasonic consolidation of 3003 aluminum. *J. of Materials Processing Tech.*, 146(2):181–187, 2004.

[21] M. Kulakov and H.J. Rack. Control of 3003-H18 Aluminum Ultrasonic Consolidation. *Journal of Engineering Materials and Technology*, 131:021006, 2009.

[22] H.A. Mohamed and J. Washburn. Mechanism of Solid State Pressure Welding. *Welding Journal*, page 302s, 1975.

[23] D.C. Montgomery. *Design and Analysis of Experiments*. John Wiley & Sons, New York, 1991.

[24] US National Institutes of Health. ImageJ. Website, 2009.

[25] E Neppiras. Ultrasonic welding of metals. *Ultrasonics*, (3):128–135, 1965.

[26] J.M. Parks. Recrystallization Welding. *Welding Journal*, pages 209s–222s, May 1953.

[27] C. Robinson, C. Zhang, G.D. Janaki-Ram, E. Siggard, B.E. Stucker, and L. Li. Maximum height to width ratio of free-standing structures built by ultrasonic consolidation. In *Proceedings of the 17th Solid Freeform Fabrication Symposium*, Austin, TX, August 2006.

[28] D.E. Schick, R.M. Hahnlen, R. Dehoff, P. Collins, S.S. Babu, M.J. Dapino, and J.C. Lippold. Microstructural Characterization of Bonding Interfaces in Aluminum 3003 Blocks Fabricated by Ultrasoninc Additive Manufacturing. *Welding Journal*, 89:105s–115s, May 2010.

[29] E. Siggard. Investigative research into the structural embedding of electrical and mechanical systems using ultrasonic consolidation. Master's thesis, Utah State University, Logan, UT, 2007.

[30] D.R. White. Ultrasonic consolidation of aluminum tooling. *Advanced materials & processes*, 161(1):64–65, 2003.

[31] Y. Yang, G.D. Janaki Ram, and B.E. Stucker. An Experimental Determination of Optimum Processing Parameters for Al/ SiC Metal Matrix Composites Made Using Ultrasonic Consolidation. *Journal of Engineering Materials and Technology*, 129:538, 2007.

[32] C. Zhang, A. Deceuster, and L. Li. A Method for Bond Strength Evaluation for Laminated Structures with Application to Ultrasonic Consolidation. *J. of Materials Engineering and Performance*, 18(8):1124–1132, 2009.